People's Democratic Republic of Algeria

Ministry of Higher Education and Scientific Research

Mohamed Boudiaf University - M'sila

Faculty Of Sciences

Physics Department

Serial number: .....

Enrolment number: D.PHM/3C/01/16

Thesis

Submitted for the diploma of

3rd cycle Doctorate (PHD) degree

Major : Physics

Speciality: Materials physics

THEME

Theoretical investigation of fundamental properties of perovskite solar cell materials

Presented By:

Adel MENEDJHI

Defended on :05/10/2021

In front of the jury composed of:

Name & First name	Grade	Establishment	Quality
Abdelmadjid BOUSSENDEL	MCA	Univ. of M'sila	President
Nadir BOUARISSA	Professor	Univ. of M'sila	Supervisor
Miloud IBRIR	Professor	Univ. of M'sila	Examiner
Samia FERAHTIA	MCA	Univ. of M'sila	Examiner
Ahmed GUEDDIM	Professor	Univ. of Djelfa	Examiner

Academic year: **2020 /2021**

Acknowledgements

I thank Allah who gave me the strength and ability to complete this thesis.

We thank our supervisor; Pr: Nadir BOUARISSA for the attention that he brought to us, and the framework of work that he offered us. As well as for his methodology and his precious advice.

I am deeply grateful to all the members of the jury, Dr. Abdelmadjid BOUSSENDEL, at the University of M'sila, for the honor she gave me by agreeing to chair the jury of this thesis, IBRIR Miloud at the University of M'sila and Professor Ahmed GUEDDIM at the University of Djelfa and also Dr. FERAHTIA for the interest they have shown in my work by agreeing to be examiners.

I also thank all the professors who helped me Pr. B .DEGHFEL, Pr. N. BAADJI and Dr. S. HAMRIT, and Professor SAIB Salima without forgetting to thank the honorable professor, Pr.F. MEZRAG

Last but not least, my strongest thanks go to my lovely parents, my sisters my parents, and my brothers.

Dedications

Through the care of Allah and all the courage and patience that he has given me during these years of study, I am now able to see the fruit of my work in this modest thesis.

I dedicate this work

To my father who has suffered a lot for us that life is better for us Thank you Father!

To my mother who gave a lot and who sacrificed so much so that I arrive at the right

Thank you Mother!

To all my family, my brothers and my sisters.

To all my friends.

I also dedicate all my respect and appreciation to those who have helped me throughout my career.

You were all a great support for me. Thank you very much

Contents

Contents

Introduction

Introduction

Classical fossil fuels have been crucial since the first industrial revolution as a primary driving force in the world today. Although past industrial revolutions catapulted human society into an unprecedented period of growth, they also resulted in massive energy and resource consumption and exacerbated the conflict between man and nature, forcing us to pay a high environmental price and ecological cost. The world's economic and social productive forces have been quickly developing, and classical fossil energy has been unable to meet our demands. As the twenty-first century began, humanity was confronted with enormous global energy and resource difficulties, as well as environmental, ecological, and climate change challenges. All of these concerns have ushered in the fourth industrial revolution, sometimes known as the green revolution. Solar energy, being the primary source of all energy, is unavoidably becoming a new reinforcement for human and social development due to its pollution-free, renewable, and massive energy potential. Optoelectronic conversion has been extensively investigated as one of the principal applications of solar energy during the last several decades, and solar cells are the most important form of optoelectronic converters. In recent years, the development of low-cost, high-efficiency solar cells has emerged as a critical concern. Perovskite solar cells (PSCs) have received a lot of interest in the last decade because of their high absorption coefficient, excellent bipolar charge mobility, long carrier difusion length, low exciton binding energy, low trap state density, and variable bandgap.Perovskite-type materials have attracted much attention in the field of photovoltaic devices. This is due to their important optical and electronic properties [1, 2]. Perovskite solar cells have improved their power conversion efficiency by roughly 20% in the last ten years, making them similar to polycrystalline silicon solar cells.

The performance of perovskite-type materials in solar devices has received a lot of interest. [1-3] . This is because to their extraordinary optical and electrical properties. Perovskite solar cells with good performance are, in reality, unstable. Furthermore, they are made of poisonous lead.[4]. Unfortunately, this make their use in photovoltaic's very limited. Alternatively, a new generation perovskites of double perovskites have been suggested so as to solve this problem [5, 6]. The proposed materials are inorganic, stable, non toxic, and have been successfully synthesized [5-7]. This makes them good candidates for photovoltaic applications.

Cs_2AgInX_6 (X: Cl,Br) is one of the double perovskites materials that has received a lot of attention in recent years. [8, 9] It has been considered as a potential option for

technological applications, particularly in the field of photovoltaics. Despite the fact that some fundamental features of the material in question were investigated, [8-10], Only a few details concerning its optical and electrical properties have been documented, which are crucial in the design and fabrication of devices that utilise the perovskite in issue. This prompted us to conduct a study utilizing density functional theory (DFT) computations on the band structure and optical spectra of the double perovskites material $Cs_2AgInBr_6$. Moreover, mechanical stability of the material under consideration has been checked via the elastic constants.

After this introduction, the work plan that we present our work according to the following following steps:

The first chapter: we give generalities on the perovskite solar cell materials and we present their an other optoelectronic applications

The second chapter focuses on the calculation method. It deals with the theoretical framework of our work. We expose the fundamental principles of the theory of the density functional functional theory (DFT). We also describe the method of pseudopotential and plane waves (PP-PW) method used in this thesis.

The third chapter: We present the main theoretical results obtained such as the study of the electronic, optical and elastic properties

Finally, we end our thesis with a general conclusion of this study.

Reference

1. Kojima, A., et al., *Organometal halide perovskites as visible-light sensitizers for photovoltaic cells.* Journal of the American Chemical Society, 2009. **131**(17): p. 6050-6051.
2. Sampath, H., et al., *Preparation and characterization of ZnIn2S4 thin film.* Emerging Materials Research, 2015. **4**(2): p. 286-289.
3. Butler, K.T., J.M. Frost, and A. Walsh, *Band alignment of the hybrid halide perovskites CH 3 NH 3 PbCl 3, CH 3 NH 3 PbBr 3 and CH 3 NH 3 PbI 3.* Materials Horizons, 2015. **2**(2): p. 228-231.
4. Walsh, A., *Principles of chemical bonding and band gap engineering in hybrid organic–inorganic halide perovskites.* The Journal of Physical Chemistry C, 2015. **119**(11): p. 5755-5760.
5. Yang, J., P. Zhang, and S.-H. Wei, *Band structure engineering of Cs2AgBiBr6 perovskite through order–disordered transition: a first-principle study.* The journal of physical chemistry letters, 2018. **9**(1): p. 31-35.
6. Fu, R., et al., *Pressure-induced structural transition and band gap evolution of double perovskite Cs 2 AgBiBr 6 nanocrystals.* Nanoscale, 2019. **11**(36): p. 17004-17009.
7. Schade, L., et al., *Structural and optical properties of Cs2AgBiBr6 double perovskite.* ACS Energy Letters, 2018. **4**(1): p. 299-305.
8. Volonakis, G., et al., *Cs2InAgCl6: a new lead-free halide double perovskite with direct band gap.* The journal of physical chemistry letters, 2017. **8**(4): p. 772-778.
9. Zhang, Z., et al., *Potential applications of halide double perovskite Cs2AgInX6 (X= Cl, Br) in flexible optoelectronics: unusual effects of uniaxial strains.* The journal of physical chemistry letters, 2019. **10**(5): p. 1120-1125.
10. Zhao, X.-G., et al., *Cu–In halide perovskite solar absorbers.* Journal of the American Chemical Society, 2017. **139**(19): p. 6718-6725.

Chapter I generality of perovskite materials for photovoltaic applications

Chapter I: generality of perovskite materials for photovoltaic applications

I.1 Introduction

In this chapter we will discuss solar cells, and mention those cells that depend on lead-containing perovskite materials in their composition. We will also mention some of the physical properties of these materials. We will also discuss the proposed perovskite materials to replace these materials that are harmful to human health.

I.2 Solar cells

During the last few decades, the energy crisis and increasing CO2 emissions have generated major environmental and political challenges. Due to the lack of coal, oil, and gas (fossil fuels) and increasing energy consumption, developing a green strategy capable of meeting human energy demand has become a critical challenge. Many energy sources have been substantially developed over the last few decades, including nuclear energy, wind energy, geothermal energy, and solar energy, among others[1].

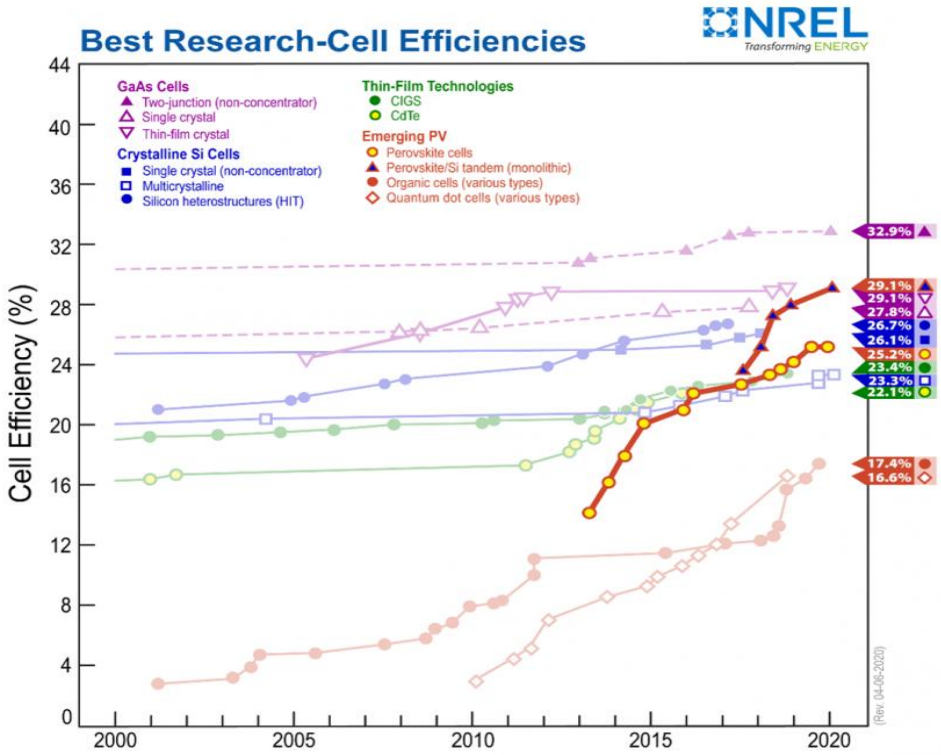

Fig I. 1: Conversion efficiencies of the best research solar cells in the world for various photovoltaic technologies. Efficiencies published by the National Renewable Energy Laboratory (NREL) [2].

Solar energy provides a number of distinct advantages over other energy sources, including low cost, low environmental impact, and inexhaustible high energy (120,000 TW/hours) of electromagnetic radiation to our planet[3]. When compared to alternative methods such as photochemical reactions and solar thermal energy, solar cells provide a cleaner, safer, and more efficient way to attain this aim. Furthermore, converting solar energy directly to electricity allows for more efficient energy transit and storage. In a nutshell, the fundamental goal of this technology is to find the most cost-effective approach to absorb solar energy.

Solar cell is a device that converts light into electricity by an photoelectric effect where it utilizes electrons that get excited from light energy, and move from valence band to the conduction band and creating an electron/hole pair in the absorber material , which is the same principle applies in semiconductor , At the heart of the solar cell is the semi-conductor absorbing layer (Fig.I.2). Semi-conductor materials are defined by a non-zero conduction-to-valence bandgap (Eg), typically of a few eV (above tens of eV the material can be considered as insulating). Their illumination promotes one conduction band electron to the valence band, creating an electron/hole pair in the absorber. Due to the energy difference between the carrier-selective layers, generated charges are separated and finally collected at the electrodes. The overall process creates an electrical current in the device and its efficiency is estimated by the produced to incident power ratio, *i. e.* the electricity to light ratio.

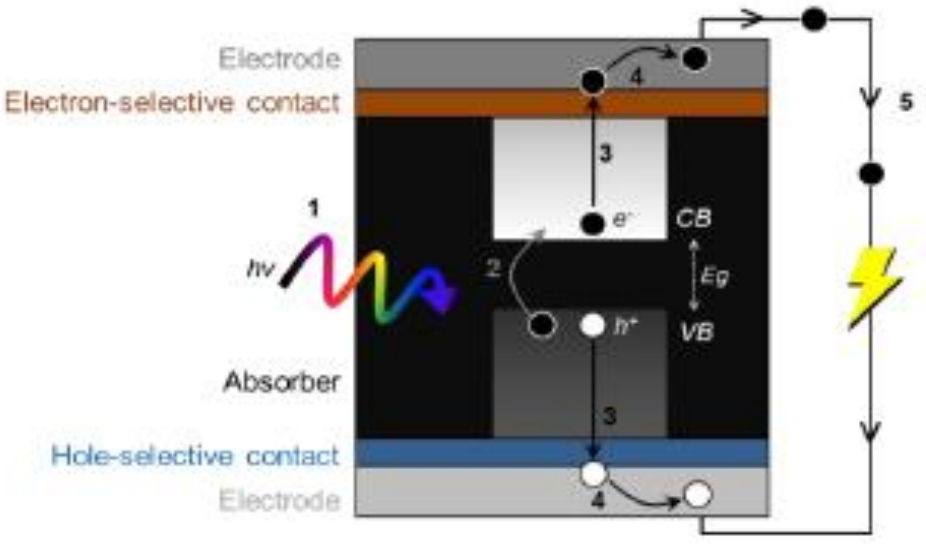

Fig. I.2. Photoconversion process steps: 1. Photon (hv) absorption; 2. electron/hole (e^-/h+) pair creation; 3. charges separation; 4. charges collection and 5. current generation (VB and CB: Valence and Conduction Bands and E_g the bandgap)[4].

Generally the classification of solar cells can be into three generations : The first generation of solar cells based on crystalline silicon, which is the most commercially used, but Silicon also requires high level of purity for it to have a high efficiency, which increases the manufacturing costs due to extra steps in dissolving impurities, or maintaining the silicon wafer purity, the second generation depends on materials e.g: CdTe (cadmium telluride) and CIGS(copper indium gallium selenide) this type has appeared as a result of high cost of the first generation (silicon material) , the second generation has some applications in the commercial field but this generation also has limited material reserves, especially tellurium and indium[5] some a problems like The low abundance of CdTe, third generation with different cells such as perovskite solar cell (PSCs) which has rapidly passed other third generation technologies such as CZTS and is starting to reach the levels of CdTe and silicon cells [6, 7].

In addition , Tandem solar cells, which utilize the two types, or more cells, and each one is optimum at absorbing a certain solar spectra, is also proven to be successful in harnessing the solar light energy and increasing the efficiency. However, as of now, this type is still cost-ineffective for household use.

I.2.1 Perovskite solar cells

PSCs cells form a new technology that can outperform silicon technology due to low cost and high efficientcy [8] .That has developed rapidly from 3.8% to of 22.7% which is comparable to multi-crystalline silicon cells and CIGS (copper indium gallium selenide) [6, 7].

In general, PSCs is made (show Fig.I.3**)** of transparent conducting oxide (electrode (-)), electron Transport layer (ETM) e.g., spiroMeOTAD (2,207,70-tetrakis(N,N-di-p-methoxyphenylamine)-9,90-spiro-bifluorene), perovskite solar absorber layer, hole transport layer (HTM)), e.g., phenyl-C61-butyric acid methyl ester (PCBM), and metal contact (electrode (+)),e.g., an indium tin oxide (ITO) or fluorine-doped tin oxide (FTO) electrode.

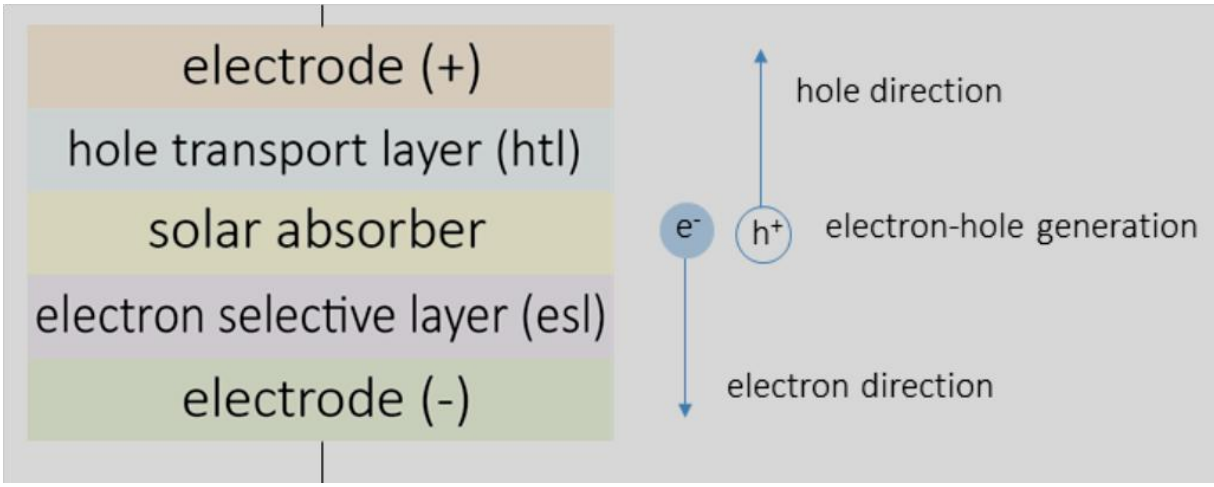

Fig. I. 3: composition of perovskite solar cell.

Perovskite material plays the role of a light absorber in the PSCs. These materials have good photovoltaic properties such as a direct bandgap, tunable bandgap,strong absorption in the visible spectrum ,high carrier mobilities,[9, 10].

I.3 Perovskite materials for solar cell

If we look at the emerging photovoltaics technologies for the past 25 years, a new photovoltaic material class, perovskite, has been gaining traction in the efficiency competition in recent years,as shown on Fig. I.4.

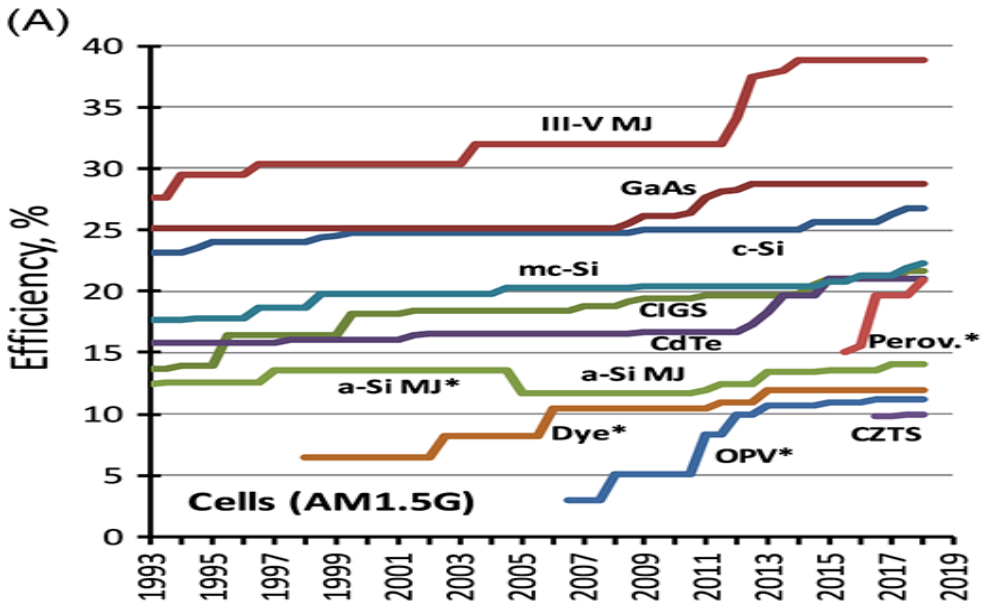

Fig. I.4. 25 year progress on various photovoltaics technologies, showing the highest certified efficiencies for ≥1 cm^2-area cells[11].

The organometal halide perovskites APbX3, in which A represents an alkylamine positive ion, such as CH_3NH^{3+}(MA) and NH_2CHNH^{2+}(FA) and X=I, Br, or Cl, have proven to be good materials for the preparation of efficient perovskite solar cells.[12, 13]wich have emerged as promising semiconductor materials owing to their excellent photovoltaic properties**.[14, 15]** However, the poor stability of these materials under ambient conditions hampers their commercial use [15]. Most of the stability studies are done in MAPI, which has 3D crystal structure, and it is really susceptible to oxygen, moisture , UV, NH3, thermal deposition condition, thermal deposition and compatibility with other layers in the device structure[16] This also applies to other 3D perovskite, such as formamidinium lead iodide (FAPI).

The inorganic perovskite halide CsPbI3 has also shown promise as a solar cell material in its own right, with pure iodide and doped iodide-bromide mixed halide perovskites achieving efficiencies of close to 10% but these materials have nonperovskite phase at room temperature which does not have the same ideal photovoltaic properties[17].

The use of lead in PSCs is a major source of concern because lead is highly toxic, and any encapsulation failures or leakages will have catastrophic consequences [18]. Lead is a well-known toxic heavy metal that builds up in living objects. It is carcinogenic, and children are more prone to it than adults due to a higher incidence of pica, as well as higher intestinal and retention rates [19, 20]. The European Union restricts the use of heavy and toxic materials for electronic devices, and in the future, more countries are bound to restrict the use of lead-based technology [21].

I.4 Lead free perovskite

Due to lead's high toxicity, researchers have attempted to look for lead-free alternatives of these perovskite materials for photovoltaics applications, by looking for Pb substitution coming from the same group,(group 14). Tin and germanium are among the ones considered, however both of them are very susceptible to oxidation [22] Tin-based perovskite, for instance,is promising in terms of its efficiencies, however, its instability and tendency to get oxidized from Sn^{+2} into Sn^{+4} is challenging.

Simple combinatorics of ionic charges in the $A^+B^{2+}X_3$ formula does not lend much hope that alternatives to the $APbX_3$ perovskites with comparable band gaps, carrier mobilities, and good moisture stability can be discovered. There are few if any suitable +2 cations with a $d^{10}s^2$ or $d^{10}s^0$ configuration that are both non-toxic and stable against oxidation. Fortunately, the situation improves if we expand the search from ternary $A^+B^{2+}X_3$ perovskites to

quaternary $A_2B^+B^{3+}X_6$ double perovskites. There are numerous combinations of +1 and +3 ions with suitable electron configurations that are quite stable when exposed to the air, such as Cu^+, Ag^+, Bi^{3+}, Sb^{3+}, and In^{3+}. Herein we document the initial investigations into the structural and optical properties of metal-halide double perovskites $Cs_2AgBiBr_6$,$Cs_2AgInCl_6$ and $Cs_2AgInBr_6$.

I.5 Crystal structure of perovskite materials

I.5.1 Crystallographic properties

Perovskites represent a large class of materials with the same crystal structure as calcium titanate (CaTiO3), called after a Russian mineralogist in 1839 [23]. in an overall manner the formula ABX_3 is used to describe this Type of structure, The unit cell comprises of a huge cation A, a little cation B and X is oxygen anions on Oxides case but it could be also Halide , Chalcogenide or Nitrogen However, we are mainly interested perovskites for solar cell and optoelectronic applications.

The perovskite crystal structure is comprised of two cation sites and one anion site. The structure is made up of corner sharing BX_6 octahedra arranged in a cage-like structure around a large central 12-coordinate A site cation. as shown on Fig.I.5 .

The B site is occupied by a second smaller cation and the X site is occupied usually by a halide (Cl^-,Br^-,I^-) or oxide anion. The A site in perovskite oxides is commonly occupied by Ca^{2+},Sr^{2+}, or Ba^+, while the B site is commonly occupied by a transition metal such as Ti^{4+} or Sn^{4+}. In the inorganic perovskite halides studied, the central A site cation is Cs^+. The B site in the perovskite halides is commonly occupied by Pb^{2+} or Sn^{2+} .The structure of an ideal perovskite can be described as cubic with space group Pm3m.

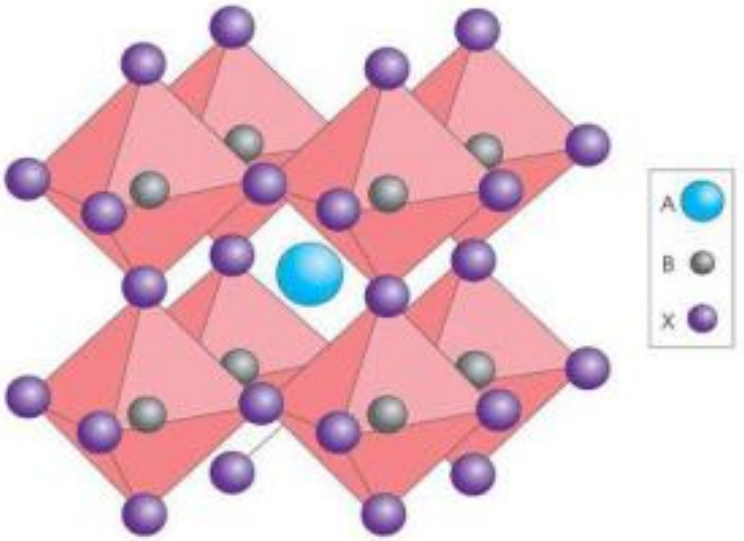

Fig.I.5 The ideal cubic perovskite structure the corner-sharing BX_6 octahedra (red) surrounding the central 12-coordinate A site (blue) [24].

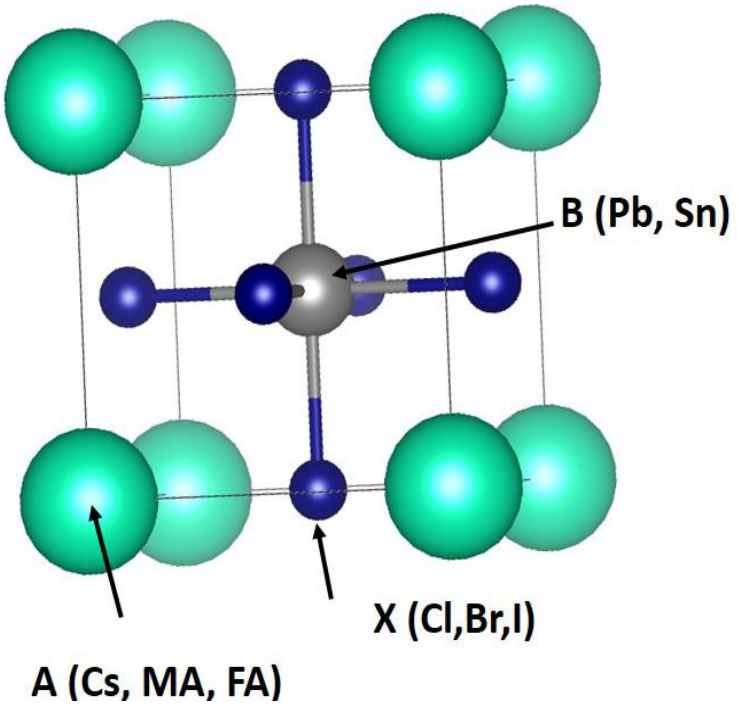

Fig.I.6**:** A halide perovskite crystal structure. Atom A is a monovalent cation, B is a divalent cation, and X is a halogen. Any crystal similar to this structure is called a perovskite crystal structure.

Fig.I.6 shows Atoms of element A are situated on the corner of a cubic cell, atoms of element B (grey) are in the center and atoms of element X (violet) are in the center of each face. The halide perovskite research community has also considered other perovskite-like structures, such as double perovskites, with $A_2BB"X_6$ structure. with A being a monovalent cation such Cs^+ or MA^+, B_I being a trivalent metal cation such Bi^{3+} or In^{3+}, B_{II} being a monovalent metal such Cu^+, Ag^+, or Na^+; and X being a halide such as Cl^-, Br^-, or I^- [25].

The cubic face-centered structure of the most studied halide double perovskites has been reported to belong to the space group. Fm-3m [26]. The structure is comparable to that of the ABX_3 perovskite, which is made up of a three-dimensional network of corner linked octahedra with Cs^+ ions in the cuboctahedron interstices. Unlike the hybrid halide perovskites where the perovskite structure is obtained by just B^{2+} centered octahedron [27], In a 3D framework known as rock salt ordering, the halide double perovskite structure is made up of alternating B_1 and B_2 centered octahedrons of B_1X_6 and B_2X_6. Figure I.7 shows the common ideal architectures of hybrid halide perovskites and halide double perovskites.

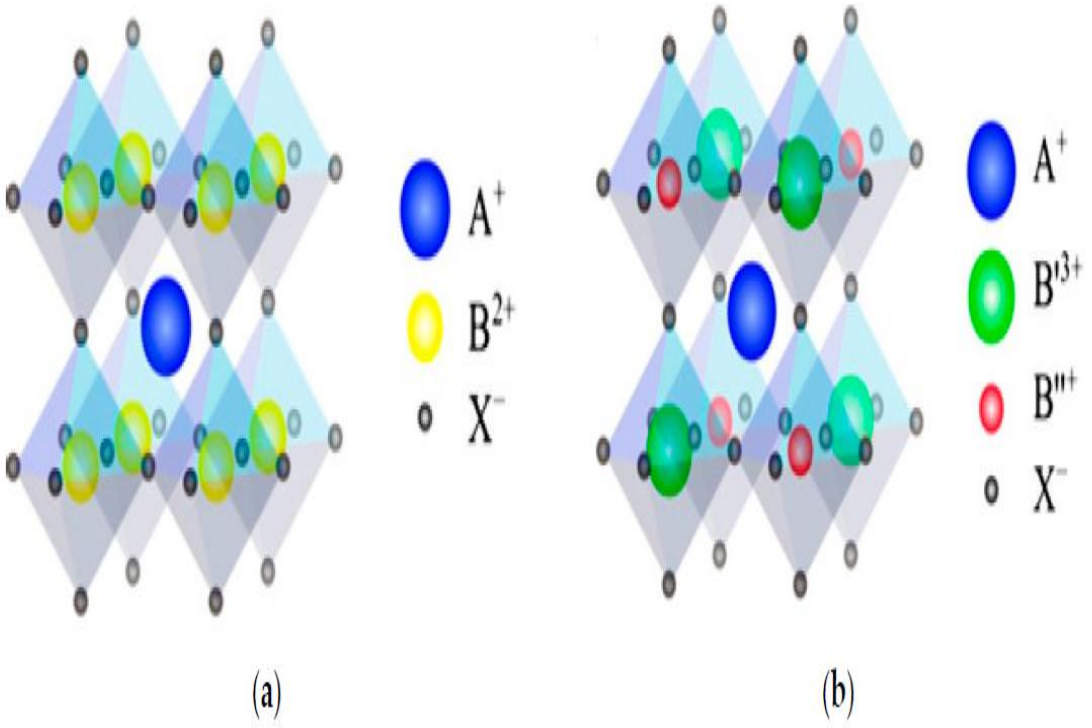

Fig. I.7: (a) Structure of ideal ABX_3 halide perovskites. (b) Structure of ideal $A_2B'B''X_6$ halide double perovskites [25].

I.5.1.1 Tolrance Factor

The formation of halide perovskites generally occurs with a Goldschmidt tolerance factor range of $0.81 < t < 1.0$ and an octahedral factor range of $0.44 < \mu < 0.9$[28] given by Equation (1):

$$t = \frac{(r_A + r_X)}{\sqrt{2}(r_B + r_X)} \qquad u = \frac{r_B}{r_X} \qquad \textbf{(I.1)}$$

Bartel at al present new tolerance factor (τ) which has the form[29] :

$$\tau = \frac{r_X}{r_B} - n_A\left(n_A - \frac{r_A / r_B}{\ln(r_A / r_B)}\right) \qquad \textbf{(I.2)}$$

where r_A, r_B, and r_X represent the ionic radius and n_A is the oxidation state of A, $r_A > r_B$ by definition, and $\tau < 4.18$ indicates perovskite [29] .

Since we have double perovskites, and therefore different radii for the $B_1$and B_2 sites, as a first

attempt we consider for r_B the average between the radii of B^{+1} and B^{+3} $r_B = \frac{(r_{B1}+r_{B2})}{2}$.

I.6 General concepts of optoelectronic properties:

I.6.1Notion of energy bands

The electrical behavior of semiconductors is generally modeled using the band theory which is a quantum model in solid state physics, determining the energies of electrons in a solid and allows to understand the notion of electrical conductivity, it is derived from the theory of molecular orbitals.In this model the possible energies for an electron in a solid form what are called allowed bands, separated by other bands called forbidden bands or band gap (Fig.I.8). At very low temperatures (T=0 K) the low energy bands are completely occupied ,they are called valence bands, on the other hand the bands of high energy are empty they are called conduction bands [30].

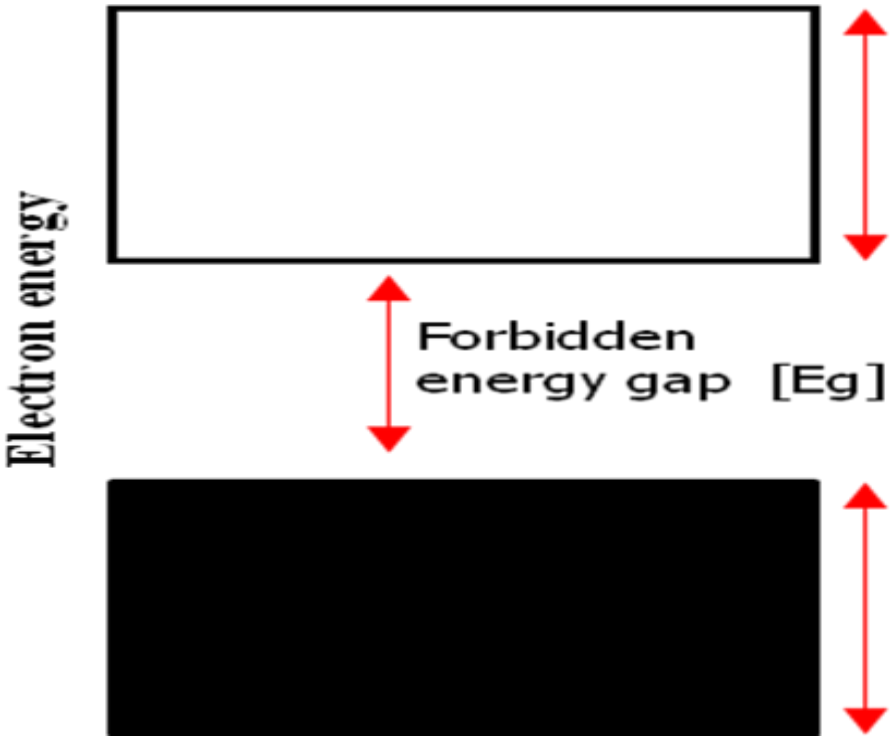

Fig.I.8 **:**energy bands of semiconductors.

I.6.2 Band structure

The band structure is the relation between the energy of the particle and its k vector: E(k). We represent the evolution of the energy of the electron by the curve E(k) by forcing the wave vector k to remain in a remarkable direction of the space of k (Fig.I.9) This diagram

allows to define the extremas of the conduction and valence bands. The band gap is by definition the difference in energy between the absolute minimum of the conduction band and the absolute maximum of the valence band. [30] It is a parameter that allows us to determine the optical and electronic properties of semiconductors and thus assess their field of application.

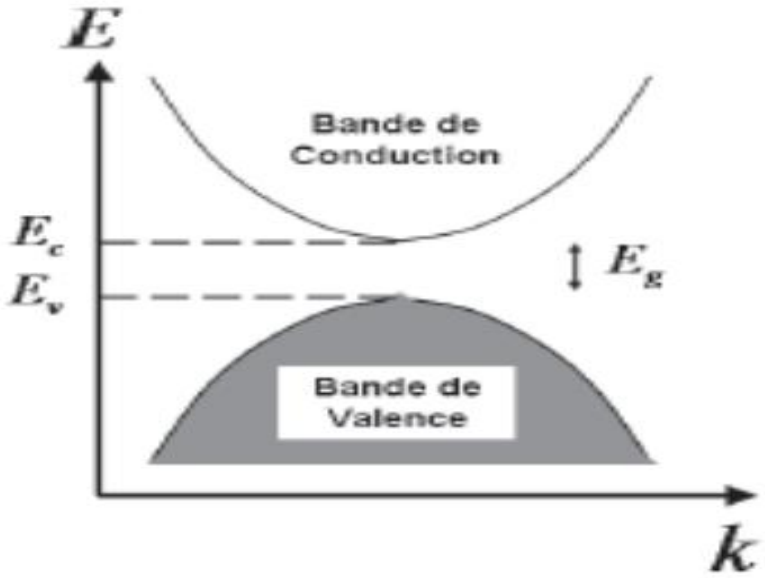

Fig. I.9: Simplified dispersion curves of the electrons in the valence band and the conduction band in the parabolic approximation [31].

In the band structure of a semiconductor, we distinguish two types of bands bands (Fig.I.10):

- The "direct" band gap: in this case, the top of the BV and the bottom of the BC are located at the same place of the Brillouin zone which allows optical transitions without any modification of the wave vector at k = 0.

- The "indirect" band gap: in this case, the band extrema are not symmetrical and the transitions are not symmetrical and the transitions are not made at constant k.

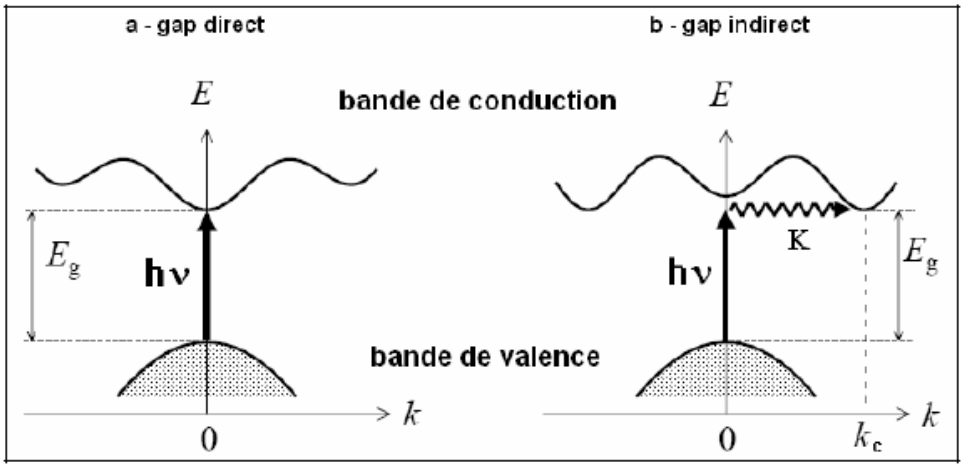

Fig.I.10**:** Energy band structure of the :a)- direct gap and b)- indirect gap [32].

I.6.3 Density of electronic states (DOS)

The total density of electronic states (DOS) is the number of states occupied by electrons with a given energy. The projection of this density on the spherical harmonics s , p , d and f gives the partial density of electronic states (PDOS). The partial density illustrates the levels of possible electronic transitions.

I.6.4 Band-to-band absorption and exciton concept

The optical properties are of great interest in knowing the ways in which A semiconductor can absorb a photon by transitioning an electron from the BV to the BC. as shown schematically in Fig.I.11. This transition can only take place when the energy hν of the incident photon is equal to or greater than the gap energy, Eg. A semiconductor is therefore perfectly transparent to photons with an energy lower than Eg. The passage of an electron from the BV to the BC is accompanied by the creation of a virtual particle of opposite charge, called hole. the majority of basic semiconductors of solar cells absorbs the visible spectrum adequately. Indeed, always uses semiconductors with a high absorption coefficient.

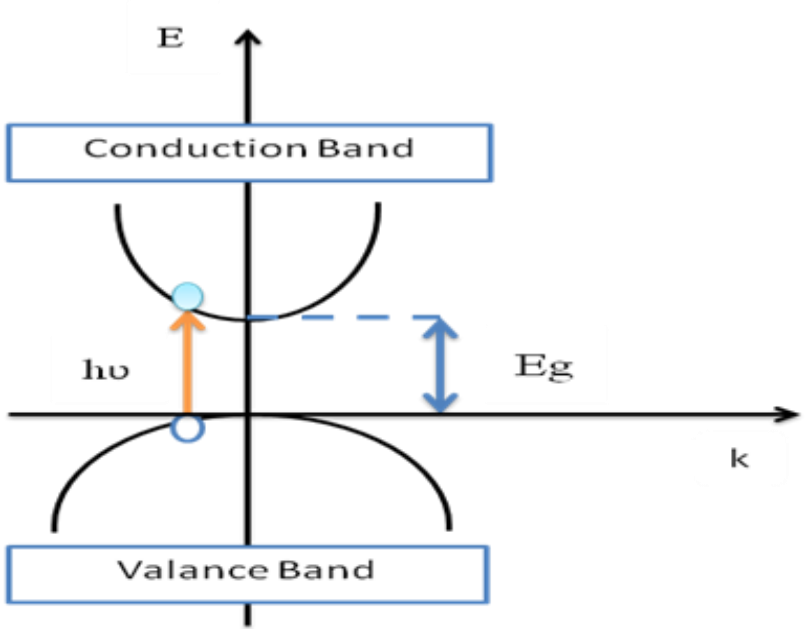

Fig.I.11. Schematic representation of the absorption of a photon in a semiconductor.

I.6.4 Exiton

When we speak about creation of an electron-hole pair by absorption of a photon, A quasi-particle called "exciton" can therefore be formed by the electrostatic coulombic attraction of the electron and the hole. The strength of this attraction depends essentially on the dielectric constant of the medium (the higher it is the weaker the attraction) and the effective masses of the electron and hole.

The exciton is characterized by its radius, defined as the average distance between the electron and the hole in coulombic interaction, and its binding energy, which represents the energy gain compared to the energy of the free particles, or the energy that must be provided to dissociate the exciton. Schematically, we distinguish the Wannier-Mott excitons, or delocalized excitons, of large radius (nm or ten nm, large compared to the lattice) and low binding energy (a few meV), found in inorganic semiconductors such as GaAs, CdTe, GaN.... and Frenkel excitons, or localized excitons, of small radius (of the order of inter-atomic distances, thus a few Angstroms) and of high binding energy (of the order of eV), found in organic materials These two kinds of excitons are schematized on Fig.I.12.

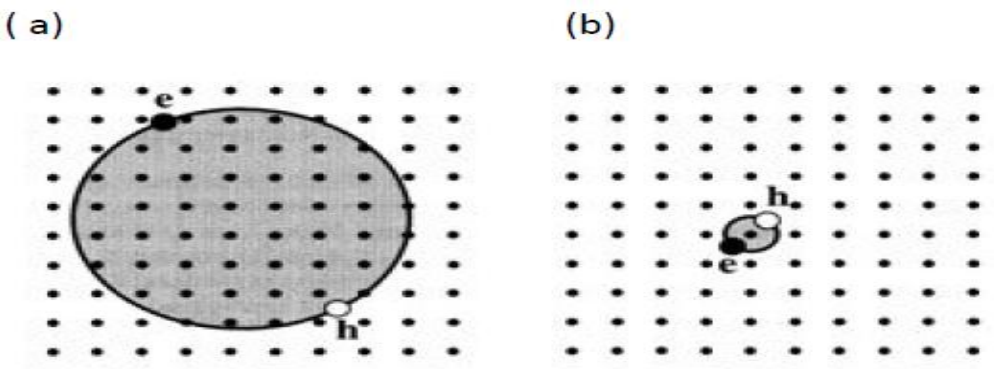

Fig.I.12 : Representative scheme of (a) free Wannier-Mott type excitons (b) bound Frenkel type excitons [31].

Wannier-Mott excitons are treated in the framework of a hydrogen model: indeed, it is a 2 body problem: a positively charged hole and a negatively charged electron bound by an attractive coulombic interaction. We can decompose the motion of this pair into a center of mass motion and a relative motion. The motion of the center of mass of the pair is free in the 3 directions of space, the total mass of the pair being $M = m_e + m_h$. The relative motion of the pair is described by the same equations that govern the relative motion of the electron and the nucleus in a hydrogen atom. We then find the binding energy and the excitonic radius of the fundamental level of the exciton:

$$E_X^{1s} = \frac{\mu}{m_0 \varepsilon_r} R_H$$
$$a_X^{1s} = \frac{m_0}{\mu} \varepsilon_r a_H \qquad \textbf{(I.3)}$$

where μ is the reduced effective mass: ε_r is the relative dielectric constant of the material, R_H is the Rydberg constant of the hydrogen atom: $R_H = 13.6$ eV and a_H is the Bohr radius.
In the context of photovoltaics: a low binding energy allows for easy separation of positive and negative charges within the solar cell.

I.6.5 effective mass of electrons and holes

An electron in the conduction band is characterized by a wave function which is a Bloch sum of anti-bonding orbitals. In corpuscular terms, it is a particle in a crystal potential. We represent this quasi-free particle of charge e^- and mass m_0 by a free quasiparticle of charge e^- and mass m_e which is called effective mass of the electron[32].

Let us consider a crystal subjected to a potential difference. A conduction electron of the crystal is subjected on the one hand to an internal force Fi resulting from the crystal field, and

on the other hand to an external force F_e resulting from the electric field applied to the crystal. The equation of the dynamics is written for this electron.

$$m_e = \frac{\hbar^2}{d^2E/dk^2} \quad m_0 \frac{dv}{dt} = F_i + F_e \qquad \textbf{(I.4)}$$

We write that the electron in the crystal responds to the solicitation of the external force F_e, as a quasi-particle of mass me in the vacuum :

$$m_e \frac{dv}{dt} = F \qquad \textbf{(I.5)}$$

The effective mass me contains the additional inertia given to the electron by the crystal potential, i.e. it contains the global effect of the crystal potential on the electron. In the crystal lattice the electronic eigenfunctions are Bloch waves.

The electron in a state k is represented by a wave packet centered on the pulsation ωk The speed of this electron is equal to the group speed of the wave packet.

$$v = \frac{dw}{dk} = \frac{1}{\hbar}\frac{dE}{dk} \qquad \textbf{(I.6)}$$

The acceleration of this electron is then given by :

$$\alpha = \frac{dv}{dt} = \frac{1}{\hbar}\frac{ddE}{dtdk} = \frac{1}{\hbar}\frac{ddE}{dkdt} \qquad \textbf{(I.7)}$$

In classical mechanics, if a particle is subjected to a force F during an interval dt, the variation of its kinetic energy is given by time interval dt, the variation of its kinetic energy is given by:

$$dE = Fvdt$$

$$\frac{dE}{dt} = Fv \qquad \textbf{(I.8)}$$

Carrying the expression (6) into the expression of the acceleration we obtain taking into account (8)

$$\alpha = \frac{1}{\hbar}\frac{d}{dk}(F.v) = F\frac{1}{\hbar^2}\frac{d^2E}{dk^2} \qquad \textbf{(I.9)}$$

which is written $F = m_e\alpha$ with:

$$m_e = \frac{\hbar^2}{d^2E/dk^2} \qquad \textbf{(I.10)}$$

This formula is the effective mass m* of an electron inside the crystal The effective mass of the electrons thus appears to be inversely proportional to the second derivative of the dispersion curve E(k) , i.e. to the curvature of the energy bands in the k Let us consider the holes of the valence band, their effective mass is defined as for the electrons, by the inverse of the second derivative of the dispersion curve (if the origin of the energies is taken at the bottom of the conduction band of a semiconductor), me depends on the value of the denominator d^2E/dk^2 , it is constant if E(k) is parabolic. The effective mass of a negative (m_e) or positive (m_h) particle depends on the nature of the semiconductor considered In the case of a direct gap semiconductor (GaAs for example) the effective mass is isotropic.

I.7 Optoelectronic Applications

I.7.1 Photodetectors

In 2017, Tang et al.[33] successfully prepared high-quality $Cs_2AgInCl_6$ single crystals with a low trap state density ((8.6±1.9)×108 cm^{-3}) by a hydrothermal method, which were further applied in UV detectors. The obtained results experimentally verifed the existence of parity-forbidden transition [31]. Shi et al.[34] used a one-step spin-coating method to prepare $Cs_2AgBiBr_6$ thin flms for photodetectors. The device exhibits high responsivity of 7.01 A W−1, ON–OFF ratio of 2.16×104 , specifc detectivity of 5.66×1011 Jones, EQE of 2146% and demonstrates remarkable stability against the water and oxygen degradation. Wang et al. [35] fabricated highly effecient and stable selfpowered UV and deep-blue detector based on $Cs_2AgBiBr_6$/ SnO2 heterojunction, The device is self-powered with two responsivity peaks at 350 and 435 nm, which is suitable for UV (320–400 nm) and deep-blue light detection, A high responsivity of 0.11 A W−1 at 350 nm and a quick response time of less than 3 ms are obtained, which are signifcantly higher than those of other semiconductor oxide heterojunction-based UV detectors.

I.7.2 X-ray Detectors

In 2017, Tang et al.[36] also prepared $Cs_2AgBiBr_6$ single crystals by controlling cooling rate in a solution for sensitive X-ray detectors with a low detection limit. The $Cs_2AgBiBr_6$ single crystals can directly convert X-rays into electrical signals due to the high average atomic number, high carrier drift length per unit electric feld, low ionization energy and high resistivity. Subsequently, Yu et al[37] used composite films of $Cs_2AgBiBr_6$ embedded in a polymer matrix for X-ray detectors. Recently, Tang et al. [38] have used lanthanide series as trivalent metals to obtain highly stable halide double perovskites ($Cs_2NaLnCl_6$, Ln=Tb or Eu) with high scintillation light yield.

Références

1. Armaroli, N. and V. Balzani, Die Zukunft der Energieversorgung–Herausforderungen und Chancen. Angewandte Chemie, 2007. **119**(1-2): p. 52-67.
2. Nazeeruddin, M.K., Perovskite Solar Cells Research in Switzerland. CHIMIA International Journal for Chemistry, 2017. **71**(11): p. 751-751.
3. Service, R.F., Is it time to shoot for the sun? Science, 2005. **309**(5734): p. 548-551.
4. Dindault, C., Development of coevaporated hybrid perovskite thin films for solar cells applications. 2019, Université Paris-Saclay (ComUE).
5. Feltrin, A. and A. Freundlich, Material considerations for terawatt level deployment of photovoltaics. Renewable energy, 2008. **33**(2): p. 180-185.
6. Kojima, A., et al., Organometal halide perovskites as visible-light sensitizers for photovoltaic cells. Journal of the American Chemical Society, 2009. **131**(17): p. 6050-6051.
7. Lee, M.M., et al., Efficient hybrid solar cells based on meso-superstructured organometal halide perovskites. Science, 2012. **338**(6107): p. 643-647.
8. Ameen, S., et al., Perovskite solar cells: influence of hole transporting materials on power conversion efficiency. ChemSusChem, 2016. **9**(1): p. 10-27.
9. Demic, S., et al., Recent Progresses in Perovskite Solar Cells, Nanostructured Solar Cells, Dr. Narottam Das (Ed.), InTech, DOI: 10.5772/65019. 2017.
10. Srivastava, R., Perovskite as light harvester: Prospects, efficiency, pitfalls and roadmap. Nanostructured Solar Cells; Das, N., Ed.; Intech: Rijeka, Croatia, 2017: p. 245-276.
11. Green, M.A., et al., Solar cell efficiency tables (version 51). Progress in photovoltaics: research and applications, 2018. **26**(1): p. 3-12.
12. Jeon, N.J., et al., Compositional engineering of perovskite materials for high-performance solar cells. Nature, 2015. **517**(7535): p. 476-480.
13. Yang, W.S., et al., Iodide management in formamidinium-lead-halide–based perovskite layers for efficient solar cells. Science, 2017. **356**(6345): p. 1376-1379.
14. Saparov, B. and D.B. Mitzi, Organic–inorganic perovskites: structural versatility for functional materials design. Chemical reviews, 2016. **116**(7): p. 4558-4596.
15. Mahapatra, A., et al., A review of aspects of additive engineering in perovskite solar cells. Journal of Materials Chemistry A, 2020. **8**(1): p. 27-54.
16. Slavney, A.H., et al., Chemical approaches to addressing the instability and toxicity of lead–halide perovskite absorbers. Inorganic chemistry, 2017. **56**(1): p. 46-55.
17. Niu, G., X. Guo, and L. Wang, Review of recent progress in chemical stability of perovskite solar cells. Journal of Materials Chemistry A, 2015. **3**(17): p. 8970-8980.
18. Asghar, M., et al., Device stability of perovskite solar cells–A review. Renewable and Sustainable Energy Reviews, 2017. **77**: p. 131-146.
19. Papanikolaou, N.C., et al., Lead toxicity update. A brief review. Medical science monitor, 2005. **11**(10): p. RA329-RA336.
20. Qiu, L., L.K. Ono, and Y. Qi, Advances and challenges to the commercialization of organic–inorganic halide perovskite solar cell technology. Materials today energy, 2018. **7**: p. 169-189.
21. Blanke, H.-J. and S. Mangiameli, The European union after Lisbon: Constitutional basis, economic order and external action. 2011: Springer Science & Business Media.
22. Ganose, A.M., C.N. Savory, and D.O. Scanlon, Beyond methylammonium lead iodide: prospects for the emergent field of ns 2 containing solar absorbers. Chemical Communications, 2017. **53**(1): p. 20-44.

23. Chen, F., Characterization and application of Pb-based organometal halide perovskite. 2015.
24. Green, M.A., A. Ho-Baillie, and H.J. Snaith, The emergence of perovskite solar cells. Nature photonics, 2014. **8**(7): p. 506-514.
25. Lozhkina, O., et al., Microstructural analysis and optical properties of the halide double perovskite Cs2BiAgBr6 single crystals. Chemical Physics Letters, 2018. **694**: p. 18-22.
26. Meyer, E., et al., Lead-free halide double perovskites: a review of the structural, optical, and stability properties as well as their viability to replace lead halide perovskites. Metals, 2018. **8**(9): p. 667.
27. Vasala, S. and M. Karppinen, A2B′ B ″O6 perovskites: a review. Progress in solid state chemistry, 2015. **43**(1-2): p. 1-36.
28. Manser, J.S., J.A. Christians, and P.V. Kamat, Intriguing optoelectronic properties of metal halide perovskites. Chemical reviews, 2016. **116**(21): p. 12956-13008.
29. Bartel, C.J., et al., New tolerance factor to predict the stability of perovskite oxides and halides. Science advances, 2019. **5**(2): p. eaav0693.
30. Mathieu, H. and H. Fanet, Physique des semiconducteurs et des composants électroniques-6ème édition: Cours et exercices corrigés. 2009: Dunod.
31. Diab, H., Propriétés optiques des pérovskites hybrides 3D pour le photovoltaique. 2017, Université Paris-Saclay.
32. Meryem, H. and D. Maroua, L'effet de la lumière solaire pour la dégradation photo-catalytique des colorants en solution aqueuse. 2020, université de jijel.
33. Luo, J., et al., Cs2AgInCl6 double perovskite single crystals: parity forbidden transitions and their application for sensitive and fast UV photodetectors. ACS Photonics, 2018. **5**(2): p. 398-405.
34. Meng, W., et al., Parity-forbidden transitions and their impact on the optical absorption properties of lead-free metal halide perovskites and double perovskites. The journal of physical chemistry letters, 2017. **8**(13): p. 2999-3007.
35. Lei, L.-Z., et al., High-efficiency and air-stable photodetectors based on lead-free double perovskite Cs 2 AgBiBr 6 thin films. Journal of Materials Chemistry C, 2018. **6**(30): p. 7982-7988.
36. Pan, W., et al., Cs 2 AgBiBr 6 single-crystal X-ray detectors with a low detection limit. Nature photonics, 2017. **11**(11): p. 726-732.
37. Li, H., et al., Lead-free halide double perovskite-polymer composites for flexible X-ray imaging. Journal of Materials Chemistry C, 2018. **6**(44): p. 11961-11967.
38. Hu, Q., et al., X-ray scintillation in lead-free double perovskite crystals. Science China Chemistry, 2018. **61**(12): p. 1581-1586.

Chapter II

The formalism of DFT

Chapter II: The formalism of DFT

II.1. Introduction :

The physical properties of a solid system, illustrated by the image of light electrons moving around heavy nuclei, depend on the behavior of its electronic structure. Quantum mechanics provides the ideal framework for this study.

A complete description of a quantum system with N electrons requires the calculation of the corresponding wave function: $\Psi(r_1,r_2, ...,r_N)$(the spin is omitted for simplicity). In principle this can be obtained from the time independent Schrödinger equation[1], but practically the potential undergone by each electron is imposed by the movement, not only of the nearest neighbors but also by all the other electrons of the real system.This would require the solution of a Schrödinger equation with$\sim 10^{23}$ simultaneous differential equations. In general, it is not possible to solve this equation and the use of approximations is necessary. In this chapter we present the theoretical foundations of the ab initio method used in this work. We start with the fundamental quantum approximations introduced to solve the Schrödinger equation for a complex system, namely the Born-Oppenheimer approximation [2] and the Hartree-Fock approximation [3, 4]. We then introduce the concept of density functional theory (DFT) which is based mainly on the theorems of Hohenberg and Kohn[5] and the approach of Kohn and Sham[6]. We explain how the exchange-correlation potential can be treated through different approximations (LDA, GGA, hybrid funional).

Then we describe the different possible choices for the basis of the wave functions and for the shape of the potential pseudopotential, more particularly the PlanWaves which is implemented in the CASTEP code that we have used.

II. 2. Solving the Schrödinger equation :

The general problem of a system of Ne electrons and N nuclei, can be posed in the form of an equation of motion of all particles present in the system. The calculation of the total energy of such an interacting system is obtained in the general case by solving the Schrödinger equation of stationary states[1].

$$H\left|\Psi\right\rangle = E\left|\Psi\right\rangle \qquad \text{(II.1)}$$

With H is the Hamiltonian operator, ψ_i s a multiparticle wave function describing the state of the system, and E is its total energy. Generally, the Hamiltonian operator is written:

$$H = (T_e + T_Z + V_e + V_Z + V_{eZ}) \qquad \text{(II.2)}$$

The total kinetic energy of the electrons :

$$T_e = \sum_{i=0}^{N_e} T_i = \sum_{i=0}^{N_e} \left(\frac{-\hbar^2 \Delta_i}{2m_e}\right) \qquad \text{(II. 3)}$$

With m_e : the mass of the electron.

The total kinetic energy of the nuclei

$$T_Z = \sum_{\alpha} T_{\alpha} = \sum_{\alpha=0}^{N_\alpha} \left(\frac{-\hbar^2 \Delta_\alpha}{2M_I}\right) \qquad \text{(II.4)}$$

With M_I the mass of the nucleus

The interaction energy of the electrons two by two: $\left|\vec{r_i} - \vec{r_j}\right|$

$$V_e = \frac{1}{2} \sum_{i,j \neq i} \frac{e^2}{\left|\vec{r_i} - \vec{r_j}\right|} = \frac{1}{2} \sum_{j \neq i} V_{ij} \qquad \text{(II.5)}$$

The interaction energy of the nuclei two by two:

$$V_Z = \frac{1}{2} \sum_{I \neq J}^{k} \frac{Z_I Z_J e^2}{\left|\vec{R_I} - \vec{R_J}\right|} = \frac{1}{2} \sum_{\alpha \neq \beta}^{k} V_{IJ} \qquad \text{(II.6)}$$

Z_I and Z_J are the atomic numbers of the nuclei I et J

The energy of interaction nuclei-electrons:

$$V_{ez} = -\sum_{i=1}^{N_e} \sum_{\alpha=1}^{N_\alpha} \frac{Z_\alpha e^2}{\left|\vec{r_i} - \vec{R_I}\right|} = \sum_{i=1}^{N_e} \sum_{\alpha=1}^{N_\alpha} V_{i\alpha} \qquad \text{(II.7)}$$

The Schrödinger equation can therefore be represented in the form:

$$(T_e + T_Z + V_e + V_Z + V_{eZ})\psi(\vec{r_1}, \vec{r_2}, \ldots\ldots \vec{R_1}, \vec{R_1}, \ldots) = E\psi(\vec{r_1}, \vec{r_2}, \ldots\ldots \vec{R_1}, \vec{R_1}, \ldots) \quad \text{(II.8)}$$

For most systems, the calculation of the energy of the fundamental state is not feasible. Indeed, except for isolated atoms, the calculations are often incommensurable because of the large number of particles to take into account and the complexity of the resulting interactions. For this reason, the solution of the Schrödinger equation in its general form cannot be completed without the introduction of a number of approximations. The first approximation introduced is the Born-Oppenheimer approximation (adiabatic approximation) which decouples the motion of electrons and nuclei [2].

Indeed, the mass of the protons being higher than that of the electrons (mp= 1836 me), one can consider that the electrons reorganize instantaneously for a given position of the nuclei. Thus, for the two terms of equation (II-2) depending only on the nuclei, T_Z can be

neglected and V_Z is constant, but can be made zero by a suitable choice of the origin. We can then solve the Schrödinger equation for this position of the nuclei.

In view of what T_Z = 0 and V_Z = 0, the wave function ψ_e can be defined as the wave function of electrons, and a new Hamiltonian, the electron Hamiltonian, is given by :

$$H_e = T_e + V_e + V_{eZ} \qquad \text{(II.9)}$$

The electronic Schrödinger equation can then be written as follows:

$$H_e \psi_e = E_e \psi_e \qquad \text{(II.10)}$$

$$\left[\sum_{i=0}^{N_e} \left(\frac{-\hbar^2 \Delta_i}{2m} \right) + \frac{1}{2} \sum_{j \neq i} \frac{e^2}{\left| \vec{r_i} - \vec{r_j} \right|} - \sum_{i=1}^{N_e} \sum_{\alpha=1}^{N_\alpha} \frac{Z_\alpha e^2}{\left| \vec{r_i} - \overrightarrow{R_\alpha^0} \right|} \right] \psi_e(\vec{r}, \overrightarrow{R_\alpha^0}) = E_e(R_\alpha^0) \psi_e(\vec{r}, \overrightarrow{R_\alpha^0}) \qquad \text{(II.11)}$$

In this equation the $\vec{R}^0{}_\alpha$ appears as a parameter

E_e : is the energy of electrons moving in the field created by fixed nuclei.

Following this approximation, the number of variables necessary to describe the function ψ is significantly reduced. In addition, all terms of the Hamiltonian involving the nuclei are eliminated. However, this approximation alone is not sufficient to solve the Schrödinger equation, because of the complexity of the electron-electron interactions. This is why it is very often coupled to the Hartree[3] and Hartree-Fock [3, 4] approximations.

II.3. Hartree's approach:

Based on the notion of independent electrons according to the Hartree approximation [3], the n-electron system becomes a set of independent electrons, each moving in the mean field created by the nuclei and the other electrons of the system. In this simplified model, each electron is treated individually, so that the wave function ψ with n electrons is reduced to a product of n wave functions ψ_i with a single electron:

$$\psi(\vec{r}) = \prod_{i=1}^{n} \psi_i(\vec{r_i}) \qquad \text{(II.12)}$$

$$H_e = \left[\sum_{i=1}^{N_e} \left(\frac{-\hbar^2 \Delta_i}{2m} \right) + \frac{1}{2} \sum_{i \neq j}^{N_e} V_{ij} + \sum_{i\alpha} V_{i\alpha} \right] = \sum_{i=1}^{N_e} \left(\frac{-\hbar^2 \Delta_i}{2m} \right) + \sum_{i=1}^{N_e} \Omega_i(\vec{r_i}) + \sum_{i=1}^{N_e} \left(\sum_{\alpha=1}^{N_\alpha} V_{i\alpha} \right) = \sum_{i=1}^{N_e} H_i \qquad \text{(II.13)}$$

$$\left(\frac{-\hbar^2 \Delta_i}{2m} + V_H(\vec{r_i}) + V_i(\vec{r_i}) \right) \psi_i(\vec{r_i}) = E \psi_i(\vec{r_i}) \qquad \text{(II.14)}$$

Where :H_i the Hamiltonian corresponding to the electron i :

$$H_i = (\frac{-\hbar^2 \Delta_i}{2m}) + V_H(\vec{r_i}) + V_i(\vec{r_i}) \quad \text{(II.15)}$$

$$V_i(\vec{r_i}) = -Ze^2 \sum_R \frac{1}{\left|\vec{r_i} - \vec{R_\alpha}\right|} \quad \text{(II.16)}$$

$$V_H(\vec{r_i}) = e\int d\vec{r'}\rho(\vec{r'}) \frac{1}{\left|\vec{r} - \vec{r'}\right|} \quad \text{(II.17)}$$

Of which $V_i\left(\vec{r}_i\right)$ represents the attractive interaction between the electron of coordinate $\vec{r}_i$ and coordinate nuclei $\vec{R_\alpha}$ and $V_H\left(\vec{r}_i\right)$ is the Hartree potential resulting from the repulsive coulombic interaction between an electron of coordinate $\vec{r}_i$ immersed in the mean field of the other electrons of coordinates $\vec{r}_j$.

Enfin on exprime le potentiel effectif comme la somme de ces deux contributions :

$$V_{eff}(\vec{r}) = V_H(\vec{r_i}) + V_i(\vec{r_i}) \quad \text{(II.18)}$$

II .4.Approximation de Hartree-Fock:

According to the Pauli exclusion principle, which follows from the Heisenberg principle, which states that any wave function for a given system must be antisymmetric with respect to the exchange of the coordinates of two particles, leading to the description of the Ne body system (electrons) by the equality :

$$\psi(\vec{r_1},\vec{r_2},\vec{r_3},.....\vec{r_i},.....\vec{r_j},.....\vec{r_{Ne}}) = -\psi(\vec{r_1},\vec{r_2},\vec{r_3},.....\vec{r_i},.....\vec{r_j},.....\vec{r_{Ne}}) \quad \text{(II.19)}$$

$\psi(\vec{r_1},\vec{r_2},\vec{r_3},.....\vec{r_i},.....\vec{r_j},.....\vec{r_{Ne}})$ is the wave function of the Ne-body system resulting from the linear combination of one-electron functions.

In the Hartry-Fock approximation [4]the antisymmetric wave function of a Ne-electron system is approximated by a Slater determinant, using a linear combination of the independent electron wave functions :

$$\psi(\vec{r_1}\vec{\sigma_1},\vec{r_2}\vec{\sigma_2},.....,\vec{r_{N_e}}\vec{\sigma_{N_e}}) = \frac{1}{\sqrt{N_e!}}\begin{pmatrix} \psi_1(\vec{r_1}\vec{\sigma_1}) & \psi_1(\vec{r_2}\vec{\sigma_2}).... & \psi_1(\vec{r_{N_e}}\vec{\sigma_{N_e}}) \\ \psi_2(\vec{r_1}\vec{\sigma_1}) & \psi_2(\vec{r_2}\vec{\sigma_2}).... & \psi_2(\vec{r_{N_e}}\vec{\sigma_{N_e}}) \\ \psi_{N_e}(\vec{r_1}\vec{\sigma_1}) & \psi_{N_e}(\vec{r_2}\vec{\sigma_2}).... & \psi_{N_e}(\vec{r_{N_e}}\vec{\sigma_{N_e}}) \end{pmatrix} \text{(II.20)}$$

Where $\frac{1}{\sqrt{N_e!}}$ is a normalization factor.

ψ represents the wave function of a system of Ne electrons in the spin-orbit representation. Interchanging two electrons is equivalent to interchanging two lines of the above determinant, which results in the change of the sign of ψ.

Where N_e is the number of electrons, σ_i represents spin and Ψ_i is the single-electron wave function that depends on the spatial coordinates $\vec{r_i}$ and of the electron spin σ_i This determinant includes single-electron wave functions as a linear combination of all Hartree functions in which permutations of $\vec{r_i}$ modulated by weights ±1 are made from so as to obey the Pauli exclusion rule according to the equation (II-21).

$$\frac{-\hbar^2}{2m}\Delta^2\psi_i(\vec{r}) + V_{ext}(\vec{r})\psi_i(\vec{r}) + V_H(\vec{r})\psi_i(\vec{r}) - \sum_j \int \frac{d\vec{r}}{|\vec{r}-\vec{r'}|}\psi_j^* = E_i\psi_i(\vec{r}) \text{ (II.21)}$$

$$(\frac{-1}{2}\Delta^2 + V_{ext}(\vec{r}) + V_H(\vec{r}) + V_x(\vec{r}))\psi_i(\vec{r}) = E_i\psi_i(\vec{r}) \text{ (II.22)}$$

The assumption of antisymmetry of the wave function ψ Thus, an exchange term appears between the electron located in $\vec{r}$ and the one located in $\vec{r'}$.

Thus, the difference between the Hartree and Hartree-Fock methods lies in the purely quantum exchange term describing the correlation between electrons with parallel spins. The basic correlation prevents two parallel spin electrons from being at the same point in space according to the Pauli exclusion principle.

The solution of the Schrödinger equation is done in a self-consistent way starting from a set of initial states; for this we proceed as follows:

For this we choose an initial basis of orbitals, generally atomic or plane wave orbitals, using this basis we calculate the interaction potentials V_H ($\vec{r}$) and Vx ($\vec{r}$) that we introduce in the mono electronic equations.

The resolution of the mono-electronic equations is then possible and provides a second mono-electronic function from which we re-evaluate the terms V_H ($\vec{r}$) and V_x($\vec{r}$).

We repeat the procedure until we obtain a function, mono electronic and stationary

eigenvalues. The total energy of the system of atoms is then calculated in order to minimize this total energy. The complexity added by taking into account the exchange is considerable. It makes Hartree-Fock type calculations difficult to carry out for systems beyond small sets of molecules.

The molecular orbitals of the Hartree-Fock method are optimized by evaluating, in each molecular orbital, the energy of an electron moving in the mean field generated by the other electrons, rather than including the instantaneous repulsion.

A wave function represented by a single Slater determinant will never be equal to the exact wave function. This means that the E_{HF} quantity is necessarily greater than the exact energy of the ground state.

The difference between the results obtained by the Hartree-Fock approximation and those obtained from the exact solution of the Schrödinger equation is called the correlation energy, defined by:

$$E_{corr} = E_{exacte} - E_{HF} \prec 0 \quad \text{(II.23)}$$

The correlation energy is a measure of the error introduced by the Hartry-Fock approximation and is mainly due to the quasi-instantaneous repulsion of the electrons which is not accounted for by the effective potential, V_{eff}. In a scheme of this type, one can consider that the electrons are often close to each other because the electrostatic interaction is only treated by averaged terms. The inter-electron repulsion term is therefore too large and the E_{HF} energy is larger than the exact E_{exact} energy.

II.5 Density functional theory :

The Hartree-Fock method and the methods derived from this formalism, are based on a multi-electron wave function. The main objective of the density functional theory is to replace the multi-electron wave function by the electron density as a basic quantity for the calculations. The Ne electrons dependent on 3n space coordinates are replaced by their density $\rho(r)$ which now depends on only 3 variables; it is therefore a quantity that is easier to handle both mathematically and conceptually.

The density functional theory (DFT) is a reformulation of the n-body quantum problem into a problem dealing only with the electron density. Today, DFT is one of the most widely used methods for quantum calculations of the electronic structure of solids, because the reduction of the problem that it brings makes it possible to calculate the fundamental state of a system with a large number of electrons. It is therefore a method of choice for the study of the physical properties of the ground state of solids. Before discussing the foundations of the

Density Functional Theory, it seems essential to define the central quantity of this theory: the electronic density (ρ) .

The electron density: electrons are indistinguishable particles. Indeed, an electron can not be located as an individual particle, but its probability of presence in a volume element can be estimated and corresponds to the electron density (ρ).The electrons must therefore be considered in their collective aspect (electron cloud) and the electron density allows us to know the regions of space where the electrons stay most often. The electron density ρ(r) is a positive function depending only on the 3 coordinates (x,y,z) of the space. This quantity cancels at infinity and is Ne (total number of electrons) when integrated over the whole space.

$$\int \rho(r)dr = N_e \quad \text{(II.24)}$$

$$\int \rho(r)dr = 0 \quad \text{(II.25)}$$

Electronic density ρ(r) represents therefore, by definition, the probability of finding an electron in a unit volume dr.

It was Thomas[7] and Fermi[8] who expressed energy in terms of density. But the DFT theory was established, formally, in 1964 by two theorems which were stated and proved by Hohenberg and Kohn in their fundamental article [5] .

II.5.1 Hohenberg-Kohn theorems:

For an electronic system with N_e electrons described by the Hamiltonian H_{el}, the external potential $V_{ext}(\vec{r})$ completely fixes the H_{el} Hamiltonian of this system. This means that if we know the number of electrons Ne of the system as well as the external potential, we can uniquely determine the Hamiltonian and thus access the energy and the wave function of the ground state.The external potential thus perfectly reflects the different characteristics of a compound.

The first theorem of Hohenberg and Kohn[5] consists in giving a theoretical justification to the idea that to a given electron density corresponds a unique external potential. The potential $V_{ext}(\vec{r})$, is indeed determined, to a constant, by the electronic density (ρ). Thus, the electron number Ne and the potential $V_{ext}(\vec{r})$ The total energy functional of any multi-particle system has a minimum that corresponds to the ground state and the density of ground state particles.

$$E(\rho_0) = Min.E(\rho) \quad \text{(II.26)}$$

According to the second Theorem of Hohenberg and Kohn [5], the true density of the ground

state is that which minimizes the energy $E[\rho]$, and all other properties are also a functional of this density. The ground state energy of an electronic system in an external potential is determined by the variational method.

$$\left.\frac{\delta E\left[\rho(\vec{r})\right]}{\delta\rho(\vec{r})}\right|_{\rho_0} = 0 \quad \text{(II.27)}$$

Consequently, the total energy E of a system of interacting electrons in an external potential is therefore a density functional $\rho(r)$, which we can rewrite by separating the parts that depend on the system (Ne, Vext) from those that do not:

$$E\left[\rho(\vec{r})\right] = F_{HK}\left[\rho(\vec{r})\right] + \int \rho(\vec{r}) V_{ext}(\vec{r}).d^3r \quad \text{(II.28)}$$

$$F_{HK}\left[\rho(\vec{r})\right] = E_{cin}\left[\rho(\vec{r})\right] + E_{el-el}\left[\rho(\vec{r})\right] \quad \text{(II.29)}$$

F_{HK} is the density functional for any multi-electron system. In fact, there is no explicit formula for the functional and in particular it is the kinetic energy functional of the electrons $E_{Kin}\left[\rho\left(\vec{r}\right)\right]$ et $E_{el-el}\left[\rho\left(\vec{r}\right)\right]$ of the electron-electron interaction potential which are unknown.

The two theorems of Hohenberg and Kohn thus offer a theoretical framework for solving the Schrödinger equation using the electron density as the main variable. The energy of a system of N interacting electrons is thus a density functional and the search for the ground state energy can be carried out iteratively. However, at this stage the DFT allows to reformulate the problem but not to solve it because of the ignorance of the form of the functional $F(\rho)$. It is therefore necessary to use approximations that correspond to the equations of Kohn and Sham [6] established with the objective of providing the necessary foundations to effectively exploit the theorems of Hohenberg and Kohn.

II.5.2.Kohn and Sham approach:

As we have seen previously, the F_{HK} functional includes two terms (E_{kin} and $E_{el\text{-}el}$) which are themselves density functions. However, their analytical expression for the system of N interacting electrons is unknown.Kohn and Sham [6] have considered this problem from another angle. In the same way that the exact expression of the classical potential energy is known (Hartree energy), they have introduced the notion de système fictif of non-interacting electrons of the same density $\rho(r)$,than the interacting electron system. Based on this reference system, it is then possible to give an exact expression to the kinetic energy of a system of N non-interacting electrons as a density functional $\rho(r)$,This correspondence between interacting

and non-interacting electron systems has, in fact, many consequences .

Passage from a description based on the wave function to Ne electrons (ψ) to N wave functions to one electron ϕ_i .Determination of the electronic density through the summation of on all occupied states instead of considering the integral of $|\psi|^2$.

According to this approach, the kinetic energy (T_{el}) and the potential energy ($E_{(el\text{-}el)}$) of the N interacting electrons are both split into two parts that we can call classical and non-classical. The classical kinetic energy (T_{ele}^{ind}) comes from the reference system of independent electrons and the classical coulombic energy (E_{el-el}^{cla}) is none other than the energy of Hartree. The rest (non-classical kinetic and potential energies) has been grouped into a quantity called exchange-correlation energy, Exc

One way to define this new functional is to say that it contains everything that is not known exactly.

$$E_{XC} = (T_{el} - T_{el}^{ind}) + (E_{ee} - E_{ee}^{ind}) \quad \text{(II.30)}$$

$$F[\rho] = \underbrace{T\left[\rho(\vec{r})\right]}_{1} + \underbrace{\frac{1}{2}.\frac{\iint \rho(\vec{r})\rho(\vec{r'})}{\left|\vec{r}-\vec{r'}\right|} d^3\vec{r}\,d^3\vec{r'}}_{2} + \underbrace{E_{xc}\left[\rho(\vec{r})\right]}_{3} \quad \text{(II.31)}$$

All the first two terms can be calculated exactly because they correspond to a term previously described for the kinetic energy part $T\left[\rho(\vec{r})\right]$ and that of Colombian repulsion (Hartree term).

The third term of the equality in (II-31) is the exchange energy correlation $E_{xc}\left[\rho(\vec{r})\right]$ appears as the difference between the true kinetic energy and that of a gas of electrons without interaction and that of Hartree, on the other hand, thus including all the multibody contributions.Thus, the functional of the total energy of the system becomes, after taking into account the term $E_{xc}\left[\rho(\vec{r})\right]$, equal to:

$$E\left[\rho(\vec{r})\right] = T_{cin}^{ind}\left[\rho(\vec{r})\right] + E_H\left[\rho(\vec{r})\right] + E_{ext}\left[\rho(\vec{r})\right] \quad \text{(II.32)}$$

either

$$E\left[\rho(\vec{r})\right] = \sum_{i=1}^{N}\left\langle \phi_i \left| \frac{-\Delta_i^2}{2} \right| \phi_i \right\rangle + \frac{1}{2}\iint \frac{\rho(\vec{r})\rho(\vec{r'})}{\left|\vec{r}-\vec{r'}\right|} d^3r\,d^3r' + \int V_{ex}\left[\rho(\vec{r})\right] d\vec{r} + E_{xc}\left[\rho(\vec{r})\right] \quad \text{(II.33)}$$

The choice of Kohn and Sham to refer to a fictitious system of N electrons without interaction implies the solution of N monoelectronic Schrödinger equations. This leads us to rewrite the problem in the form of three independent equations, the Kohn-Sham equations:
The first one gives the definition of the effective potential in which the electrons bathe

$$\rho(r) \rightarrow V_{eff}\left[\rho(r)\right] = V_{ext(r)} + \int \frac{\rho(r')}{|r-r'|} dr + V_{xc}\left[\rho(r)\right] \text{ (II.34)}$$

The second uses this effective potential in the N Schrödingermonoelectronic equations in order to obtain the ϕ_i

$$V_{eff}(r) \rightarrow \left[-\frac{1}{2}\Delta + V_{eff}\right]\phi_i(r) = \varepsilon_i \phi_i(r) \text{ (II.35)}$$

The third shows how to access the density from the N single-electron wave functions:

$$\phi_i(r) \rightarrow \rho(r) = \sum_{i=1}^{N} \left|\phi_{i(r)}\right|^2 \text{ (II.36)}$$

II.5.2.1-Solution of the Kohn-Sham equations :

The solution of the Schrödinger equation in the framework of the Kohn-Sham approximation is reduced to the solution of an equation of the following form:

$$\left|H_{ks}\phi_{i(r)}\right| = \left|E_i \phi_{i(r)}\right| \text{ (II.37)}$$

$$H_{ks} = -\frac{\hbar^2 \Delta_i^2}{2m} + \frac{e^2}{4\pi\varepsilon_0}\int \frac{\rho(\vec{r'})}{|\vec{r}-\vec{r'}|} dr' + V_{XC} + V_{ext} \text{ (II.38)}$$

H_{ks} Kohn-Sham Hamiltonian

The different methods of calculating the electronic structure based on DFT can be classified according to the representations used for the density, the potential and the Kohn-Sham orbitals. The latter are described by :

$$\phi_{i(r)}(\vec{r}) = \sum C_{ij}\phi_j(\vec{r}) \text{ (II.39)}$$

$\phi_j(\vec{r})$: are the basic functions

C_{ij} : development coefficients.

The resolution of the Kohm-Sham equation consists then in determining the coefficients C_p^m .

Ayant choisi une base et une valeur finie de P, l'équation (II-37) se transforme sous la forme

séculaire :

$$S_g = \left\langle \phi_i^b \middle| \phi_j^b \right\rangle \left[\phi_i^b \middle| \hat{H} \middle| \phi_j^b - \varepsilon \left\langle \phi_i^b \middle| \phi_j^b \right\rangle \right] \begin{bmatrix} C_1^m \\ \vdots \\ C_p^m \end{bmatrix} = \begin{bmatrix} 0 \\ \vdots \\ 0 \end{bmatrix} \text{ (II.40)}$$

In which appear the matrix elements of the single-particle Hamiltonian H and the elements of the covering matrix S, that is :

$$(H_g - \varepsilon_i S_g) C_p^i = 0 \quad \text{(II.41)}$$

$$H_g = \left\langle \phi_i^b \middle| \hat{H} \middle| \phi_i^b \right\rangle \text{(II.42)}$$

$$S_g = \left\langle \phi_i^b \middle| \phi_j^b \right\rangle \text{(II.43)}$$

For a solid, these equations must be solved for each point k in the irreducible Brillouin zone.The eigenfunction is approximated all the more accurately as the value of P is large, but the diagonalization time of the matrix is also higher.

The resolution of these equations is then done in an iterative way using a self-consistent iteration cycle illustrated by the flowchart of Figure (II.l).We start by injecting the initial charge density ρ_{in} , constructed from a superposition of atomic densities:

$$\rho_{in} = \rho_{cristal} = \sum_{at} \rho_{at} \text{ (II.44)}$$

Then the orbitals are occupied and a new density is determined as follows:

$$\rho_{out}(r) = \sum_{i=1}^{N} \left| \phi_{i(r)} \right|^2 \text{ (II.45)}$$

II.5.2.2. Self-consistency in the calculation:

To simplify the computations, we solve the Kohn-Scham equations for the symmetry points in the first draft area. These solutions will be obtained in an iterative way using a self-consistent cycle of iterations illustrated by the flowchart of Figure(I-1), we start with a test density ρ_in for the first iteration. Typically we use a superposition of the atomic densities then we calculate the Kohn - Sham equations, and solving the equations for the expansion coefficient to obtain the kohn-Sham orbitals, at this step, calculating the new density ρ out .if the density or the energy has changed a lot (convergence criterion), we go back to the first step, and mixing the two charge densities ρ_{in} et ρ_{out} as follows:

$$\rho_{in}^{i+1} = (1-\alpha)\rho_{in}^{i} + \alpha \rho_{out}^{i} \text{ (II.46)}$$

i: represents the ith iteration

α : a mix parameter represents the i^{th} iteration age.

Thus the iterative procedure can be continued until convergence is achieved.

This procedure can be represented by the following diagram:

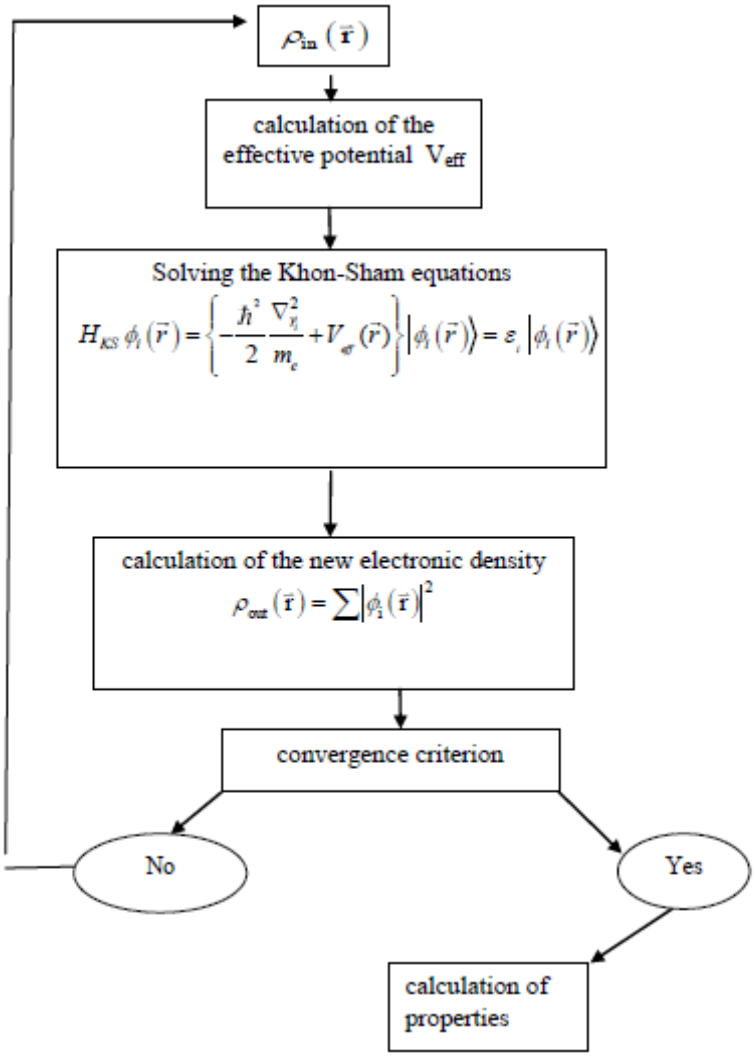

Figure.II.1 : Diagram of the self-consistent cycle in the framework of the density functional theory (DFT).

Different types of approximations of the exchange-correlation functional have been developed, among which we quote the following ones.

II.6.1. The local density approximation (LDA):

The simplest approximation of the exchange-correlation energy E_{xc} is the local density approximation (LDA). The idea of LDA is to substitute the electron density of a real system

by that of a homogeneous electron gas. In other words, it is assumed that in a small spatial region, the charge distribution of a non-homogeneous gas at a similar density has a charge distribution of a homogeneous gas.

Thus, the fundamental assumption contained in the LDA formalism is to assume that the exchange-correlation potential is a functional of the local electron density[6]and to consider that the contribution of $E_{xc}^{LDA}(\rho)$ the total energy of the system can be summed up from each portion of the non-uniform gas as if it were locally uniform

The exchange-correlation energy is written:

$$E_{XC}^{LDA}(\rho) = \int \rho(\vec{r})\varepsilon_{xc}\left[\rho(\vec{r})\right]d\upsilon \quad \text{(II.47)}$$

Where $\varepsilon_{xc}(\vec{r})$ is the exchange-correlation energy of a homogeneous electron gas of uniform density $\rho(\vec{r})$.

The term $\varepsilon_{xc}\left[\rho(\vec{r})\right]$ can be approximated by a sum of two contributions, one corresponding to the exchange term, the other to the correlation term :

$$\varepsilon_{xc}^{LDA}(\rho(\vec{r})) = \varepsilon_{x}^{LDA}(\rho(\vec{r})) + \varepsilon_{c}^{LDA}(\rho(\vec{r})) \quad \text{(II.48)}$$

II.6.2. The generalized gradient approximation (GGA) :

In the generalized gradient approximation (GGA), the gradient of the density is introduced to account for the non-homogeneity of the real electron density. The GGA (Generalised Gradient Approximation) allows to introduce a combination of local terms and gradient dependent terms. Such functionals have the general form given by the equation:

$$E_{xc}^{GGA}\left[\rho(r)\right] = \int dr f_{xc}^{GGA}\left|\rho(\vec{r}), \vec{\nabla}\rho(r)\right| \quad \text{(II.49)}$$

Where f_{xc}^{GGA} depends in particular on the GGA used. Several expressions of exchange and correlation energies have been proposed. In principle, it is possible to combine them at will, but in practice, only a few combinations are used. In particular, the correlation functional of Lee, Yang and Par (LYP)[7], the exchange functional of Becke (B88)[8] and the exchange-correlation functional proposed by Perdew and Wang (PW91)[9] as well as the functional proposed by Perdew-Burke-Ernzerhof (PBE)[10], the one used in the present thesis, are used. The GGA approximation has been proven in many cases and is known to give better results than the LDA, especially for magnetic systems. Systems with strong variations of electron density are thus described more correctly.

DFT has a number of flaws that need to be addressed. DFT's failure to estimate band gap values for insulators and semiconductors is one of them. DFT appears to be underestimating the band gap by up to 50%[10, 11].

There are several methods for correcting underestimate of the electronic band gap, including LDA+U, hybrid functional, and GW approximation.

II.6.3.The local density approximation (LDA+U)

LDA+U formalism uses the Hubbard U correction to move the LDA d/f orbitals and, in some cases, the delocalized s and p electrons. Anisimov et al.[9] proposed a smi-local DFT with a Hubbard model correction that accounts for the localized electrons' on-site repulsion, while the rest is still described by normal DFT.

The Hubbard (U value) is added to the energy to describe the interactions between the electrons in the d-orbitals:

$$E = E_{LDA} - U\frac{N(N-1)}{2} + \frac{1}{2}\sum_{i\neq j} n_i n_j \quad \text{(II.50)}$$

where E_{LDA} is the normal LDA term for delocalized s and p orbitals, UN(N- 1)/2 is the Coulomb energy of d-d electrons, which is a function of the total number of d-electrons, N, and the third component is the additional Hubbard term for orbital occupancies ni. The orbitals' potential, which describes the change in charge density, is given by

$$V_i(r) = V_{LDR}(r) - U(\frac{1}{2} - n_i) \text{(II.51)}$$

II.6.4. Hybrid functionals:

The B3LYP hybrid density functional [7, 10] was created to better the description of small molecule ground state energetics. It has now been shown to be much more trustworthy than the local density approximation (LDA) and generalized gradient approximation (GGA) functionals for computing atomization enthalpies, geometries, and vibrational frequencies [11, 12]. Because of the significant Coulomb resistance between the two 3d electrons on the transition metal ions, some specific features are not adequately represented in LDA and GGA calculations on solids, particularly transition metal oxides, which are prototypes of Mott insulators [13] .Due to the lack of self-interaction, the simple Hartree-Fock (HF) approximation is able to forecast the right ground states for strongly correlated insulators, although the energy gaps and magnetic moments are always overstated due to poor treatment of correlations. In the B3LYP hybrid functional scheme, the nonlocal Hartree-Fock (HF) approach is mixed into the energy functional of the GGA. Here, the Perdew-Wang[14] gradient-corrected correlation energy, which was used in the original work of Becke [10], is

replaced by Lee-Yang-Parr correlation energy [7]. The exchange-correlation energy functional can be written as:

$$E_{xc} = (1-A)(E_x^{LDA} + BE_x^{Becke}) + AE_x^{HF} + (1-C)E_c^{VWN} + CE_c^{LYP} \quad \text{(II.52)}$$

in which the local density functional of Vosko, Wilk, and Nusair is used for LDA Ex and Ec VWN[15] , E_x^{HF} is the exact nonlocal HF exchange energy. Becke Ex and LYP Ec are the Becke's and Lee-Yang-Parr's gradient corrections for the local exchange and correlation energies, respectively. The weight coefficients for the gradient-correlated correlation energy, local exchange energy, and the exact HF exchange terms were determined by a linear least-square fitting of the thermochemical properties of some atoms and molecules to the experiments. 20 % of the exact HF exchange energy in the exchange-correlation energy gives theoretical results in good agreement with experiments. The optimum values for the parameters A (Fock exchange percentage), B (exchange weight of the non-local part of exchange), and C (weight of the non-local correlation) are 0.20, 0.9, and 0.81, respectively.

II.7. Method of calculation:

II.7.1. The Pseudopotential (PP) method

The atoms which compose a crystal or a molecule are surrounded by several electronic layers. The electrons in the layers closest to the nucleus are very little influenced by the external environment. Conversely, the electrons of the outer layers are very sensitive. Thus, to simulate the behavior of an atom, it is sufficient to simulate the behavior of the external electrons by considering that the electrons of the internal layers are not influenced by the environment.

This is the idea of pseudopotentials[16, 17] We speak then of "valence" electrons for the electrons of the external layers which will be explicitly simulated in the calculation, and of "core" electrons for the electrons frozen in the pseudopotential. These core electrons are not affected by the environment, but influence it. They have two main effects: - to screen the charge of the nucleus: far from the nucleus, in the upper layers, the apparent charge of the nucleus is the sum of the charge of protons and core electrons. - to cause strong oscillations on the wave functions of the electrons of the upper layers: the electronic wave functions must be orthogonal between them to satisfy the principle of exclusion of Pauli. The more the electrons are in higher layers, the more the number of nodes of their wave functions will be large. The pseudopotentials must therefore mimic the effect of the core electrons (ecreted charge, eigenstate energies, scattering properties, ...) while having the softest possible effective potential, as seen on figure (II-2). Moreover, beyond a cut-off radius rc defined

during the creation of the pseudopotential, the quantities "all electrons" and "pseudo" must be identical. Thanks to the use of pseudopotentials the calculation will be faster because :

- there are less electrons to treat, the calculation is thus less heavy.
- there are less degrees of freedom (the core electrons being "frozen"), so the convergence algorithm is more efficient, and convergence is faster.

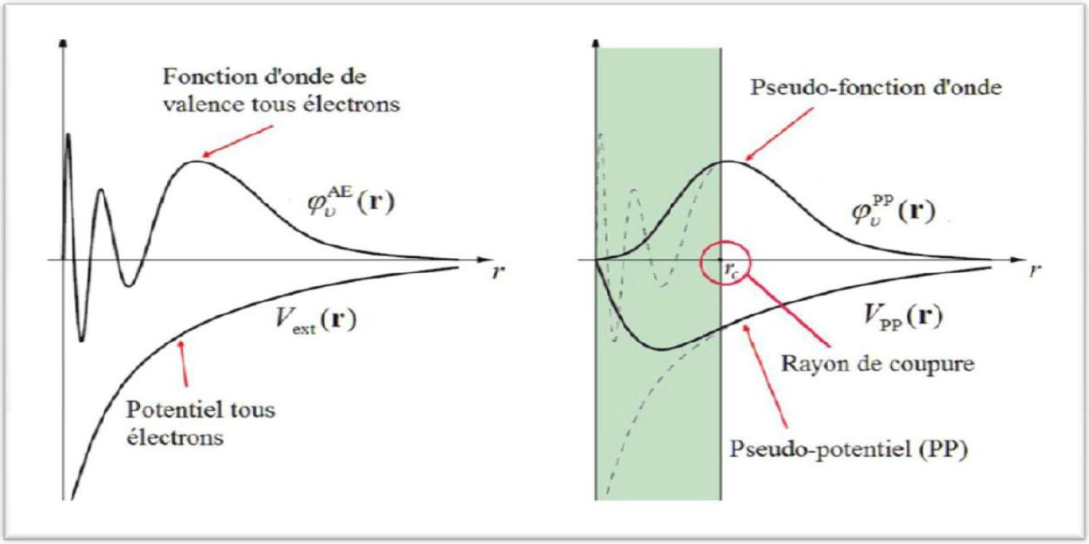

Fig. II.2.Schematic representation of the construction of the pseudo wave function and the pseudo potential [18].

There are four main types of pseudopotentials, each of which has its advantages and disadvantages:

- conserved norm pseudopoentials introduced by hamann et al [19].
- the ultra-soft pseudopoentials introduced by Vanderbilt [20].
- dual-space Gaussian pseudopoentials introduced by Geodecker et al[21] .
- the projected pseudopoentials PAW , acronym of the English <Projector augmented-wave>, which do not conserve the norm [22].

We chose to use Normconserving pseudopotentials for their conceptual simplicity of use and numerical implementation in the Castep computational code. In the following section, we will focus on this type of pseudopotential.

II.7.2. Plan waves method (PW)

Plane wave bases are intensively used in electronic structure calculations since they offer the possibility to improve the convergence on structure calculations since they offer the possibility to improve the convergence on the calculations by increasing their dimensions. Thus, the plane wave basis is completely independent of atomic positions, and it is

particularly well adopted for periodic systems. Indeed, one of the main problems of numerical computation is that of the dimension of the studied systems. In most physical problems, the systems studied have one or more studied have one or more dimensions which can be considered as infinite (wire, surface, solid). The number of electrons in the system is also infinite, a problem numerically intractable. We must then return to periodic systems and thus Bloch's theorem, which is fundamental for solid state physics, to overcome this Problem.

II.7.2. 1.Symmetries in a crystal and Brillouin zone

Cyclic Born-Von Karman conditions (translational symmetry superconditions) preserve the translational symmetry of a finite perfect crystal, lead to the quantization of the *k*-vectors of the reciprocal space, and introduce the notion of density of states. These periodic conditions remove edge effects and the modeled crystals become infinite. The symmetry properties of the crystal are then used for the solution of the single-electron equation, and all properties of the crystal then possess the same symmetry as the space group. This implies that the Hamiltonian is operator invariant for any symmetry operation of the space group and it then becomes possible to simplify the search for the eigenelements of the Schrödinger equation. The invariance of the properties of the crystal in direct space for any translation of the direct lattice leads to the invariance of the properties of the crystal in the reciprocal space. Thus for any translation $\vec{G}$ of the reciprocal space, the single-electron energy states $E_n(\vec{K})$ functions of the vectors of the reciprocal space, can be written:

$$E_n(\vec{K}) = E_n(\vec{K} + \vec{G}) \quad \text{(II.53)}$$

where n is the band index and *k* belongs to the first Brillouin zone defined as the smallest portion of the reciprocal space centered on one of the points of the reciprocal lattice, allowing, by translations $\vec{G}$, to generate all points of the reciprocal space. It then becomes unnecessary to calculate the $E_n(\vec{K})$ energy states at any point in the reciprocal space, but only in the first Brillouin zone and better yet in the first Brillouin zone reduced by the use of the point symmetries of the crystal.

II.7.2.2 Bloch's theorem and plane wave basis

Any periodic function can be decomposed into a complete basis of Fourier coefficients C_n. Bloch's theorem allows us to write the wave function in the form:

$$\psi_{nk}(r) = u_{nk} e^{ikr} \text{ (II.54)}$$

where $u_{nk}(r$) is a periodic function possessing lattice periodicity, n is the band index The

kinetic energy term is diagonal and the potentials are expressed in terms of their Fourier coefficients and are the non-diagonal terms of the Hamiltonian matrix. However, there is no method to determine the values propres. By organizing the Hamiltonian matrix of sorte If the diagonal terms are increasing and the non-diagonal terms decreasing, the Hamiltonian matrix is said to be "dominant diagonal", and beyond a certain value, it becomes possible to approximate the potentials to zero. The infinite matrix then becomes a finite matrix and the search for the first electronic energy bands then consists of the determination of the eigenvalues. The expansion of $\psi_{n,\,k}$ is then truncated and the infinite sums over all k vectors become finite sums and k is any vector in the first Brillouin zone.

II.8. CASTEP calculation code

All the calculations presented in the manuscript have been performed using the numerical modeling code called CASTEP (Cambridge Serial Total Energy Package) originally developed in 1988 by Payne et al [23, 24]. It is an ab initio calculation code and is part of a set of numerical simulation software called Material Studio marketed by Accelrys. CASTEP uses the DFT for the solution of the Schrödinger equation and employs periodic conditions, supercells, integration over the Brillouin zone, a plane wave basis and pseudopotentials to calculate the total energy of a given system. The electron wave functions are developed in a plane wave basis defined by the use of periodic boundary conditions and Bloch "s theorem. The electron-ion potential is described by means of ab initio pseudopotentials with the two formulations; norm-conserving pseudopotentials and ultra-soft pseudopotentials. Direct energy minimization procedures are used to obtain the electronic wave functions and the corresponding charge density. Only the Kohn-Sham orbitals whose G vector belongs to the irreducible part of the Brillouin zone are calculated, because the electron density can be constructed only from these states, with a symmetrization step that uses the space group matrices. A symmetrization step is also necessary for the forces and the stress. Consequently, the electron density is explicitly symmetrized. The use of symmetrization allows a significant reduction of the computational time, especially for small meshes containing many k-points because CASTEP is efficiently parallelized according to the k-points. As mentioned earlier, CASTEP uses the Monkhorst-Pack method for Brillouin zone sampling [25]. This method generates a uniform grid along the three axes of the reciprocal space. The symmetry of the system is used to reduce the number of k-points of the primitive cell. The forces on the atoms, the stress tensor and consequently the atomic displacements and the variations of the crystal lattice parameters are always symmetrized.

II.8.1. Definition of some parameter used in the calculation

II. 8.1.1. The cut-off energy

Represents a stopping criterion corresponding to the minimization of the error committed in the kinetic energy. The plane wave set is bounded by a sphere in the reciprocal space represented in terms of the cutoff energy, E_{cut}

such as:

$$\frac{\hbar^2}{2m}\left|\vec{K}+\vec{G}\right|^2 \prec E_{cut} \quad \text{(II.55)}$$

II.8.1.2. The grids of k points

The total energy of the system is not simply equal to the sum of the energies of the fictitious particles, but it is obtained by equation (II-16) and thus just like the electronic density via integrals in the Brillouin zone (BZ). Theoretically, it is necessary to calculate the eigenvalues of the Hamiltonian at an infinite number of k points in order to determine the total energy of the system. The symmetries already allow to simplify the problem. Indeed, it is possible to limit the problem to the irreducible Brillouin zone (IBZ), because the symmetry operations allow to regenerate the complete BZ, but the different points considered are always infinitely close to each other. A method proposed by Monkhorst and Pack [26]allows to approximate the integral by a sum of terms computed on a finite three-dimensional grid of k points. The basic idea is that the wave functions do not vary very rapidly in the neighborhood of a k-point, so that it is possible to condense the information over an entire region of the BZ to a single point. In this way, it will be possible to reduce the integrals to discrete sums, so that the determination of the eigenvalues has to be performed in a limited number of points[15].

II.9. Conclusion

In this chapter we have presented the methodology that we will use throughout this work. of this work. It is a method of calculation of electronic structure centered on the formalism of the formalism of the theory of the density functional, we also showed the bass of the potential in combination with plane waves (PP-PW) on which was built the DFT theory.

The DFT requires a number of approximations to make it practical in atomistic simulations Some of them are not very controllable during the calculations like the mesh of the first

Brillouin zone or the size of the wave base. The implementation is done with the help of the CASTEP calculation code.

Références

1. Ashcroft, N.W. and N.D. Mermin, *Solid state physics*. 1976, holt, rinehart and winston, new york London.
2. Born, M. and R. Oppenheimer, *Zur quantentheorie der molekeln.* Annalen der physik, 1927. **389**(20): p. 457-484.
3. Hartree, D.R. *The wave mechanics of an atom with a non-coulomb central field. Part II. Some results and discussion*. in *Mathematical Proceedings of the Cambridge Philosophical Society*. 1928. Cambridge University Press.
4. Fock, V., *Näherungsmethode zur Lösung des quantenmechanischen Mehrkörperproblems.* Zeitschrift für Physik, 1930. **61**(1-2): p. 126-148.
5. Hohenberg, P. and W. Kohn, *Density functional theory (DFT).* Phys. Rev, 1964. **136**: p. B864.
6. Kohn, W. and L.J. Sham, *Self-consistent equations including exchange and correlation effects.* Physical review, 1965. **140**(4A): p. A1133.
7. Lee, C., W. Yang, and R.G. Parr, *Development of the Colle-Salvetti correlation-energy formula into a functional of the electron density.* Physical review B, 1988. **37**(2): p. 785.
8. Becke, A.D., *Density-functional exchange-energy approximation with correct asymptotic behavior.* Physical review A, 1988. **38**(6): p. 3098.
9. Anisimov, V.I., J. Zaanen, and O.K. Andersen, *Band theory and Mott insulators: Hubbard U instead of Stoner I.* Physical Review B, 1991. **44**(3): p. 943.
10. Becke, A.D., *Density-functional thermochemistry. I. The effect of the exchange-only gradient correction.* The Journal of chemical physics, 1992. **96**(3): p. 2155-2160.
11. Curtiss, L.A., et al., *Assessment of Gaussian-2 and density functional theories for the computation of enthalpies of formation.* The Journal of Chemical Physics, 1997. **106**(3): p. 1063-1079.
12. Curtiss, L., *Raghavachari, k.; Redfern, PC; Pople, JA.* Chem. Phys. Lett, 1997. **270**: p. 419.
13. Mott, N.F., *Metal-insulator transitions.* 1974.
14. Perdew, J.P., P. Ziesche, and H. Eschrig, *Electronic structure of solids' 91*. 1991, Akademie Verlag, Berlin.
15. Vosko, S.H., L. Wilk, and M. Nusair, *Accurate spin-dependent electron liquid correlation energies for local spin density calculations: a critical analysis.* Canadian Journal of physics, 1980. **58**(8): p. 1200-1211.
16. Hellmann, H., *A new approximation method in the problem of many electrons.* The Journal of Chemical Physics, 1935. **3**(1): p. 61-61.
17. Yin, M. and M.L. Cohen, *Theory of ab initio pseudopotential calculations.* Physical review B, 1982. **25**(12): p. 7403.
18. Hamann, D., M. Schlüter, and C. Chiang, *Norm-conserving pseudopotentials.* Physical Review Letters, 1979. **43**(20): p. 1494.
19. Blöchl, P.E., *Projector augmented-wave method.* Physical review B, 1994. **50**(24): p. 17953.
20. Vanderbilt, D., *Soft self-consistent pseudopotentials in a generalized eigenvalue formalism.* Physical review B, 1990. **41**(11): p. 7892.
21. Troullier, N. and J.L. Martins, *Efficient pseudopotentials for plane-wave calculations.* Physical review B, 1991. **43**(3): p. 1993.
22. Anderson, E., et al., *LAPACK users' guide*. 1999: SIAM.
23. Stewart, J.C., et al., *IJ Probert Matt, K. Refson and C. Payne Mike.* Cryst. Mater, 2005. **220**: p. 567.

24. Payne, M.C., et al., *Iterative minimization techniques for ab initio total-energy calculations: molecular dynamics and conjugate gradients.* Reviews of modern physics, 1992. **64**(4): p. 1045.
25. Monkhorst, H.J. and J.D. Pack, *Special points for Brillouin-zone integrations.* Physical review B, 1976. **13**(12): p. 5188.
26. Sahni, V. and M. Slamet, *Interpretation of electron correlation in the local-density approximation for exchange.* Physical Review B, 1993. **48**(3): p. 1910.

Chapter III Results and discussion

Chapter III: Results and discussion

III.1 Introduction

The perfect optoelectronic features of organic-inorganic lead-halide perovskites have aided the astonishing development of perovskite solar cells. The prototypical compound, $CH_3NH_3PbI_3$, methylammonium lead iodide[1] is a direct band gap semiconductor with a visible band gap, strong charge carrier mobility, long diffusion length, and low excitonic binding energy[2] $CH_3NH_3PbI_3$ is attracting interest in a variety of applications outside of photovoltaics, such as light emitting devices, due to its perfect characteristics[3], lasers[4]

The advancement of metal-halide perovskite optoelectronics is dependent not only on a thorough understanding of the electrical and optical properties of these materials, but also on the development of new materials. also on the creation of practical ways for tuning their qualities by manipulating parameters like chemical composition. Ab initio computer modeling can help provide a physical interpretation of experimental results and guide the construction of innovative halide perovskites with customized features in this setting.

This chapter is divided into two parts. The first part includes some previous studies (experimental and theoretical) concerning some structural and optoelectronic properties of hybrid perovskite $CH_3NH_3PbI_3$. The second Part we will investigate the electronic and optical properties especially the absorption coefficient of the Lead Free perovskites materials.

III.2.Part one

III.2.1 Methylammonium Lead Iodide

Methylammonium lead-iodide, $CH_3NH_3PbI_3$, belongs to the ABX_3 perovskite structural family[5] .As shown in Fig. 1, the Pb^{2+} and I^- ions form a three-dimensional network of corner-sharing octahedra. The organic $CH_3NH_3^+$ cations occupy the center of the cuboctahedral cavities enclosed by the inorganic PbI_6 network[5] $CH_3NH_3PbI_3$, methylammonium lead-iodide, is a member of the ABX_3 perovskite structural family[5].

As seen in Fig.1, the ions Pb^{2+} and I^- form a three-dimensional network of corner-sharing octahedra. The organic $CH_3NH_3^{3+}$ cations at the core of the cuboctahedral cavities are encased by the inorganic PbI_6 network [5]. The temperature-dependent crystal structure of $CH_3NH_3PbI_3$ undergoes two phase transitions.[5-8] from the orthorhombic Pnma structure at low temperatures to the tetragonal *I4/mcm* structure at 160 K, and the cubic *Pm*3*m* structure at 315–330 K, The corner sharing connectivity of the PbI_6 octahedra is maintained in all phases of $CH_3NH_3PbI_3$, although the degree of octahedral tilting decreases as the temperature rises.

Furthermore, only the orthorhombic phases of the organic $CH_3NH_3^+$ cations have ordered orientations across the unit cell, whereas the tetragonal and cubic phases have orientationally disordered cations[5-8].

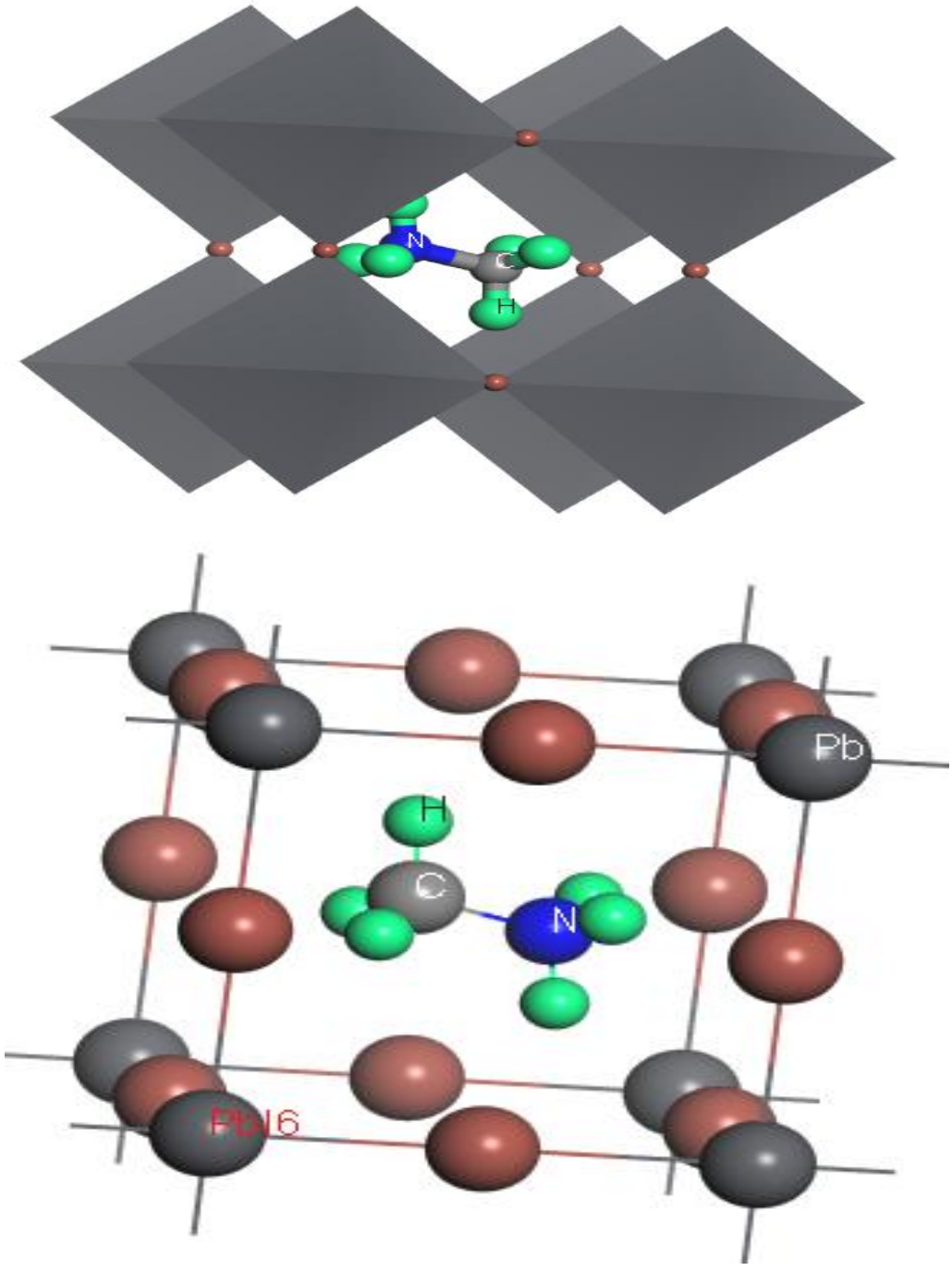

Fig.III.1 crystal Structure of $CH_3NH_3PbI_3$.

The characteristics of $CH_3NH_3PbI_3$ in the excited state have been extensively studied. $CH_3NH_3PbI_3$ has a direct band gap semiconductor optical absorption spectrum with a rapid absorption beginning around 1.6 eV In the solar spectrum range , and it has a high absorption

coefficient is order of 10^4 cm^{-1} [9].

Theoretical studies of the fundamental, electronic characteristics of $CH_3NH_3PbI_3$ have aided in the understanding of the above-mentioned experimental data. The projected density of states of $CH_3NH_3PbI_3$ in the low temperature orthorhombic Pnma scenario is shown in Fig.III 2. I-p and Pb-s electrons occupy the valence band top, whereas I-p and Pb-p electrons occupy the conduction band bottom. The states on the $CH_3NH_3^+$ cation are, as expected, positioned away from the band edges.

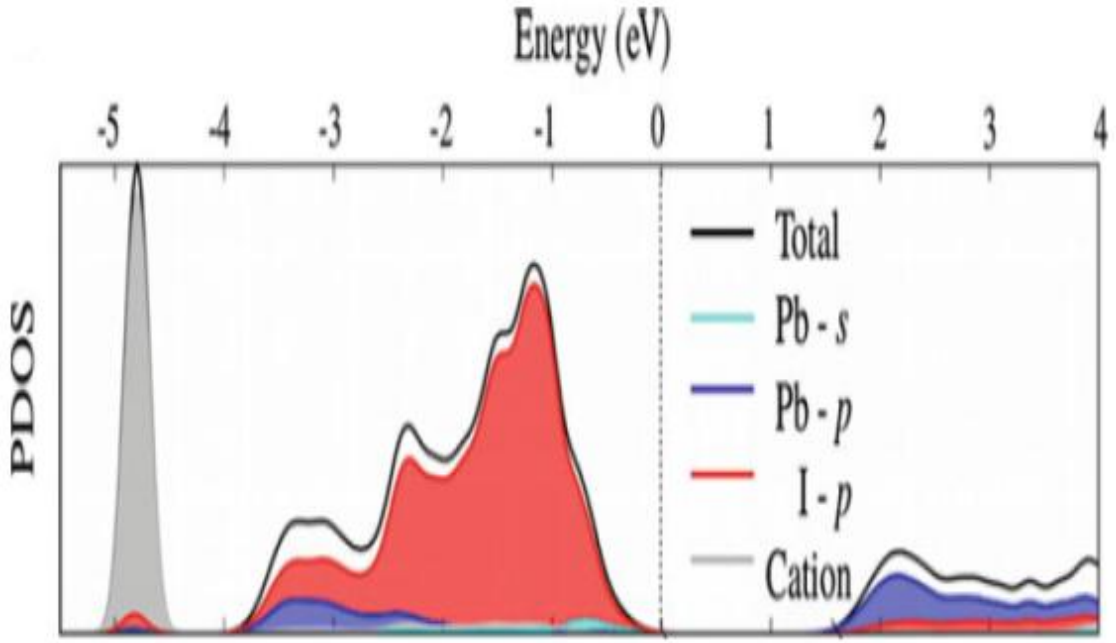

Fig.III. 2 :Projected density of states of $CH_3NH_3PbI_3$ calculated within the local density approximation to density functional theory (DFT/LDA) without spin-orbit coupling for the orthorhombic crystal structure [10].

III.3. Part Two

Because of the existence of lead in lead-halide perovskites, concerns have been raised about the environmental impact of perovskite solar cells. so It's highly appealing to develop lead-free perovskites. In this part, we go over some of the most notable studies on new halide perovskites that could have this unusual mix of optoelectronic features. First principles computational design has emerged as an effective method for screening new materials and identifying good candidates among the various ways to developing new lead-free perovskites.

III.3.1 Double perovskite $A_2B^{(I)}B^{(III)}X_6$

Recently, Pb-free halide double perovskites (HDPs) [11] with a formula of $A_2B^IB^{III}X_6$ have emerged as potential candidates for PV absorbers to overcome the toxicity and instability issues inherent within $MAPbI_3$. Besides of the conventional PV applications, HDPs have also been found to be promising functional materials in many other fields such as X-ray detectors .

We then referred to the periodic table to observe the ideal elements for stable LFDP structures as shown in Figure III.3 Sun et al.[12].

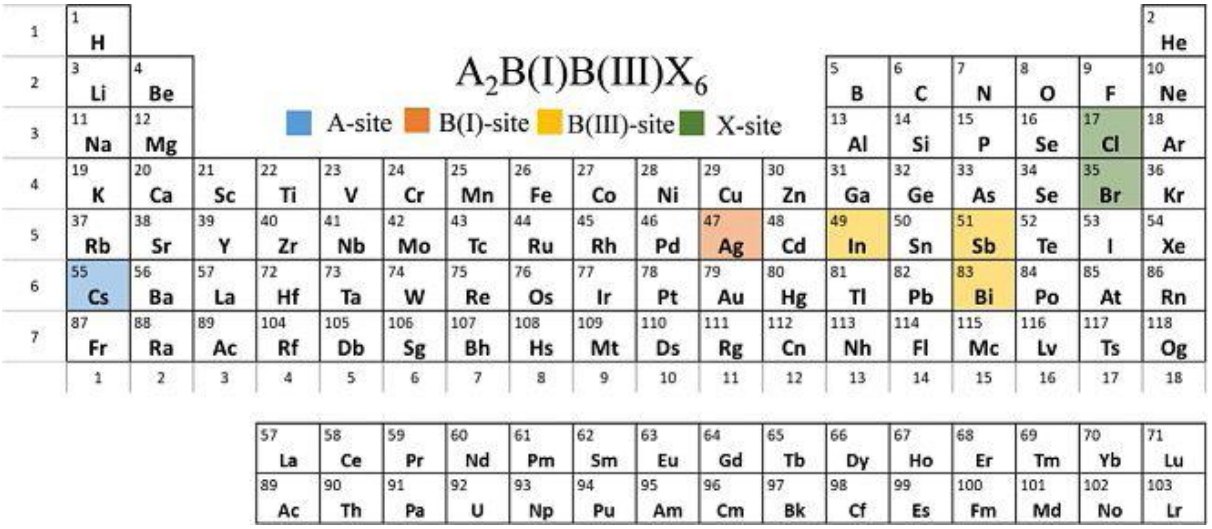

Fig. III.3 Representation of stable double perovskite structure of elements through the periodic table [13].

III.3.1.1 Double Perovskites Based on Bi (III) and Ag(I)

A new generation of perovskites materials such as $Cs_2AgBiBr_6$ was proposed [14-17]. These materials are inorganic, stable, and non-toxic. Besides, they are regarded as useful materials for photovoltaic applications since they were reported to be successfully synthesized [18].The perovskite solar cells based on $Cs_2AgBiBr_6$ film have reported efficiency of 2.43% [19].

The fundamental properties of perovskite solar cell materials, mainly the electronic and optical properties play a crucial role in the design and fabrication of devices based on these materials. For that, the current contribution attempts to investigate the electronic properties and absorption coefficient of the double perovskites material $Cs_2AgBiBr_6$ using first-principles calculations.

III.3.1.1.1 Electronic properties

The double perovskite $Cs_2AgBiBr_6$ has a cubic crystal structure as shown in Fig. III.4 ,The type of crystal structure and the lattice constant are two important elements before starting to calculate the electronic properties.

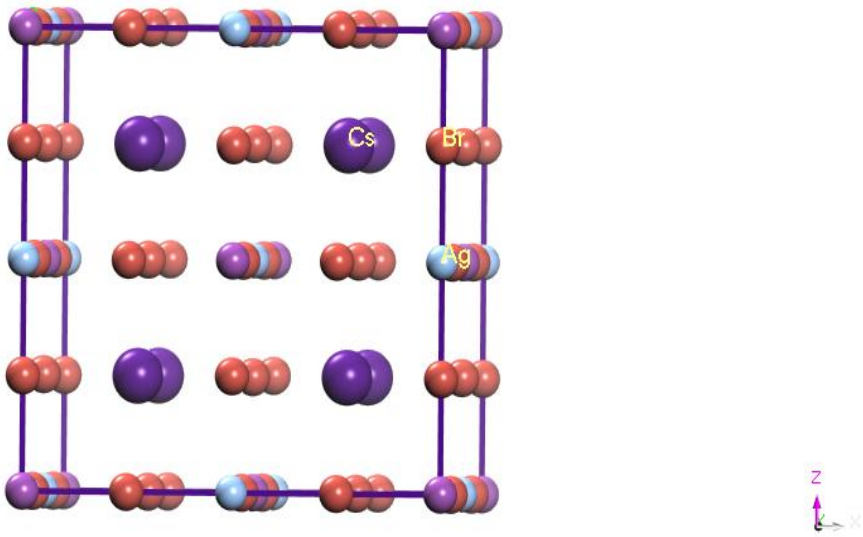

Fig. III.4. Crystalline cell of double perovskite $Cs_2AgBiBr_6$ with a face-centered cubic crystal (*Fm*3*m* space group).

We calculated the lattice constant in this work, as its value was close to some other theoretical values , but somewhat far from the experimental value as shown in Table III. 1

theorical lattice constant value	exprimental lattice constant value
11.42 Å (our work) 11.47 Å [20]	11.27 Å [21]

Table III.1: a lattice constant of $Cs_2AgBiBr_6$ calculated in our work compared with other theorical and exprimental result.

The electronic band structure is a useful tool for researching semiconductor electronic and optical properties. [22-26]. The accurate knowledge of these parameters is an important information for synthesizing and fabricating devices based on these semiconductors[27-30] . In this regard, the electronic band structure of $Cs_2AgBiBr_6$ double perovskite has been

computed . Our findings are displayed in Fig.III.5. The picture appears to be qualitatively similar to those of other semiconducting materials[31, 32] . A close inspection of Fig.III.4 shows the absence of intersection points between the Fermi level and energy bands. This indicates that the material of interest is a semiconductor. By observing Fig.III. 5, one can note that the valence band maximum is located at the high symmetry point L in the Brillouin zone, whereas the conduction band minimum occurs at the Γ point. This suggests that the material in question is an indirect (L- Γ) band gap semiconductor. The computed magnitude of this band gap is found to be 1.32 eV. While the exprimental value is 2.19 eV[21] As a matter of fact, the nature and the value of the band gap of $Cs_2AgBiBr_6$ limits its application in photovoltaics. In this case, We followed the suggestion made by some researchers, where we replace Bi with In in order to change the nature of the band gap , this what we did in the next work.

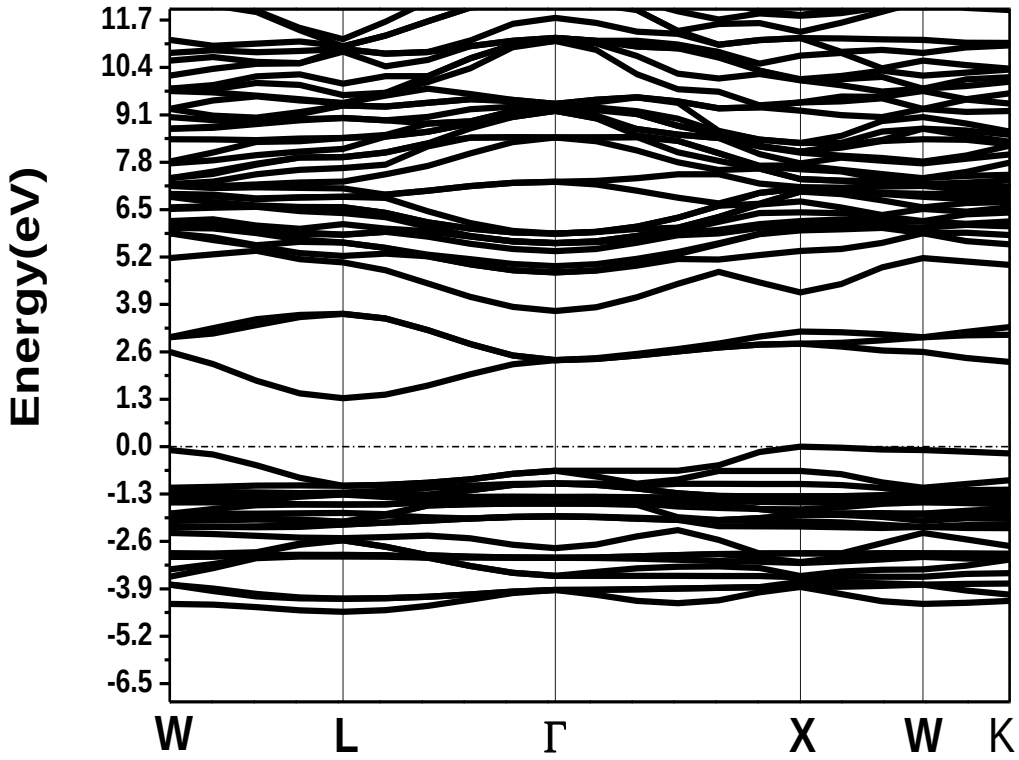

Fig.III.5. Electronic band structure for $Cs_2AgBiBr_6$.

Fig.III.6 shows the partial densities of states (PDOS) for $Cs_2AgBiBr_6$ double perovskite material that correspond to the electronic band structures presented in Fig.III.5.The Fermi level is set to be at the zero energy. Through the Partial density of states diagram, we can

know the orbitals that make up the valence band and the conduction band, as well as the orbitals that dominate in each band, as we note that The dominant orbital in the valence band is p-Br, While the p-Bi orbital and to a lesser extent the s-Ag orbital dominate the conduction band. The presence of Ag 4d states in the valence band helps to reduce the band gap and is partly responsible for these phases' indirect band gap**.**

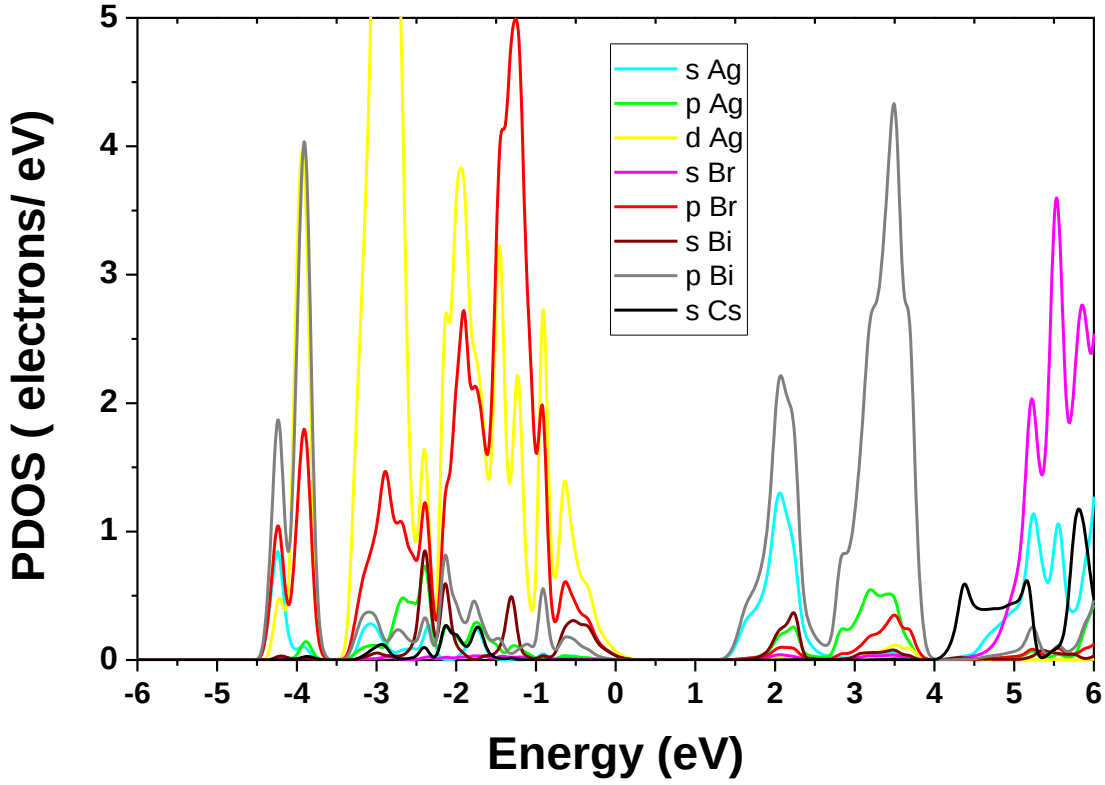

Fig.III.6**.** Partial density of states (PDOS) of cubic double perovskite $Cs_2AgBiBr_6$.

III.3.1.1.2 Absorption coefficient

The optical characteristics of semiconductors are critical physical parameters in quantum structure modeling [33, 34]. Incident light of a specific wavelength penetrates a material and travels a certain distance before being absorbed. The absorption coefficient[35-37] is a physical parameter that describes this distance.

The evolution of the absorption coefficient as a function of photon incoming energy is depicted in Figure III.5. It's worth noting that for photon incidence energies below the fundamental absorption edge, the absorption coefficient is nearly null, before increasing in magnitude. This can be explained by an increase in the amount of electrons with enough energy to interact with photons. The optical absorption coefficient's magnitude is proportional to the frequency of the electromagnetic wave. When it comes to the material of interest, it

exhibits good light absorption in the visible spectrum region. Fig.III.6 shows that $Cs_2AgBiBr_6$ have very strong optical absorption in the high-energy part of the solar spectrum with an absorption coefficient of the order of 10^4 cm^{-1}.

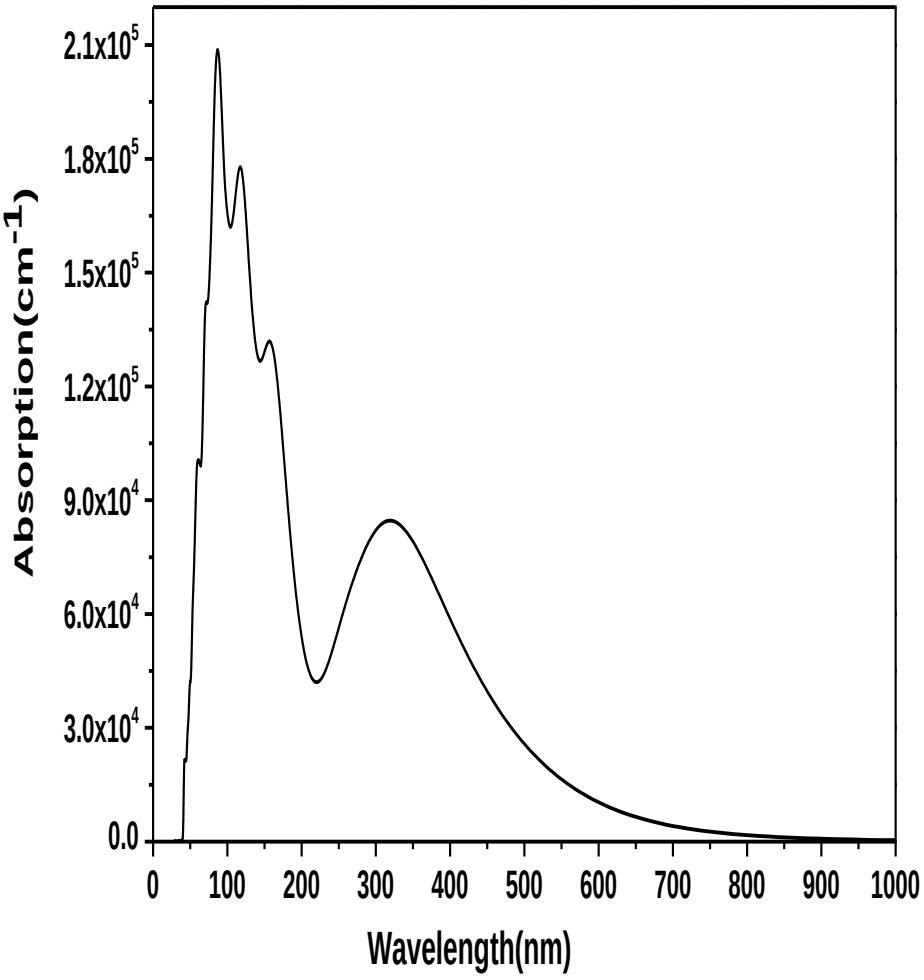

Fig.III.7. Optical absorption coefficient spectrum for $Cs_2AgBiBr_6$.

In fact, solar cells using $Cs_2AgBiBr_6$ as the active layer were demonstrated by **Greul et al.** [19], and power conversion efficiencies of 2.5% were reported.

III.3.1.1.3 Computational details

The calculations in this study are based on the CASTEP code [38], which employs a pseudopotential plane-wave approach. The generalized gradient approximation (GGA) of Perdew et al. (PBE)[39] is used to explain the exchange and correlation potential. 1400 eV is assumed to be the plane wave cutoff energy. The k-point meshes of Monkhorst and Pack [40] are used so as to perform the Brillouin zone integrations with a 10 x10 x10 special k points mesh.

III.3.1.2 Double Perovskites Based on In (III) and Ag(I)

Following up on the successful design and synthesis of lead-free halide double perovskites based on pnictogen/noble metals combinations, several groups set to improve the design by targeting double perovskites with a direct band gap.[41] reasoned that the origin of the indirect band gap of $Cs_2AgBiBr_6$ lies in the hybridization between Bi *s*-states and Ag *d*-states near the valence band top.[41] proposed to replace Bi with a +3 cation with the outermost *s*-shell unoccupied. Among these materials, Cs_2AgInX_6 where X are Cl or Br[41].

III.3.1.2.1 $Cs_2AgInCl_6$

$Cs_2AgInCl_6$ has attracted much attention during the last years[42-46]. This is because of its interesting optoelectronic properties that make it favorable for solar cells as an absorber layer[42]. Besides, due to its exceptional sensitivity, reasonable stability and good response time, this material is a candidate in use fire, missile flame detection and optical communication[47]. As a matter of fact, different methods were reported in the literature for the design of the band gap of $Cs_2AgInCl_6$ [46, 48, 49]. In addition, ideal growth conditions for $Cs_2AgInCl_6$ have been revealed for photovoltaic purposes [50].

The ability to evaluate the quality of samples and design and fabricate optoelectronic devices requires a thorough understanding of optical and electrical properties of materials. [29, 51-55]. In this regard, some experimental and theoretical studies have been carried out for $Cs_2AgInCl_6$ double perovskite material [41] Despite this, some essential features of $Cs_2AgInCl_6$ have still to be precisely characterized. In addition, knowledge of the strain effect on these properties is critical for the application. The current study focuses on the electronic and optical characteristics of $Cs_2AgInCl_6$. Our goal in this part of the study is to contribute to the data already accessible in the literature about the fundamental properties of the material under consideration, with a focus on their dependence on strain. The computations are based on a hybrid functional and density functional theory (DFT).

III.3.1.2.1.a .Electronic properties

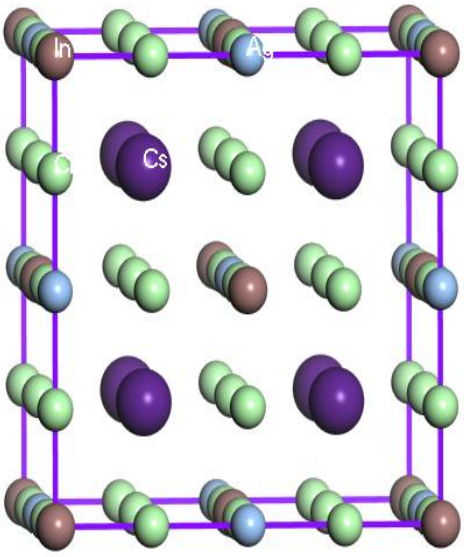

Fig III. 8. Crystalline cell of double perovskite $Cs_2AgInCl_6$.

Fig. III.8 illustrates the crystalline cell of $Cs_2AgInCl_6$ double perovskite material. In our case, the cell has a lattice parameter of 10.4905 Å This value is near to exprimental value 10.47 Å [41] . The Cs is shown by the violet color, the Ag by the blue color, the In by the brown color and the Cl by the green color.

theorical lattice constant value	exprimental lattice constant value
10.4905 Å (our work)	10.47 Å [41]

Table III. 2: a lattice constant of $Cs_2AgInCl_6$ calculated in our work compared with other exprimental result.

The understanding of band structure and electronic properties of solid materials is very important from both basic and applied points of view [23, 26, 56, 57]. For that, the electronic band structures of the unstrained and strained $Cs_2AgInCl_6$ double perovskite materials are depicted in Fig.III 9.a:

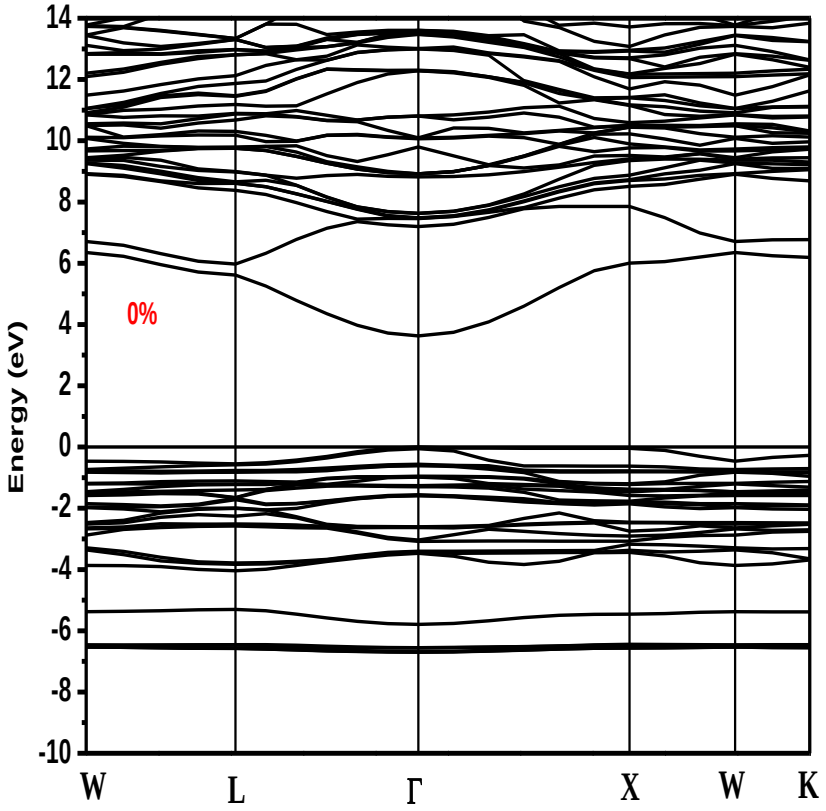

Fig. III.9 a. Electronic band structure for double perovskite $Cs_2AgInCl_6$.

Note that the overall picture of these band structures resembles to that reported for semiconducting materials [31, 58]. Remark that for the unstrained material under focus, the Fermi level which is taken as zero reference energy level does not cross the energy bands. In addition, the maximum of the valence band appears to be at the Γ high-symmetry point in the Brillouin zone, and the lowest conduction band is located at the Γ-point as well. Accordingly, the unstrained $Cs_2AgInCl_6$ is a direct (Γ→Γ) band-gap semiconductor. This accords well with experimental and previous theoretical results reported in the present literature [41-43, 45, 46, 48, 49] The authors obtained energy band-gap is recorded as 3.62 eV.

Theorical band gap value (eV)	Experimental band gap value (eV)
3.62 (our work) 1.1 [44] 1.04, 3.01 , 2.95 [45]	3.53 [46]

Table III. 3: band gap value of $Cs_2AgInCl_6$ calculated in our work compared with other theorical and exprimental results.

This value is in very good accord with the experimental one of 3.53 eV reported recently by Tran et al[46]. using UV-Vis diffuse reflectance spectra measurements (the authors result deviates by less than 3% from experiment[46]). As compared to previous theoretical calculations, the authors recorded value is closer to experiment [46] than those of 3.33 eV calculated by Zhou et al.[42] using projector-augmented wave pseudopotentials as implemented in the Vienna Ab-initio simulation package code, 1.1 eV calculated by Mathew et al. [44] using the Quantum-Espersso suite and 1.04, 3.01 and 2.95 eV computed by Soni et al.[45] using full-potential linearized augmented plane wave (FP-LAPW) method within PBE, mBJ and mBJ (with spin-orbit coupling) for the exchange-correlation potential, respectively.

Under strain effects (Figs.III. 8b and III.8c), one can observe a similar qualitative picture of the band structure to that of the unstrained material under focus (Fig. III.7.a). From the quantitative point of view, they differ in magnitude of their energy band gaps. In this context, the authors results recorded a value of 3.54 eV when the compressive strain of 5% is applied and a value of 3.7 eV when the material of interest is subjected to a tensile strain of -5%. It is worth noting that although the magnitude of the fundamental energy band-gap of $Cs_2AgInCl_6$ changes under compressive and tensile strain effects, the nature of the band-gap remains a ($\Gamma \rightarrow \Gamma$) direct-gap.

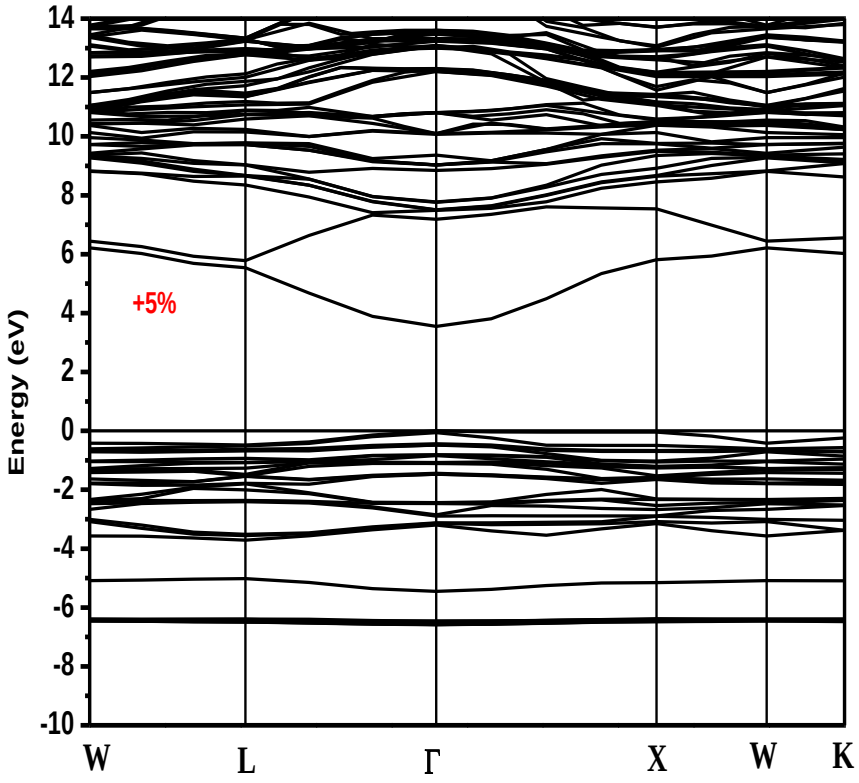

Fig.III .9.b. Electronic band structure strained (+5%) double perovskite.

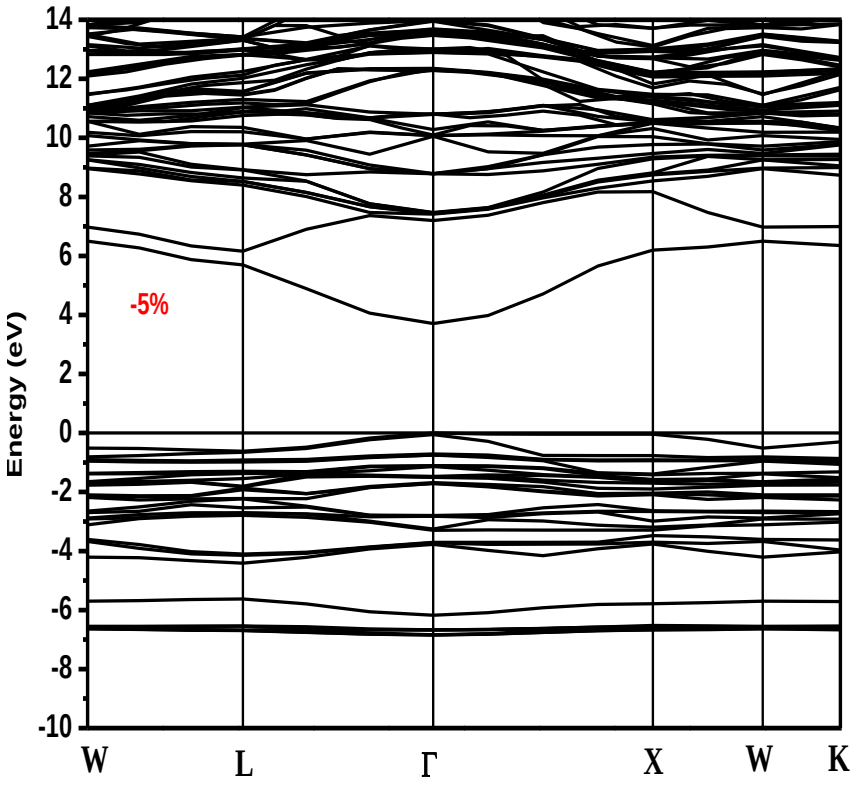

Fig.III. 9.c. Electronic band structure strained (-5%) double perovskite.

The evolution of the fundamental energy band-gap (E_g) against strain is depicted in Fig.III.9 Remark that by applying a tensile strain (from -5% to 0%), E_g increases with respect to that of the unstrained $Cs_2AgInCl_6$. However, when the material under focus is subjected to a compressive strain (from 0% to 5%), the E_g decreases with respect to that of the unstrained $Cs_2AgInCl_6$. The behavior of E_g versus strain is monotonous for both compressive and tensile strains. The tuning of the E_g under strain effects may give more diverse opportunities for the applications of $Cs_2AgInCl_6$ in optoelectronic applications. The compressive strain is expected to make the material of interest as a good candidate for the applications in the infrared and visible ranges of the electromagnetic spectrum.

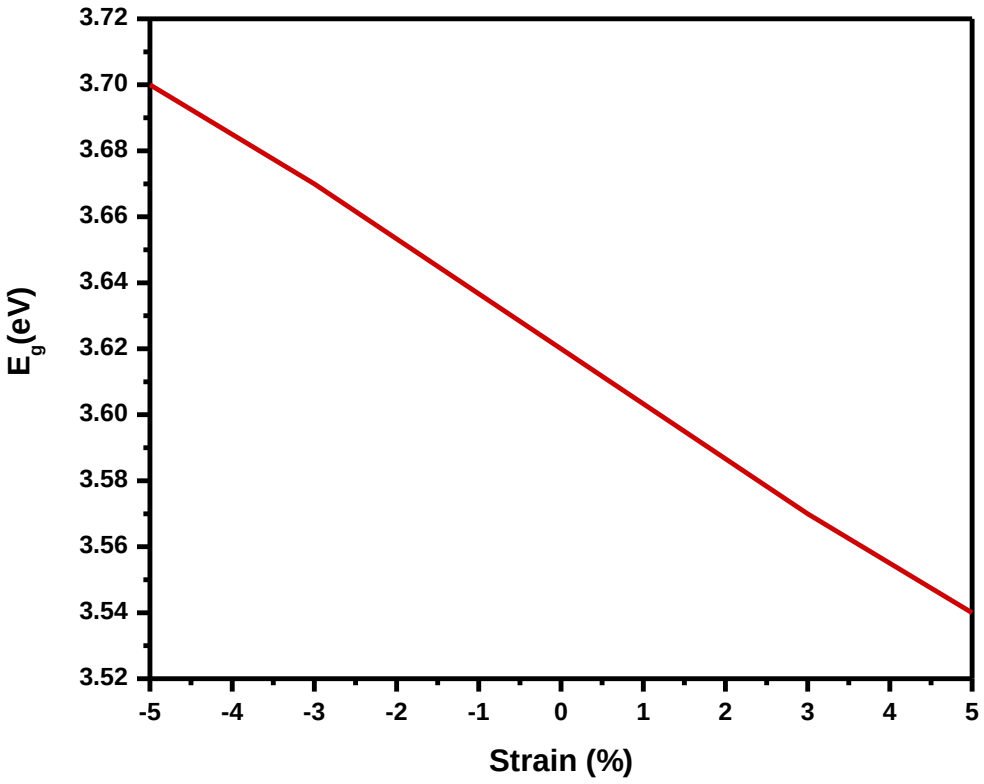

Fig. III.10. Fundamental band-gap energy (E_g) as a function of strain for double perovskite $Cs_2AgInCl_6$.

Fig.III.11 shows the partial densities of states (PDOS) for unstrained $Cs_2AgInCl_6$ double-perovskite material that correspond to the electronic band structures presented in Fig.III.8a. The Fermi level is set to be at the zero energy. Note that for the unstrained $Cs_2AgInCl_6$, the contribution of the Ag-4d electrons is predominant in the energy bands interval from -4 to 0 eV. In the energy bands range from 4 to 8 eV, the contribution of Ag-5s electrons is predominant with a minor contribution of Ag-p electrons. In the interval from -7

to -6 eV, the contribution of Cs-6p seems the predominant, whereas in the energy bands range lying between -4 and -2 eV, the contribution of In-p seems the predominant. In the energy band region from -6 to 0 eV, the main contribution comes from the Cl-3p states. For the energy bands near the Fermi level of the unstrained $Cs_2AgInCl_6$ crystal, the contribution of the mixing of In-5s and Cl-3p states electrons is predominant. Therefore, these electrons are useful for the conductibility of the material under focus. The energy bands in the valence regions (-7 to 0 eV energy) comes from the hybridization of Cs-6p, Ag-4d, In-5p and Cl-3p states. Based on the results of the electronic band structures, one may expect that there is no significant strain effect on the PDOS of the material under focus.

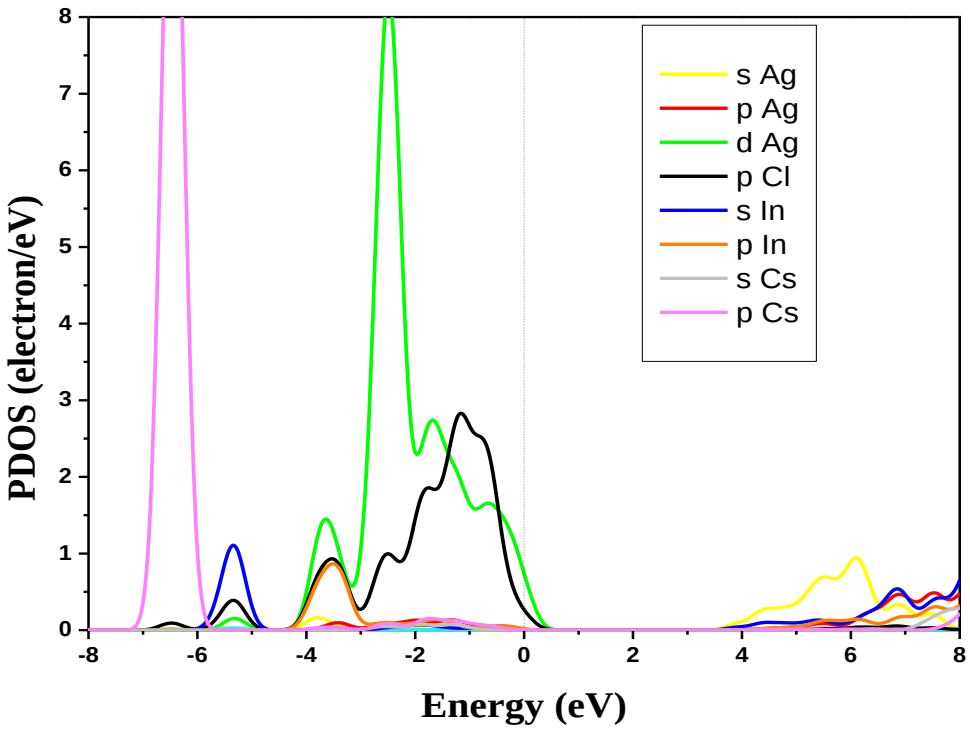

Fig. III.11. (a) , (b), (c) and (d) Partial density of states (PDOS) for unstrained double perovskite $Cs_2AgInCl_6$ for Ag ,Cs, In and Cl respectively.

.III.3.1.2.1.b .Optical properties

Figs.III.12 and 13 are respectively plots of the calculated real (ϵ_1) and imaginary (ϵ_2) parts of the dielectric function against the photon energy for $Cs_2AgInCl_6$ double perovskite material. Remark that for unstrained $Cs_2AgInCl_6$ the real part of the dielectric function exhibits several peaks and valleys against the photon energy. The main peak is located at a photon energy of about 7.5 eV (Fig.III.12). This peak is followed by peaks that have less

intensities. Similar trend of the real part of the dielectric function against photon energy was reported by Khan and Bouarissa [59] for ZnS compound using first-principles molecular dynamics simulation. The peaks are attributed to the optical transitions that happen between valence and conduction bands [60]. The static dielectric constant has been estimated in this work and recorded as about 3.1. This value is larger than that of 2.078 calculated very recently by Soni et al.[45] using FP-LAPW method. By applying strain, all the peaks are shifted with respect to those in unstrained $Cs_2AgInCl_6$. The shift is upward when the applied strain is tensile and it is downward when the applied strain is compressive. This affects the optical transitions in the material under focus. It also slightly affects the static dielectric constant which becomes about 3 in the case of compressive strain of 5% and about 3.2 in the case of tensile strain of -5%. Very recently, Soni et al.[45] reported values of static dielectric constant of 3.78 for -5% and 3.09 for a strain of 5%. The former value is somewhat larger than that recorded by the present authors, whereas the latter value agrees to within 3% with that reported in this work.

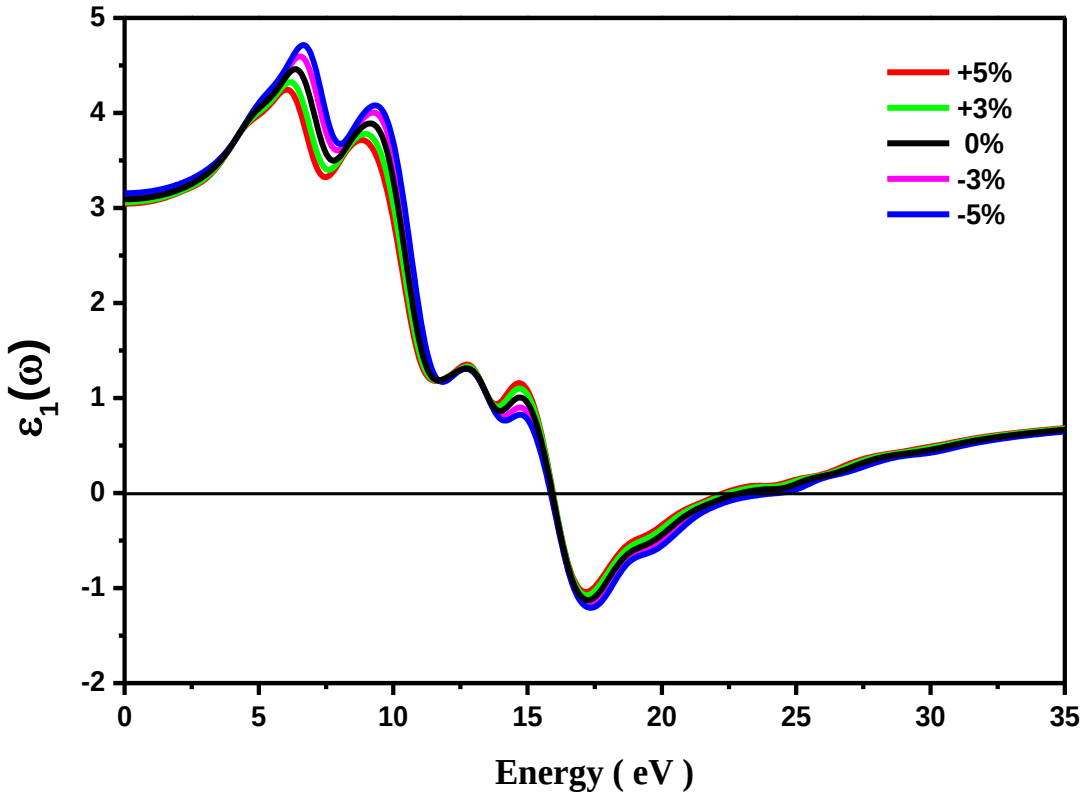

Fig. III.12. Real part of the dielectric function (ϵ_1) spectra for unstrained and strained double perovskite $Cs_2AgInCl_6$.

The imaginary part of the dielectric function allows to defines the energy losses of the

material , As for The imaginary part of the dielectric function obtained in our study (Fig. III.12), for unstrained $Cs_2AgInCl_6$, the representative curve increases first steeply exhibiting a set of peaks thereafter. Furthermore, the threshold energy in the spectrum of (Fig.III.12) is recognized to indicate an electron transition between the valence and conduction bands. The threshold energy obtained in this case is 3.6eV, which is closer to the band gap of the compound .The imaginary part of the dielectric function typically rises to a peak which is an asymmetric. This peak is attributed to the transitions that occur along the (111) directions in the Brillouin zone[61]. spectrum There are also different peaks (Fig.III.12) that can be described in terms of different interband transitions. For example, the peak at about 6 eV, occurs due to the transition of electrons from Ag-4d to In 5s states. Similarly to the real part of the dielectric function, the effect of tensile strain shifts the imaginary part of the dielectric function upwards with respect to that of the unstrained $Cs_2AgInCl_6$ and that of compressive strain shifts it downwards with respect to that of the unstrained material in question.

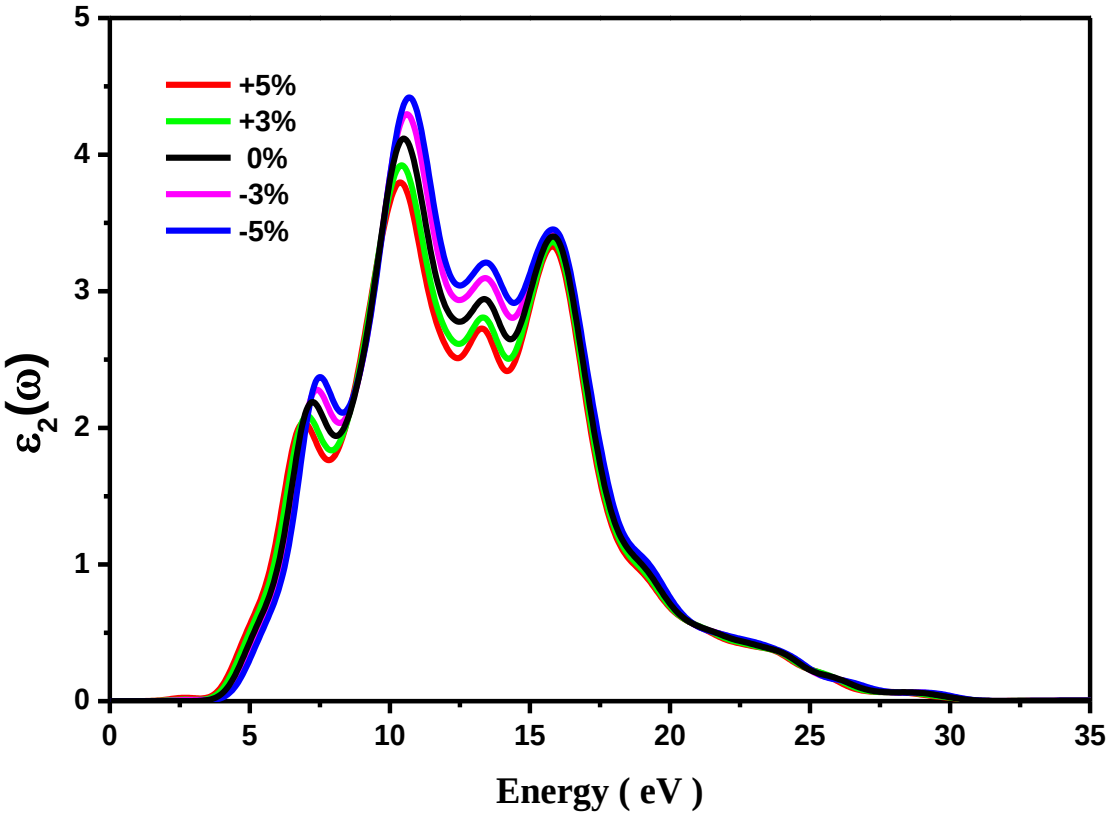

Fig. III.13. Imaginary part of the dielectric function (ϵ_2) spectra for unstrained and strained double perovskite $Cs_2AgInCl_6$.

The refractive index of solid materials is an interesting optical parameter that can serve in the design and fabrication of optoelectronic devices[62-68]. It serves also in the investigation of the transparency of materials for technological purposes[69] . In the current work, the refractive index spectrum is computed and plotted in Fig. III.14 against the photon energy for unstrained $Cs_2AgInCl_6$ double-perovskite material, Also shown in Fig. III.14 are the refractive index spectra obtained under compressive and tensile strains. Remark that for the unstrained $Cs_2AgInCl_6$, the values of the refractive index at low-photon energy region are larger than those at high-photon energy region. One can note a series of peaks in the refractive index spectrum. These peaks are attributed to the excitonic transitions. The static refractive index obtained at zero limits of the photon energies is recorded as about 1.75. This value is somewhat larger than that of 1.45 reported very recently by Soni et al.[45] using FP-LAPW calculations. The transparent nature of the unstrained material under focus is obtained for a wide range of solar spectrum covering the infrared and visible regions. Nevertheless, in the photon energy interval from about 17 to 35 eV, $Cs_2AgInCl_6$ behaves as opaque.

The shape of the refractive index spectra of the material under focus when subjected to strain appears to resemble to that of the unstrained $Cs_2AgInCl_6$. This is true for both compressive and tensile strains. However, from the quantitative point of view, the refraction spectra are slightly shifted under strains effect in such a way that it increases the maximum amplitudes of the refractive index spectra for tensile strains and decreases them for compressive strains in the transparent region. This affects the optical nature of the material under focus when it is under strain.

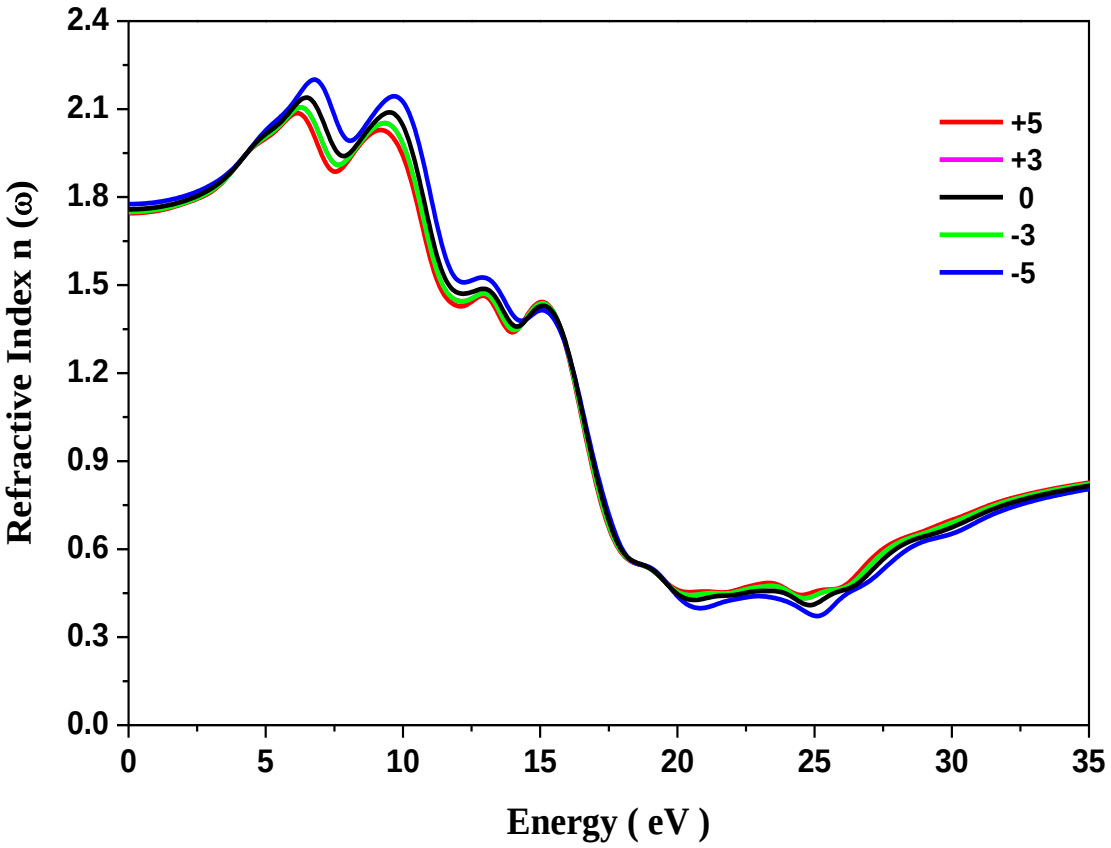

Fig. III. 14.Refractive index spectra for unstrained and strained double perovskite $Cs_2AgInCl_6$.

Another interesting optical parameter is the optical absorption coefficient α(E), where E is the photon energy. The accurate knowledge of the latter is very important for the evaluation of solid materials in order to check their ability to be used in the design and fabrication of photovoltaic devices [60]. In this context, α(E) is computed for the unstrained $Cs_2AgInCl_6$ double-perovskite material. We obtained data are shown in Fig. III.15. Note that the optical absorption coefficient spectrum for the material under focus exhibits sufficiently high optical absorption of the order of 10^6 cm^{-1}. The interval of the light absorption is wide and extended from about 5 to 30 eV. The maximum amplitude in the spectrum is recorded as about 3.7 cm^{-1} at around 17 eV.

Applying strains shifts the absorption coefficient spectra with respect to that of the unstrained $Cs_2AgInCl_6$. The shift is upward when the strain is tensile and is downward when the strain is compressive. This will increase the absorption when the strain is tensile. This results in the augmentation of the integrated intensities of the α(E) and hence might improves the potential application of the material under focus for optoelectronic applications.

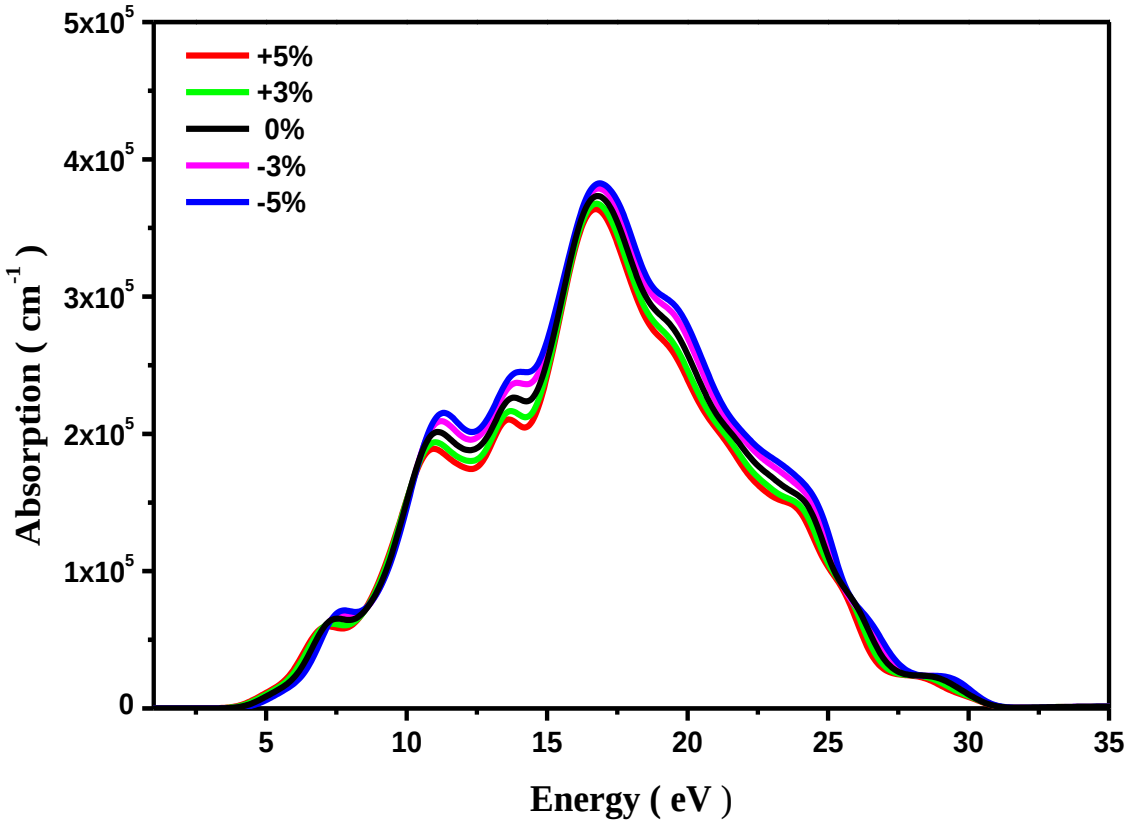

Fig. III.15. Absorption coefficient spectra for unstrained and strained double perovskite $Cs_2AgInCl_6$.

Due to its outstanding stability and non-toxicity, this new double perovskites is garnering attention for applications in UV detectors because the band gap of $Cs_2InAgCl_6$ is too large for photovoltaics.. In particular Luo et al. [47] and Zhou et al. [42] succeeded in growing mm-sized single crystals, and Luo et al._[47]fabricated UV detectors with high on/off ratios, fast photoresponse, low dark current, and high sensitivity.

III.3.1.2.1.c. Computational details

The double-perovskite under focus crystallizes in a cubic unit cell with the Fm3m space group. It is composed of [$AgCl_6$] and [$InCl_6$] octahedra alternating in an ordered rocksalt structure.

All DFT computations are carried out using the norm-conserving pseudopotential plane-wave method as implemented in the CASTEP code[38]. The exchange-correlation potential is described by the conventional generalized-gradient approximation (GGA) of Perdew et al.[39] . In the structural optimization, the Monkhorst and Pack k point meshes[40] are taken to be 5 ×5×5 special k points mesh, while the plane wave cutoff energy is set to be 950 eV.

In order to improve the band-gap accuracy, the functional hybrid B3LYP is used for the electronic structure. In that case, the plane wave basis set cutoff is 650 eV and the k-points used for the Brillouin zone sampling are $2\times2\times2$.

The optical properties are calculated using GGA of Perdew et al., and the scissors operator has been used for correction. For that, we have taken a plane wave basis set cutoff of 950 eV and we have used k-points of $15\times15\times15$ for sampling the Brillouin zone.

The relaxations of electrons and ions are allowed only when the change in the successive total energies and forces on each atom is greater than 10^{-5} eV/atom and 0.05 eV/ Å, respectively.

The single crystal elastic coefficients (C_{ij}) are determined using the finite strain-stress method [70]. By deriving the C_{ij}'s, the polycrystalline elastic parameters are calculated using the Voigt-Reuss-Hill approximations [71-73].

When the material under focus is subjected to strain, which is taken here from -5% to 5%, the lattice parameters are obtained from the energy optimization using a similar procedure to that used for unstrained $Cs_2AgInCl_6$.

III.3.1.2.2 $Cs_2AgInBr_6$

Cs2AgInBr6 is one of the double perovskites materials that has received a lot of attention in recent years and has been recommended as an ideal option for technological applications, particularly in the field of photovoltaics. Despite the fact that some fundamental features of the material in question were investigated,[41, 43, 74, 75], only a few data were reported about its optical and electronic properties which have an important role in designing and fabricating devices that use the perovskite in question[66, 76, 77] . In fact, Liang[75] has carried out a systematic modeling so as to formulate a new system of solar absorption layer based on Cs_2InAgX_6 and its hetero-junction device. The optimized $Cs_2InAgBr_5Cl$ compound is a marvelous solar absorption layer which is consistent with $Cs_2InAgBr_6$ at standard room temperature (298 K). On the other hand, Zhang et al. [74] have discovered that the Cs_2AgInX_6 (X=Cl, Br) have provided an efficient way to search promising solar cell absorbers. Despite the fact that Cs2AgInX6 (X=Cl, Br) has a similar structure, the physical characteristics of strained Cs2AgInX6 (X=Cl, Br) differ. In compressive $Cs_2AgInBr_6$, the direct-to-indirect phase transition occurs. As a result, the material of interest is suitable for radiation detection. Furthermore, stresses obtain a negligible absorption coefficient. As a result, the material could be used in future photovoltaic applications. This prompted us to conduct a study utilizing density functional theory (DFT) computations on the band structure and optical spectra of the

double perovskites material Cs2AgInBr6. Furthermore, the elastic constants were used to check the phonon spectrum computation and mechanical stability of the material under investigation.

III.3.1.2.2 a. Electronic properties

The crystalline cell of the double perovskite $Cs_2AgInBr_6$ material is shown in Fig.III.16(a). The violet hue represents the Cs, the blue color represents the Ag, the brown color represents the In, and the red color represents the Br. Cubic is the crystal structure. FM3M is the symmetry of the group.. The lattice constant of the primitive cell is 7.94 Å. And the conventional cell is 11.22 Å is very near to other theorical calculation 11.20 Å[20].

lattice constant value calculated in this work	lattice constant value other theorical calculation
11.22 Å	11.20 Å[20]

Table III. 4: a lattice constant value of $Cs_2AgInBr_6$ calculated in our work compared with other theorical result.

Fig.III.16 (b) displays the crystal structure of double perovskite $Cs_2AgInBr_6$ with two types of octahedral $InBr_6$ (brown color) and $AgBr_6$ (blue color) and Cs atoms with (violet color).Fig .III.16 (b) displays the crystal structure of double perovskite $Cs_2AgInBr_6$ with two types of octahedral $InBr_6$ (brown color) and $AgBr_6$ (blue color) and Cs atoms with (violet color).

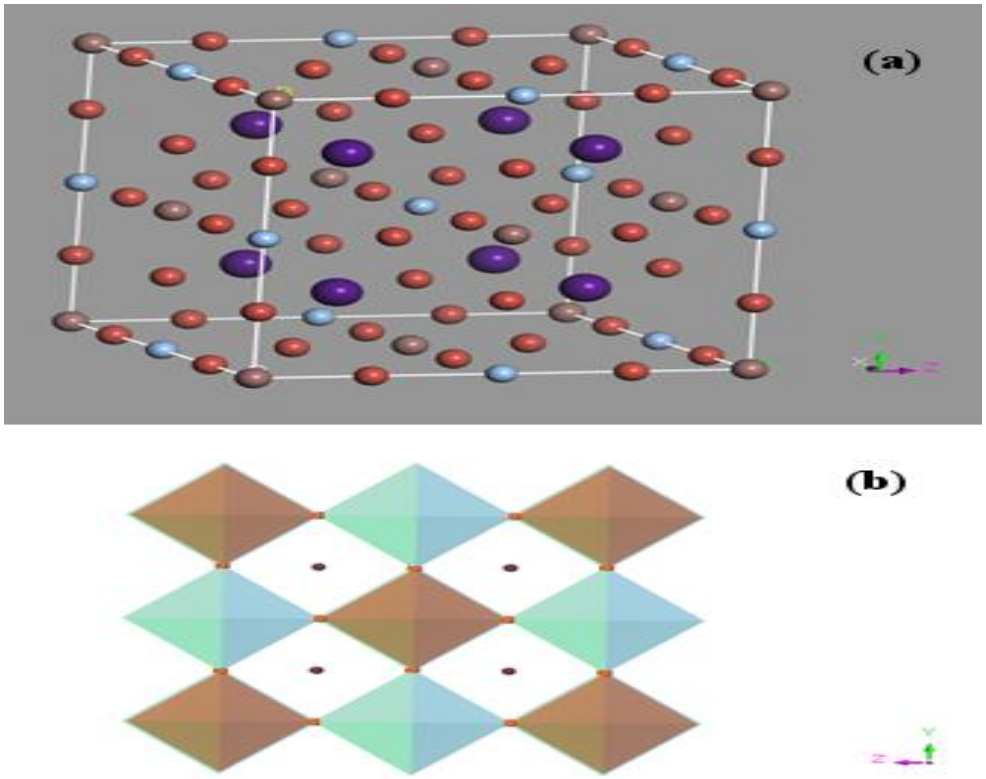

Figure III.16: (a) Crystalline cell of double perovskite $Cs_2AgInBr_6$ (b) Crystal structure of double perovskite $Cs_2AgInBr_6$ with two types of octahedral $InBr_6$ (Brown color) and $AgBr_6$ (blue color) and Cs atoms with violet color.

The electronic band structure and its associated parameters are significant physical characteristics for defining materials' optoelectronic properties. [26, 58, 78] The electronic band structure and its associated parameters are significant physical characteristics for defining materials' optoelectronic properties. [22, 28, 29]. The electronic structure of $Cs_2AgInBr_6$ double perovskite was estimated utilizing the functional hybrid B3LYP technique in this study. Figure III.17 depicts our findings. The situation appears to be comparable to that which is frequently observed for semiconducting materials [24, 31].

The fundamental energy gap between the materials is the most significant difference. The Fermi level does not intersect the energy bands, as can be seen. This denotes that the substance in question is a semiconductor. Because both the valence band top and the lowest conduction band are located at a position in the Brillouin zone, Fig. III.17 reveals that $Cs_2AgInBr_6$ possesses a direct ($\Gamma \rightarrow \Gamma$) gap energy.

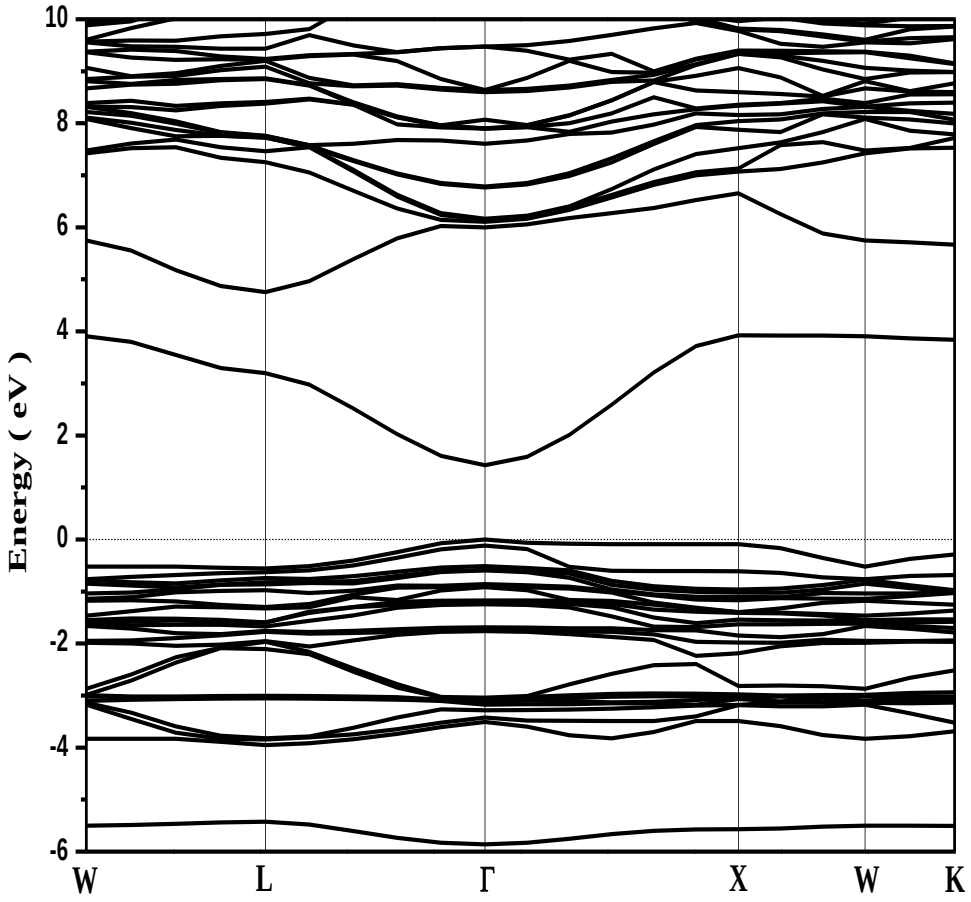

Fig. III.17. Electronic band structure for cubic double perovskite $Cs_2AgInBr_6$.

The lowest conduction band is dominated by σ* antibonding. It is mostly made up of Ag-s AgBr6 octahedran states and In-s InBr6 octahedran orbitals.The valence band maximum is dominated by Ag-d and Br-p orbitals of the $AgBr_6$ octahedran with the small In-d orbitals of the $InBr_6$ octahedran [74]. The direct (Γ→Γ) energy gap of $Cs_2AgInBr_6$ recorded by the authors results is 1.427 eV. This value is larger than that of 0.58 eV reported in Refs. [41, 74] and obtained by using local density approximation (LDA). As a matter of fact, LDA methods are known to underestimate the band gap values with respect to experiment[79, 80]. In general, the theoretical electron effective mass is found to be a tensor. As a result, the electron effective mass is a number that is direction dependent. The electron effective mass, on the other hand, becomes a scalar that is independent of direction in a very idealized simple scenario. As a result, we just employ one scalar effective mass. The electron effective mass of $Cs_2AgInBr_6$ was employed in the electron conduction band minimum calculated from the band curvature in this method. $Cs_2AgInBr_6$'s electron effective mass has thus been calculated. Our findings yield a value of $m^*_e=3.47\ m_o$, where m_0 is the electron free-particle mass and

$m^*_e=0.24m_0$, $m^*_{hh}= 0.3\ m_o$ and $m^*_{lh} = 1.25\ m_o$ for other theoretical calculation[20].

We attribute the significant difference in our results in calculating the effective mass to a difference in the use of approximations as well as the limits of our capabilities, because calculating the effective mass requires a large number of K points, which becomes very expensive when using Hybrid Functional.

To explore the distribution of electrons on various orbitals, the partial density of states (PDOS) has been estimated. In this context, PDOS for $Cs_2AgInBr_6$ double perovskite has been displayed in Fig. III.18. A closer look at Fig. III.18 reveals that the first PDOS zone is the most tightly bound energy band. In the energy range of -4 to 0.5 eV, the contribution of the Ag-d and Br-p electrons is prominent, whereas the Ag-s and In-p electrons are dominant in the energy range of 1 to 5 eV. The antibonding states of the Ag-d and Br-p orbitals create the upper valence bands, whereas the antibonding states of the In-s/p orbitals with the Br-p orbital dominate the conduction bands. The Ag-d electrons dominate the contribution to energy bands near the Fermi level of the $Cs_2AgInBr_6$ double perovskite material. This suggests that the Ag-d electrons have a significant influence in the conductibility of the perovskite under investigation.

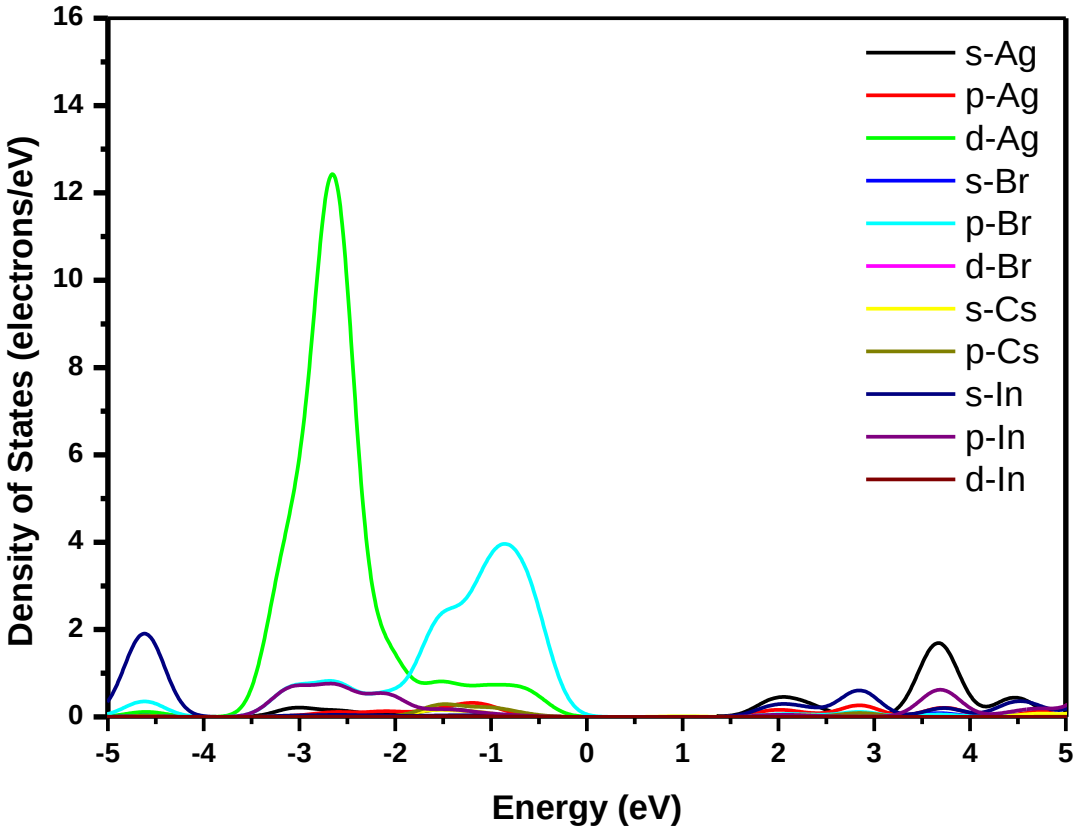

Fig. III.18. Partial density of states (PDOS) of cubic double perovskite $Cs_2AgInBr_6$.

III.3.1.2.1.b .Optical properties

Solid materials have optical properties that can be employed in research and device applications. [34, 62, 66]. The refractive index (n) is a significant optical property that can help in device design and fabrication. It can be thought of as the parameter that reduces the radiation speed and wavelength in comparison to their vacuum values. For the $Cs_2AgInBr_6$ material, n is calculated against photon energy in the current study. The n(E) spectrum, is illustrated in Fig. III.19. At zero photon energy, the static refractive index is recorded as n(0)=2.09. The present discovery is a forecast because there are no theoretical or experimental values for n(0) for $Cs_2AgInBr_6$ to the authors' knowledge. The values of n are big in the low photon energy zone but drop in the high photon energy region, as can be seen. Peaks originating from excitonic transitions can be seen. The peaks are more pronounced in low photon energy region than in high photon energy region. The effect of excitonic tends to increase the oscillator strength [68].

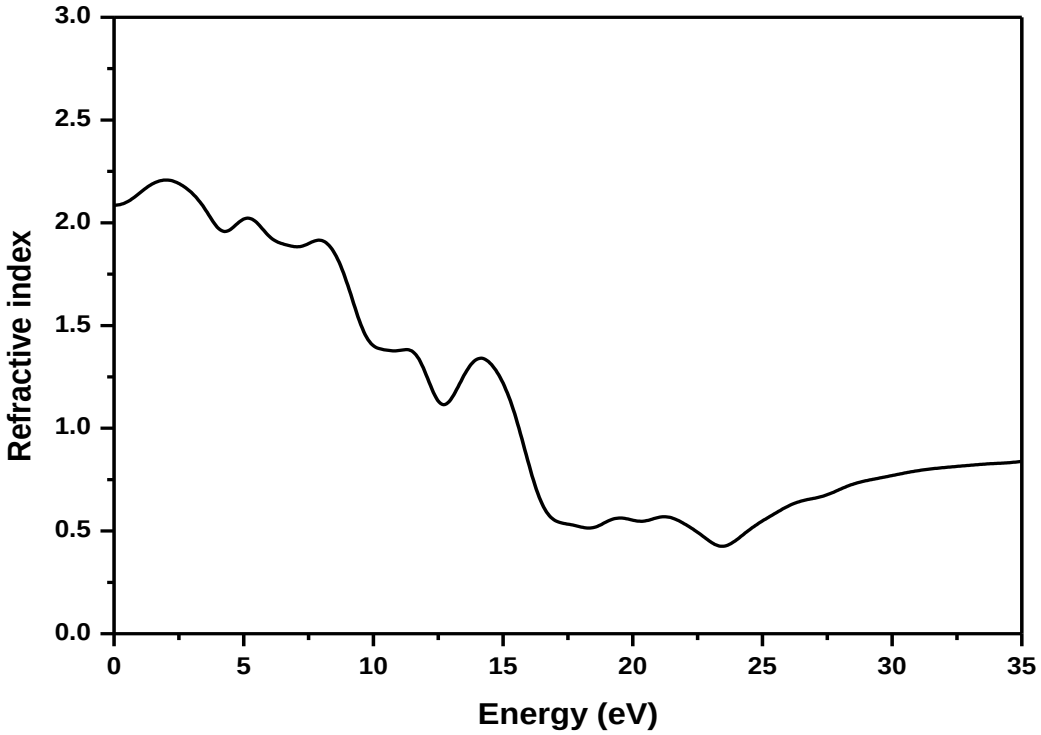

Fig. III.19. Refractive index spectrum for cubic double perovskite $Cs_2AgInBr_6$.

The optical absorption coefficient α(ω) is one of the most essential parameters for evaluating semiconductors for usage in photovoltaic devices. This optical parameter describes how far incident light travels into a substance before being absorbed. [37]. In the present work

α(ω) has been calculated for $Cs_2AgInBr_6$. Figure III.19 depicts our findings. We find that for photon incidence energies less than the basic absorption edge, is practically nil. Finally we find peaks at the energy threshold, followed by a plateau, and then a sudden drop in α. Light absorption appears to be greater at low photon wavelengths. This is due to an increase in the amount of electrons with sufficient energy to interact with photons. The prominent value bands of the optical transition channels of Ag-d/Br-p orbitals to the In-s/p conduction bands orbitals contribute to the absorption around the threshold. [43]. The photon energy of roughly 17 eV appears to be the top of α(ω) for $Cs_2AgInBr_6$. The perovskite in issue exhibits an absorption band in the energy range of 2.5-35 eV. The visible spectrum has a high absorption rate, which can be used in technological applications.

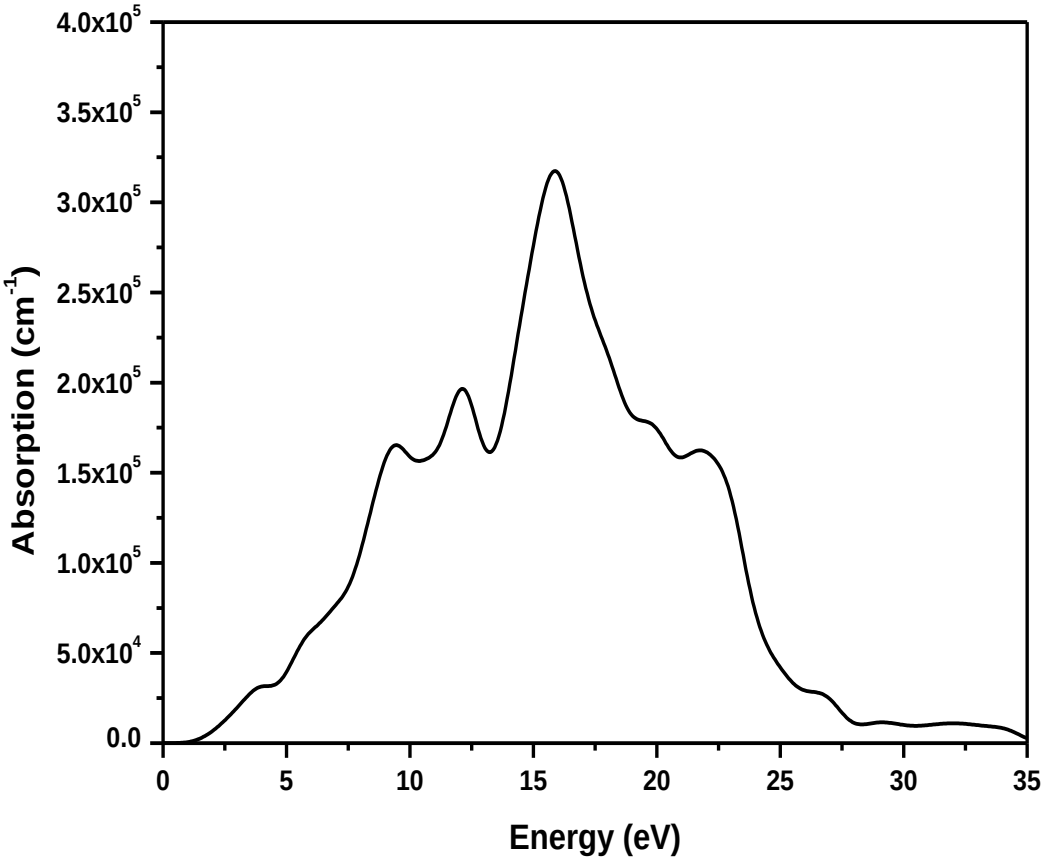

Fig. III.19 Absorption coefficient spectrum for cubic double perovskite $Cs_2AgInBr_6$.

III.3.1.2.1.c .Phonon stability

A phonon spectrum calculation was performed to determine the stability of this molecule. Indeed, understanding many characteristics of solid materials necessitates a thorough understanding of their lattice-dynamical properties, where phonons play an important role. The phonon dispersions curves were derived after performing lattice dynamics

simulations. In fact, a crystal lattice with n atoms per unit cell will have three n branches, three of which are acoustic and the rest are optical. All normal vibration modes must have a real and limited frequency, according to the dynamical stability criteria for a structure. Figure III.20 depicts our findings. As a result of the current computations, $Cs_2AgInBr_6$ is predicted to be dynamically unstable in this structure. Note that the phonon spectrum estimates are extended up to roughly -175 cm^{-1}, with negative values indicating a negative phonon spectrum in this region.

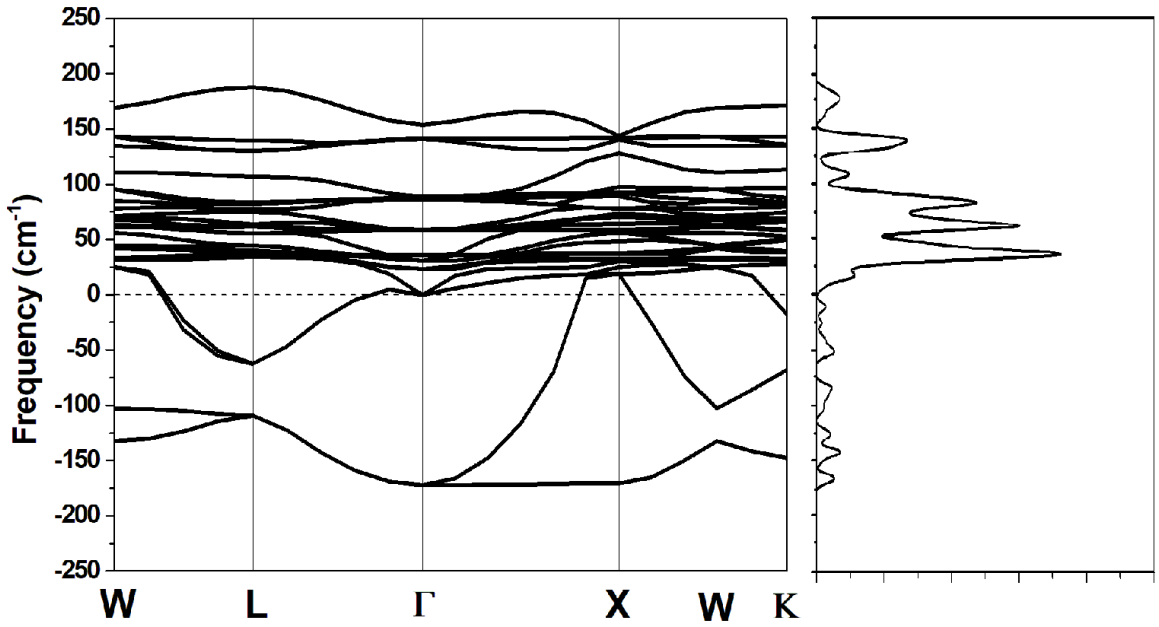

Fig. III.20. Phonon spectrum calculation for cubic double perovskite $Cs_2AgInBr_6$.

Zhao et al claim that after accounting for the finite temperature anharmonic effect, the imaginary phonons of $Cs_2AgInBr_6$ are totally stabilized**.** [43] justified this by the appearance of unstable phonons for $Cs_2AgBiCl_6$ which was synthesized experimentally[43] After accounting for the finite temperature anharmonic effect, the imaginary phonons of $Cs_2AgBiCl_6$ are clearly stabilized. This also applies to $Cs_2AgInBr_6$.

III.3.1.2.1.d . Elastic constant

The elastic parameters are fascinating physical numbers that are linked to many material properties. They define solid mechanical properties and give stability information. [81-84]. The number of distinct stiffness constants in cubic crystals with symmetry elements is three: C_{11}, C_{12}, and C_{44}. C_{11}, C_{12}, and C_{44} have been determined for the $Cs_2AgInBr_6$ double perovskite material in this paper. C_{11}=35.73 GPa, C_{12}=12.08 GPa, and C_{44}=10.71 GPa are the results of our research. These values appear to be low, indicating that strains in $Cs_2AgInBr_6$ are common. Because there isn't enough data in the literature to compare with, our findings

are only meant to be used as a guide. The mechanical stability of the $Cs_2AgInBr_6$.

The elastic parameters		
C_{11}	C_{12}	C_{44}
35.73 GPa	12.08 GPa	10.71 GPa

Table III. 5: The elastic parameters of $Cs_2AgInBr_6$ calculated in our work.

double perovskite at equilibrium is investigated using Cij's and the stability criteria presented in.

$$(C_{11} - C_{12}) \rangle 0 \quad \text{(III.1)}$$

$$C_{11} \rangle 0 \quad \text{(III.2)}$$

$$C_{44} \rangle 0 \quad \text{(III.3)}$$

$$(C_{11} + 2C_{12}) \rangle 0 \quad \text{(III.4)}$$

According to our obtained C_{ij}'s, all the stability criteria are satisfied

III.3.1.2.2 e. Computational details

The norm-conserving pseudopotential approach, as implemented in the CASTEP package[38], is used for all computations. The typical generalized gradient approximation of Perdew et al. (GGA-PBE) [39] is used to represent the exchange-correlation potential. To improve the accuracy of the band gaps, the functional hybrid B3LYP has been used. The functional hybrid B3LYP was employed to improve the precision of the band gaps. The plane wave cutoff energy for GGA-PBE computations is set to 1350 eV, whereas the k point meshes of Monkhorst and Pack [40]are selected to be $4\times4\times4$ special k points mesh. The cut-off plane wave basis set for functional hybrid B3LYP is 1224.5 eV, and the k-points for Brillouin zone sampling are $2\times2\times2$. The relaxations of electrons and ions are allowed only when the variation of the successive energies and forces is larger than 10^{-5} eV and 0.02 eV/Å, respectively.

Optical properties are computed using the GGA-PBE plus scissors.

The finite strain-stress method [70] is used for calculating the elastic constants (C_{ij}). By deriving the C_{ij}'s, polycrystalline elastic parameters are obtained using the Voigt-Reuss-Hill approximations [71-73].

III.4. conclusion

In this chapter, We focused on environmentally friendly lead-free perovskite materials in this work, in particular the lead free double perovskite. Where we chose the compounds $Cs_2AgBiBr_6$,$Cs_2AgInCl_6$ and $Cs_2AgInBr_6$ as samples for our study and based on the functional density theory, we calculated the electronic and optical properties of $Cs_2AgBiBr_6$, where the results of the electronic properties showed the presence of an indirect gap, which is a negative point that prevents it from being a good alternative to lead perovskite, On the other hand, the calculation of the electronic properties of compound $Cs_2AgInCl_6$ showed that this compound has a direct band gap, which is a very positive point, but the results of the calculation of the optical properties were disappointing,It showed a significant weakness in the absorption of light in the visible field, which makes it unsuitable for photovoltaic applications In addition, it has a wide energy gap.

Replacing base Cl with base Br in the previous compound gives compound $Cs_2AgInBr_6$, the latter has not yet been synthesized, but the results of our theoretical calculations of electronic properties were encouraging, as the results of our calculations showed that it has a direct bandgap of a suitable value (1.42 eV) for photovoltaic applications. Also, the light absorption coefficient in the visible field is a good value of the order of 10^4 Cm^{-1}. Although our calculations of the elasticity constants for this compound showed the mechanical stability of this compound. However, according to the criteria of dynamic stability of the structure, and from the results we obtained, we found that $Cs_2AgInBr_6$ is expected to be dynamically unstable in this structure.

Reference

1. Stranks, S.D. and H.J. Snaith, *Metal-halide perovskites for photovoltaic and light-emitting devices.* Nature nanotechnology, 2015. **10**(5): p. 391-402.
2. Johnston, M.B. and L.M. Herz, *Hybrid perovskites for photovoltaics: charge-carrier recombination, diffusion, and radiative efficiencies.* Accounts of chemical research, 2016. **49**(1): p. 146-154.
3. Tan, Z.-K., et al., *Bright light-emitting diodes based on organometal halide perovskite.* Nature nanotechnology, 2014. **9**(9): p. 687-692.
4. Wehrenfennig, C., et al., *Homogeneous emission line broadening in the organo lead halide perovskite ch3nh3pbi3–x cl x.* The journal of physical chemistry letters, 2014. **5**(8): p. 1300-1306.
5. Poglitsch, A. and D. Weber, *Dynamic disorder in methylammoniumtrihalogenoplumbates (II) observed by millimeter-wave spectroscopy.* The Journal of chemical physics, 1987. **87**(11): p. 6373-6378.
6. Baikie, T., et al., *Synthesis and crystal chemistry of the hybrid perovskite (CH 3 NH 3) PbI 3 for solid-state sensitised solar cell applications.* Journal of Materials Chemistry A, 2013. **1**(18): p. 5628-5641.
7. Stoumpos, C.C., C.D. Malliakas, and M.G. Kanatzidis, *Semiconducting tin and lead iodide perovskites with organic cations: phase transitions, high mobilities, and near-infrared photoluminescent properties.* Inorganic chemistry, 2013. **52**(15): p. 9019-9038.
8. Weller, M.T., et al., *Complete structure and cation orientation in the perovskite photovoltaic methylammonium lead iodide between 100 and 352 K.* Chemical communications, 2015. **51**(20): p. 4180-4183.
9. Herz, L.M., *Charge-carrier dynamics in organic-inorganic metal halide perovskites.* Annual review of physical chemistry, 2016. **67**: p. 65-89.
10. Filip, M.R., et al., *Steric engineering of metal-halide perovskites with tunable optical band gaps.* Nature communications, 2014. **5**(1): p. 1-9.
11. Xu, J., et al., *Unique ion diffusion properties in lead-free halide double perovskites: A first-principles study.* Journal of Power Sources, 2019. **412**: p. 689-694.
12. Sun, Q. and W.-J. Yin, *Thermodynamic stability trend of cubic perovskites.* Journal of the American Chemical Society, 2017. **139**(42): p. 14905-14908.
13. Dave, K., et al., *Recent Developments in Lead-Free Double Perovskites: Structure, Doping, and Applications.* Chemistry–An Asian Journal, 2020. **15**(2): p. 242-252.
14. Zhang, Z., et al., *Improvement of Cs2AgBiBr6 double perovskite solar cell by rubidium doping.* Organic Electronics, 2019. **74**: p. 204-210.
15. Schade, L., et al., *Structural and optical properties of Cs2AgBiBr6 double perovskite.* ACS Energy Letters, 2018. **4**(1): p. 299-305.
16. Yang, J., P. Zhang, and S.-H. Wei, *Band structure engineering of Cs2AgBiBr6 perovskite through order–disordered transition: A first-principle study.* The journal of physical chemistry letters, 2018. **9**(1): p. 31-35.

17. Fu, R., et al., *Pressure-induced structural transition and band gap evolution of double perovskite Cs 2 AgBiBr 6 nanocrystals.* Nanoscale, 2019. **11**(36): p. 17004-17009.
18. García-Espejo, G., et al., *Mechanochemical synthesis of three double perovskites: Cs 2 AgBiBr 6,(CH 3 NH 3) 2 TlBiBr 6 and Cs 2 AgSbBr 6.* Nanoscale, 2019. **11**(35): p. 16650-16657.
19. Greul, E., et al., *Highly stable, phase pure Cs 2 AgBiBr 6 double perovskite thin films for optoelectronic applications.* Journal of Materials Chemistry A, 2017. **5**(37): p. 19972-19981.
20. Xu, J., et al., *Intrinsic defect physics in indium-based lead-free halide double perovskites.* The journal of physical chemistry letters, 2017. **8**(18): p. 4391-4396.
21. McClure, E.T., et al., *Cs2AgBiX6 (X= Br, Cl): new visible light absorbing, lead-free halide perovskite semiconductors.* Chemistry of Materials, 2016. **28**(5): p. 1348-1354.
22. Bouarissa, N., *Optoelectronic properties of InAs1− xPx semiconducting alloys.* Materials Science and Engineering: B, 2001. **86**(1): p. 53-59.
23. Cohen, M.L. and J.R. Chelikowsky, *Wurtzite Structure Semiconductors*, in *Electronic Structure and Optical Properties of Semiconductors*. 1989, Springer. p. 140-160.
24. Bouarissa, N., *Electron and positron energy levels and deformation potentials in group-III Nitrides.* physica status solidi (b), 2002. **231**(2): p. 391-402.
25. Bechiri, A., F. Benmakhlouf, and N. Bouarissa, *Band structure of III–V ternary semiconductor alloys beyond the VCA.* Materials chemistry and physics, 2003. **77**(2): p. 507-510.
26. Martin, R.M., *Electronic structure: basic theory and practical methods*. 2020: Cambridge university press.
27. Bouarissa, N., *Pressure dependence of optoelectronic properties of GaN in the zinc-blende structure.* Materials chemistry and physics, 2002. **73**(1): p. 51-56.
28. Vurgaftman, I., J.á. Meyer, and L.á. Ram-Mohan, *Band parameters for III–V compound semiconductors and their alloys.* Journal of applied physics, 2001. **89**(11): p. 5815-5875.
29. Adachi, S., *Properties of semiconductor alloys: group-IV, III-V and II-VI semiconductors*. Vol. 28. 2009: John Wiley & Sons.
30. Bouarissa, N. and F. Annane, *Electronic properties and elastic constants of the ordered Ge1− xSnx alloys.* Materials Science and Engineering: B, 2002. **95**(2): p. 100-106.
31. Bouarissa, N., *Effects of compositional disorder upon electronic and lattice properties of GaxIn1− xAs.* Physics Letters A, 1998. **245**(3-4): p. 285-291.
32. Hannachi, L. and N. Bouarissa, *Band parameters for cadmium and zinc chalcogenide compounds.* Physica B: Condensed Matter, 2009. **404**(20): p. 3650-3654.
33. Mezrag, F., W.K. Mohamed, and N. Bouarissa, *The effect of zinc concentration upon optical and dielectric properties of Cd1− xZnxSe.* Physica B: Condensed Matter, 2010. **405**(9): p. 2272-2276.
34. Saib, S., et al., *Structural and dielectric properties of AlN under pressure.* Physica B: Condensed Matter, 2008. **403**(21-22): p. 4059-4062.
35. Djaili, S., et al., *Temperature dependence of the optical properties of MgO: Ab initio molecular dynamics calculations.* Optik, 2020. **200**: p. 163421.

36. Bouarissa, A., et al., *Band structure and optical properties of polyaniline polymer material.* Polymer Bulletin, 2018. **75**(7): p. 3023-3033.
37. Khaldi, A., N. Bouarissa, and L. Tabourot, *First-principles study of pressure dependence of optical spectra of MnS.* Journal of Superconductivity and Novel Magnetism, 2018. **31**(5): p. 1643-1647.
38. Clark, S.J., et al., *First principles methods using CASTEP.* Zeitschrift für Kristallographie-Crystalline Materials, 2005. **220**(5-6): p. 567-570.
39. Perdew, J.P., K. Burke, and M. Ernzerhof, *Generalized gradient approximation made simple.* Physical review letters, 1996. **77**(18): p. 3865.
40. Monkhorst, H.J. and J.D. Pack, *Special points for Brillouin-zone integrations.* Physical review B, 1976. **13**(12): p. 5188.
41. Volonakis, G., et al., *Cs2InAgCl6: a new lead-free halide double perovskite with direct band gap.* The journal of physical chemistry letters, 2017. **8**(4): p. 772-778.
42. Zhou, J., et al., *Composition design, optical gap and stability investigations of lead-free halide double perovskite Cs 2 AgInCl 6.* Journal of Materials Chemistry A, 2017. **5**(29): p. 15031-15037.
43. Zhao, X.-G., et al., *Cu–In halide perovskite solar absorbers.* Journal of the American Chemical Society, 2017. **139**(19): p. 6718-6725.
44. Mathew, N.P., N.R. Kumar, and R. Radhakrishnan, *First principle study of the structural and optoelectronic properties of direct bandgap double perovskite Cs2AgInCl6.* Materials Today: Proceedings, 2020. **33**: p. 1252-1256.
45. Soni, A., K. Bhamu, and J. Sahariya, *Investigating effect of strain on electronic and optical properties of lead free double perovskite Cs2AgInCl6 solar cell compound: A first principle calculation.* Journal of Alloys and Compounds, 2020. **817**: p. 152758.
46. Tran, T.T., et al., *Designing indirect–direct bandgap transitions in double perovskites.* Materials Horizons, 2017. **4**(4): p. 688-693.
47. Luo, J., et al., *Cs2AgInCl6 double perovskite single crystals: parity forbidden transitions and their application for sensitive and fast UV photodetectors.* Acs Photonics, 2018. **5**(2): p. 398-405.
48. Zhou, J., et al., *Exploring the transposition effects on the electronic and optical properties of Cs 2 AgSbCl 6 via a combined computational-experimental approach.* Journal of Materials Chemistry A, 2018. **6**(5): p. 2346-2352.
49. Luo, J., et al., *Efficient and stable emission of warm-white light from lead-free halide double perovskites.* Nature, 2018. **563**(7732): p. 541-545.
50. Li, T., et al., *Intrinsic defect properties in halide double perovskites for optoelectronic applications.* Physical Review Applied, 2018. **10**(4): p. 041001.
51. Adachi, S., *Properties of Group-IV, III–V and II–VI Semiconductors, Wiley.* Chichester, England, 2005.
52. Heriche, H., Z. Rouabah, and N. Bouarissa, *New ultra thin CIGS structure solar cells using SCAPS simulation program.* International Journal of Hydrogen Energy, 2017. **42**(15): p. 9524-9532.
53. Bouarissa, A., et al., *Modeling of ZnO/MoS2/CZTS photovoltaic solar cell through window, buffer and absorber layers optimization.* Materials Science and Engineering: B, 2021. **263**: p. 114816.

54. Suzuki, N., K. Sawai, and S. Adachi, *Optical properties of PbSe.* Journal of applied physics, 1995. **77**(3): p. 1249-1255.
55. Kanazawa, H. and S. Adachi, *Spectroellipsometry and electroreflectance of PbS.* Journal of applied physics, 1998. **84**(9): p. 5342-5344.
56. Zerroug, S., F.A. Sahraoui, and N. Bouarissa, *Ab initio calculations of yttrium nitride: structural and electronic properties.* Applied Physics A, 2009. **97**(2): p. 345-350.
57. Benmakhlouf, F., A. Bechiri, and N. Bouarissa, *Zinc-blende ZnS under pressure: predicted electronic properties.* Solid-State Electronics, 2003. **47**(8): p. 1335-1338.
58. Kassali, K. and N. Bouarissa, *Effect of nitrogen concentration on electronic energy bands of Ga1− xInxNyAs1− y alloys.* Microelectronic engineering, 2000. **54**(3-4): p. 277-286.
59. Khan, M.A. and N. Bouarissa, *Optical and energy-loss spectra of ZnS from ab initio molecular dynamics simulation: temperature effect.* Optik, 2013. **124**(21): p. 5095-5098.
60. Bouarissa, A., et al., *Optical response and magnetic moment of MoS2 material.* Optik, 2020. **208**: p. 164080.
61. Bouarissa, N., *The effect of hydrostatic pressure on the electronic and optical properties of InP.* Solid-State Electronics, 2000. **44**(12): p. 2193-2198.
62. Ozaki, S. and S. Adachi, *Optical constants of ZnS x Se1− x ternary alloys.* Journal of applied physics, 1994. **75**(11): p. 7470-7475.
63. Suzuki, K.-i. and S. Adachi, *Optical constants of Cd x Zn 1− x Se ternary alloys.* Journal of applied physics, 1998. **83**(2): p. 1018-1022.
64. Rizwan, M., et al., *First principles investigation of electronic and optical properties of AgAlO2.* Chinese journal of physics, 2018. **56**(5): p. 2186-2190.
65. Herve, P. and L. Vandamme, *General relation between refractive index and energy gap in semiconductors.* Infrared physics & technology, 1994. **35**(4): p. 609-615.
66. Ravindra, N. and P. Ganapathy, *Choi Infrared Phys.* Technol, 2007. **50**: p. 21.
67. Bouarissa, N., *Energy gaps and refractive indices of AlxGa1− xAs.* Materials chemistry and physics, 2001. **72**(3): p. 387-394.
68. Gueddim, A., S. Zerroug, and N. Bouarissa, *Optical characteristics of ZnTe1− xOx alloys from first-principles calculations.* Journal of luminescence, 2013. **135**: p. 243-247.
69. Haq, B.U., et al., *Optoelectronic properties of PbSe monolayers from first-principles.* Applied Surface Science, 2020. **525**: p. 146521.
70. Milman, V. and M. Warren, *Elasticity of hexagonal BeO.* Journal of Physics: Condensed Matter, 2001. **13**(2): p. 241.
71. Voigt, W., *Lehrbuch der Kristallphysik (Textbook of crystal physics).* BG Teubner, Leipzig und Berlin, 1928.
72. Hill, R., *The elastic behaviour of a crystalline aggregate.* Proceedings of the Physical Society. Section A, 1952. **65**(5): p. 349.
73. Hill, R., *Elastic properties of reinforced solids: some theoretical principles.* Journal of the Mechanics and Physics of Solids, 1963. **11**(5): p. 357-372.

74. Zhang, Z., et al., *Potential applications of halide double perovskite Cs2AgInX6 (X= Cl, Br) in flexible optoelectronics: unusual effects of uniaxial strains.* The journal of physical chemistry letters, 2019. **10**(5): p. 1120-1125.
75. Liang, Y., *Exploring inorganic and nontoxic double perovskites Cs2AgInBr6 (1− x) Cl6x from material selection to device design in material genome approach.* Journal of Alloys and Compounds, 2021. **862**: p. 158575.
76. Adachi, S., *Band gaps and refractive indices of AlGaAsSb, GaInAsSb, and InPAsSb: Key properties for a variety of the 2–4-μm optoelectronic device applications.* Journal of applied physics, 1987. **61**(10): p. 4869-4876.
77. Boucenna, M. and N. Bouarissa, *Refractive index and dielectric constants of GaxIn1− xP: Disorder effect.* Optik, 2014. **125**(22): p. 6611-6615.
78. Bouarissa, N., *Effective masses of electrons, heavy holes and positrons in quasi-binary (GaSb) 1− x (InAs) x crystals.* Journal of Physics and Chemistry of Solids, 2006. **67**(7): p. 1440-1443.
79. Saib, S. and N. Bouarissa, *High-pressure band parameters for GaAs: first principles calculations.* Solid-state electronics, 2006. **50**(5): p. 763-768.
80. Zerroug, S., F.A. Sahraoui, and N. Bouarissa, *Structural parameters and pressure coefficients for CdS x Te 1-x: FP-LAPW calculations.* The European Physical Journal B, 2007. **57**(1): p. 9-14.
81. Bouarissa, N. and K. Kassali, *Erratum to phys. stat. sol.(b) 228, No. 3, 663–670 (2001): Mechanical Properties and Elastic Constants of Zincblende Ga1—xInxN Alloys.* physica status solidi (b), 2002. **231**(1): p. 294-294.
82. Kim, K., W.R. Lambrecht, and B. Segall, *Elastic constants and related properties of tetrahedrally bonded BN, AlN, GaN, and InN.* Physical Review B, 1996. **53**(24): p. 16310.
83. Bouarissa, N., *Elastic constants and acoustical phonon properties of GaAsxSb1− x.* Materials chemistry and physics, 2006. **100**(1): p. 41-47.
84. Daoud, S., N. Bioud, and N. Bouarissa, *Structural phase transition, elastic and thermal properties of boron arsenide: pressure-induced effects.* Materials Science in Semiconductor Processing, 2015. **31**: p. 124-130.

.

General Conclusion

General Conclusion

we have theoretically studied the lead-free perovskite compounds, which are a large family, and our interest was in the lead free double perovskite. Where we chose the compounds $Cs_2AgBiBr_6$,$Cs_2AgInCl_6$ and $Cs_2AgInBr_6$ as samples for our study ,and we studied the electronic and optical properties of these materials. And we added the elastic and dynamic properties in particular for the compound $Cs_2AgInBr_6$.

Our study relied on The DFT computations that were carried out using ab initio pseudopotential plane-wave method within the GGA-PBE exchange-correlation functional. To improve the accuracy of the fundamental gap, a functional hybrid B3LYP was used , All calculations were made using CASTEP code.

The obtained results showed that $Cs_2AgBiBr_6$ has good absorption in the visible spectrum region. However, the basic bandgap energy was found to be indirect. This indicates that its application in photovoltaic cells is limited. The indirect energy gap of this compound made us move towards another compound of double perovskite so that In this compound, base Bi is replaced by base In known by the formula Cs_2AgInX_6 (x= Cl,Br). The results obtained from calculating the electronic properties of compound $Cs_2AgInCl_6$ showed that this compound has a direct band gap, but with a large value (3.62 eV). Also, the results of calculating the optical properties showed that its absorption of visible light is weak. In order to reduce the energy gap value, we calculated the energy gap for this compound under strain, but the results were not sufficient as the gap value did not change much, and the same was true for the absorption coefficientWe moved to the third compound $Cs_2AgInBr_6$, and through the results of calculating the electronic properties, it appeared that replacing halide Cl with halide Br in compound $Cs_2AgInBr_6$ leads to a decrease in the value of the direct band gap, where we found its value of 1.427 eV, which is a good value for photovoltaic applications. In addition, through the results of our calculation of the optical properties, it was found that this compound has a large absorption coefficient($> 10^4$ cm^{-1}). Although our studies of the elasticity constants for this chemical revealed that it is mechanically stable. However, we discovered that $Cs_2AgInBr_6$ is projected to be dynamically unstable in this structure based on the structure's dynamic stability criteria and the data we got. Moreover, this compound has not been synthesized so far.

In general, by calculating the electronic properties of Compounds $Cs_2AgBiBr_6$, $Cs_2AgInCl_6$ and $Cs_2AgInBr_6$ we observed a flat band at the level of VBM in direction $\Gamma \rightarrow X$ These flat bands greatly increase the mass. Effective and can prevent the charge carrier

transfer in the solar cell.

In the end, it can be said that replacing lead perovskite with lead-free perovskite is not an easy task. Through our study of the compounded perovskite compounds $Cs_2AgBiBr_6$, $Cs_2AgInCl_6$, and $Cs_2AgInBr_6$, it became clear that these compounds are not ready to be the best alternative to lead perovskite due to some problems such as the difficulty of manufacturing that compound 1 suffers from. Facing these problems will constitute a challenge in the future for researchers in this field, as there is another solution that can be more effective by moving to another family of lead-free perovskite, which is chalcogenide perovskite.

Abstract

Our work focused on studying the electronic and optical properties of lead-free halide double perovskite materials Cs_2AgInX_6 (X = Cl,Br) and $Cs_2AgBiBr_6$, These properties help to obtain the required photovoltaic and optoelectronic properties of these materials. Our computations will be based on the first-principles calculations Using castep code within GGA and hybrid functional (B3LYP) Our calculations showed that compound $Cs_2AgBiBr_6$ has an indirect band gap, which makes it unsuitable for photovoltaic applications. As for compound $Cs_2AgInCl_6$, the calculations showed that it has a direct band gap ($\Gamma \rightarrow \Gamma$) with a value of 3.62 eV, but it is considered a discouraging result because of its high value, so it is not suitable for applications in the field of solar energy while the results of the $Cs_2AgInBr_6$ were encouraging and promising as the calculations gave a small Γ to Γ direct band gap in the visible range 1.427 eV for $Cs_2AgInBr_6$ and The optical absorption coefficient has been determined showing a high-absorption ($> 10^4$ cm^{-1}) with a wide absorption band suggesting that the material of interest-based solar cells may reach a good solar efficiency. But the Synthesis of this material has not yet been achieved. In addition, our theoretical results showed that it is dynamically unstable.

Keywords: Electronic properties; Optical absorption ; Photovoltaic applications ; Halide double perovskite.

Resumé

Notre travail a porté sur l'étude des propriétés électroniques et optiques des matériaux halogénures double pérovskite sans plomb Cs_2AgInX_6 (X = Cl,Br) et $Cs_2AgBiBr_6$, Ces propriétés permettent d'obtenir les propriétés photovoltaïques et optoélectroniques requises de ces matériaux. Nos calculs seront basés sur les calculs des premiers principes Utilisation du code castep dans GGA et fonctionnelle hybride (B3LYP) Nos calculs ont montré que le composé $Cs_2AgBiBr_6$ a une bande interdite indirecte, ce qui le rend inadapté aux applications photovoltaïques. Quant au composé $Cs_2AgInCl_6$, les calculs ont montré qu'il a une bande interdite directe ($\Gamma \rightarrow \Gamma$) avec une valeur de 3,62 eV, mais il est considéré comme un résultat décourageant en raison de sa valeur élevée, il n'est donc pas adapté aux applications sur le terrain de l'énergie solaire tandis que les résultats du $Cs_2AgInBr_6$ étaient encourageants et prometteurs car les calculs donnaient une petite bande interdite directe de Γ à Γ dans le domaine visible 1,427 eV pour $Cs_2AgInBr_6$ et Le coefficient d'absorption optique a été déterminé montrant une forte absorption ($> 10^4$ cm^{-1}) avec une large bande d'absorption suggérant que le matériau des cellules solaires basées sur l'intérêt peut atteindre un bon rendement solaire. Mais la synthèse de ce matériel n'a pas encore été réalisée. De plus, nos résultats théoriques ont montré qu'il est dynamiquement instable.

Mots clés : Propriétés électroniques ; Absorption optique ; Applications photovoltaïques ; Pérovskite double aux halogénures.

الملخص

ركز عملنا على دراسة الخصائص الإلكترونية والبصرية لمواد البيروفسكايت المزدوجة الهاليدي الخالية من الرصاص Cs_2AgInX_6 (X = Cl، Br) و $Cs_2AgBiBr_6$ ، تساعد هذه الخصائص في الحصول على الخصائص الكهروضوئية والإلكترونية الضوئية المطلوبة لهذه المواد، ستعتمد حساباتنا على حسابات المبادئ الأولى باستخدام كود castep داخل GGA والوظيفة الهجينة .(B3LYP)

اظهرت حساباتنا ان المركب $Cs_2AgBiBr_6$ له فجوه نطاق غير مباشره مما يجعله غير مناسب للتطبيقات الكهروضوئيه اما المركب $Cs_2AgInCl_6$ فاظهرت الحسابات انه يملك فجوة نطاق مباشرة $(\Gamma \rightarrow \Gamma)$ بقيمة تبلغ تبلغ 3.62 eV لكنها تعتبر نتيجة غير مشجعة بسبب قيمتها العاليه ، لذا فهي غير مناسبة للتطبيقات في مجال الطاقة الشمسية،بينما كانت نتائج $Cs_2AgInBr_6$ مشجعة وواعدة حيث أعطت الحسابات فجوة نطاق صغيرة إلى مباشرة في النطاق المرئي 1.427 eV لـ $Cs_2AgInBr_6$ و تم تحديد معامل الامتصاص البصري مما يدل على امتصاص عالي ($> 10^4$ cm^{-1}) مع نطاق امتصاص عريض مما يوحي بأن مادة الخلايا الشمسية القائمة على الفائدة قد تصل إلى كفاءة شمسية جيدة لكن تصنيع هذه الماده لم يتحقق بعد اضافه الى ذلك فقد اظهرت نتائجنا النظريه انه غير مستقر ديناميكيا.

الكلمات المفتاحية: الخصائص الإلكترونية ؛ امتصاص بصري؛ التطبيقات الكهروضوئية ؛ هاليد مزدوج بيروفسكايت.

UNIVERSITY MOHAMED BOUDIAF OF M'SILA - M'SILA

Faculty of Sciences

Department of Physics

Candidate: MENEDJHI Adel

Thesis is submitted to obtain the degree of 3rd Cycle Doctorate

Title: Theoretical investigation of fundamental properties of perovskite solar cell materials

INTERNATIONAL PUBLICATIONS

1. Halide double perovskite $Cs_2AgInBr_6$ for photovoltaic's applications: Optical properties and stability Adel Menedjhi [a], Nadir Bouarissa [a,b],*, Salima Saib a,b, Khaled Bouamama [c], Optik - International Journal for Light and Electron Optics
Received 1 February 2021; Received in revised form 30 April 2021; Accepted 12 May 2021

Available online 25 June 2021

2. Band Structure and Optical Spectra of Double Perovskite Cs2AgBiBr6 for Solar Cells Performance

A. Menedjhi [a;b], N. Bouarissaa;[b;]*, S. Saiba;[b,] M. Boucenna[b] and F. Mezraga;[b]

. journal of ACTA PHYSICA POLONICA A .2020

INTERNATIONAL COMMUNICATIONS

1.Electronic and optical properties of Lead Free double perovskite Cs2AgInCl6 for optoelectronic applications MENEDJH. A., BOUARISSA .N 1st International Conference on Sustainable Energy and Advanced Materials IC-SEAM'21 April 21-22, 2021, Ouargla, ALGERIA (Virtual) IC-SEAM'21 April 21-22, 2021, Ouargla, ALGERIA,

NATIONAL COMMUNICATIONS

1. Band structure and optical spectra of cubic perovskite CsSnX3 for solar Cells performance MENEDJHI.A, BOUARISSA.N . La 1 ére conference Nationale sur la Transition Energétique en Algérie CNTEA-2020,du 08 09 Mars 2020 à l'Université Mohamed Boudiaf de M'sila –Algerie

PEOPLE'S DEMOCRATIC REPUBILC OF ALGERIA

MINISTRY OF HIGHER EDUCATION AND SCIENTIFIC RESEARCH
UNIVERSITY OF KASDI MERBAH OUARGLA
FACULTY OF MATHEMATICS AND MATTER SCIENCES

****

N° : TAM428/2021

1st International Conference on Sustainable Energy and Advanced Materials
IC-SEAM'21 April 21-22, 2021, Ouargla, ALGERIA (Virtual conference)

****

CERTIFICATE OF PARTICIPATION

The organizing committee of the first International Conference on Sustainable Energy and Advanced Materials IC-SEAM'21 April 21-22, 2021, Ouargla, ALGERIA, certifies that:

Adel MENEDJHI

presented a Poster communication entitled:

Electronic and optical properties of Lead Free double perovskite Cs2AgInCl6 for optoelectronic applications

Co-author (s): NADIR BOUARISSA

Dean of the Faculty
Pr. Djamel BECHKI

Coordinator of IC-SEAM'21
Dr. Lazhar BENMEBROUK

Chairman of the IC-SEAM'21
Dr. Lazhar MOHAMMEDI

République Algérienne Démocratique et Populaire
Ministère de l'Enseignement Supérieur et de la Recherche Scientifique
Université Mohamed Boudiaf de M'sila
Département de Physique, Faculté des Sciences
1ère ConférenceNationale sur la TransitionEnergétique en Algérie

Attestation de Participation

Le comité d'organisation de la 1ère Conférence Nationale sur la Transition Energétique en Algérie

"CNTEA1-2020 " qui s'est tenue du 08 au 09 Mars 2020 à l'Université Mohamed Boudiaf de M'sila- Algérie, atteste que :

MENEDJHI Adel

A participé (e) avec succès aux travaux de la conférence en présentant une communication **Poster** *intitulée:*

Band Structure and Optical Spectra of Cubic Perovskite $CsSnX_3$ for Solar Cells Performance

Co-auteur(s) : ***N. BOUARISSA***

Président de la Conférence

Dr. SALMI Mohamed

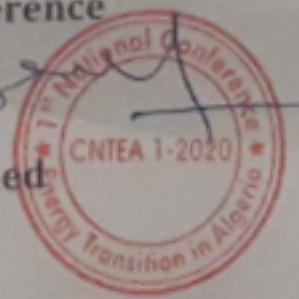

Doyen de la Faculté

Pr. BENSACI Ettayib

Optik - International Journal for Light and Electron Optics 243 (2021) 167198

Contents lists available at ScienceDirect

Optik - International Journal for Light and Electron Optics

journal homepage: www.elsevier.com/locate/ijleo

Original research article

Halide double perovskite $Cs_2AgInBr_6$ for photovoltaic's applications: Optical properties and stability

Adel Menedjhi [a], Nadir Bouarissa [a,b,*], Salima Saib [a,b], Khaled Bouamama [c]

[a] Laboratory of Materials Physics and Its Applications, University of M'sila, 28000 M'sila, Algeria
[b] Physics Department, Faculty of Science, University of M'sila, 28000 M'sila, Algeria
[c] LESIMS, Département de Physique, Université Ferhat Abbas, Sétif 19000, Algeria

ARTICLE INFO

Keywords:
$Cs_2AgInBr_6$
Halide double perovskite
Electronic structure
Optical spectra
Photovoltaic's
Stability

ABSTRACT

Theoretical calculations on halide double perovskite $Cs_2AgInBr_6$ electronic properties and optical spectra are carried out. The hybrid functional B3LYP calculations have been used indicating a 1.427 eV direct to band gap. The optical absorption coefficient has been determined showing a high-absorption ($> 10^4$ cm^{-1}) within a large absorption range suggesting that the perovskite of interest-based solar cells may reach a good solar efficiency. Based on the refractive index spectrum, the $Cs_2AgInBr_6$ static refractive index is estimated and found to be 2.09. The stability, phonon spectrum, electron effective mass and absorption spectrum with solar spectrum at AM1.5 of $Cs_2AgInBr_6$ have been computed and verified.

1. Introduction

Much attention has been given to perovskite-type materials for photovoltaic devices performances [1–5]. This is principally due to their amazing optical and electronic properties. As a matter of fact, perovskite solar cells with good performance are instable. Moreover, they are based on lead which is toxic [6]. Unfortunately, this make their use in photovoltaic's very limited. Alternatively, a new generation perovskites of double perovskites have been suggested so as to solve this problem [7–9]. The proposed materials are inorganic, stable, non toxic, and have been successfully synthesized [7–11]. This makes them good candidates for photovoltaic applications. $Cs_2AgInBr_6$ is among double perovskites materials which has been given many considerations during the last years and proposed to be an excellent candidate for technological applications, especially in the photovoltaic field. Although some fundamental properties of the material under focus were studied [12–15], only a few data were reported about its optical and electronic properties which have an important role in designing and fabricating devices that use the perovskite in question [16–18] . In fact, Liang [15] has carried out a systematic modeling so as to formulate a new system of solar absorption layer based on Cs_2AgInX_6 and its hetero-junction device. The optimized $Cs_2$2$InAgBr_5Cl$ compound is a marvelous solar absorption layer which is consistent with $Cs_2AgInBr_6$ at standard room temperature (298 K). On the other hand, Zhang et al. [13] have discovered that the Cs_2AgInX_6 (X=Cl, Br) have provided an efficient way to search promising solar cell absorbers. Even though that Cs_2AgInX_6(X=Cl, Br) have a similar structure, the strained Cs_2AgInX_6 (X=Cl, Br) physical properties vary differently. The direct-to-indirect phase transition is undergone in compressive $Cs_2AgInBr_6$. This makes the material of interest as a good radiation detection material. Furthermore, its absorption coefficient is obtained negligibly by strains. This makes the material as a potential one for further applications of photovoltaics. This has motivated us to take such a study on the band structure and optical spectra of the double perovskites material $Cs_2AgInBr_6$ using the density functional theory (DFT) computations. Moreover, phonon spectrum calculation and mechanical stability of the material under consideration has been checked via the elastic constants.

* Corresponding author.
E-mail address: nadir.bouarissa@univ-msila.dz (N. Bouarissa).

https://doi.org/10.1016/j.ijleo.2021.167198
Received 1 February 2021; Received in revised form 30 April 2021; Accepted 12 May 2021
Available online 25 June 2021

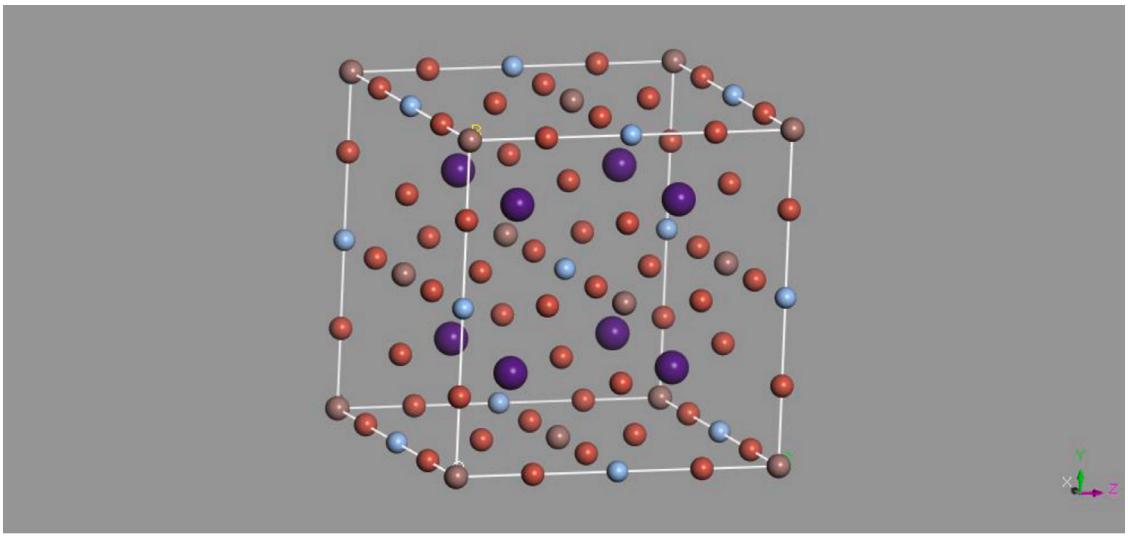

(a)

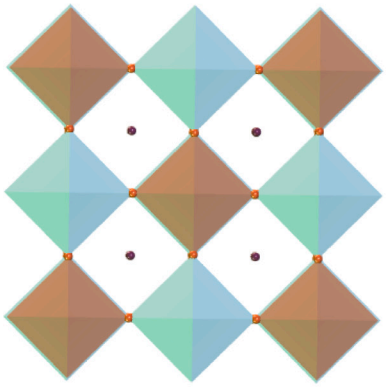

(b)

Fig. 1. (a) Crystalline cell of double perovskite $Cs_2AgInBr_6$ (b) Crystal structure of double perovskite $Cs_2AgInBr_6$ with two types of octahedral $InBr_6$ (Brown color) and $AgBr_6$ (blue color) and Cs atoms with violet color. (For interpretation of the references to color in this figure legend, the reader is referred to the web version of this article.)

2. Computational details

All computations are executed using the norm-conserving pseudopotential method as implemented in the CASTEP package [19]. The exchange–correlation potential is represented by the conventional generalized gradient approximation of Perdew et al. (GGA-PBE) [20]. To improve the accuracy of the band gaps, the functional hybrid B3LYP has been used. For the GGA-PBE calculations, the plane wave cutoff energy is set to be 1350 eV, whereas the k point meshes of Monkhorst and Pack [21] are selected to be 4 × 4x4 special k points mesh. When using functional hybrid B3LYP, the cut-off plane wave basis set is 1224.5 eV and k-points for Brillouin zone sampling are 2 × 2x2. The relaxations of electrons and ions are allowed only when the variation of the successive energies and forces is larger than 10^{-5} eV and 0.02 eV/Å, respectively.

Optical properties are computed using the GGA-PBE plus scissors.

The finite strain–stress method [22] is used for calculating the elastic constants (C_{ij}.

By deriving the C_{ij}'s, polycrystalline elastic parameters are obtained using the Voigt–Reuss–Hill approximations [23–26].

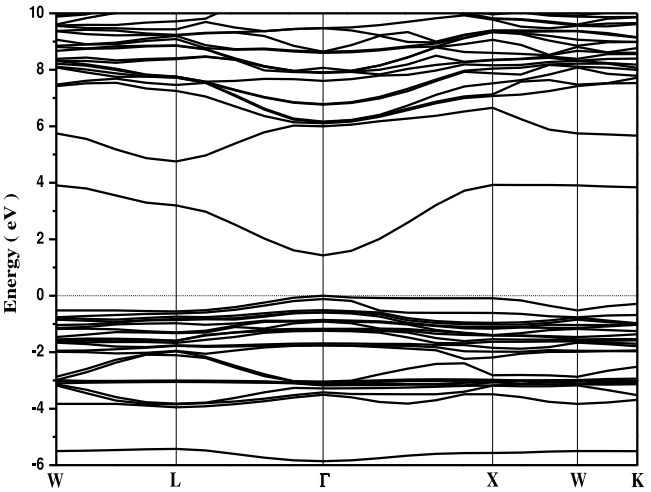

Fig. 2. Electronic band structure for cubic double perovskite $Cs_2AgInBr_6$. (For interpretation of the references to color in this figure legend, the reader is referred to the web version of this article.)

3. Results and discussion

Fig. 1(a) displays the crystalline cell of double perovskite $Cs_2AgInBr_6$ material. The Cs is represented by the violet color, the Ag by the blue color, the In by the brown color and the Br by the red color. The crystal structure is cubic. The group symmetry is FM3M. The lattice constant of the primitive cell is 7.94 Å. Fig. 1 (b) displays the crystal structure of double perovskite $Cs_2AgInBr_6$ with two types of octahedral $InBr_6$ (brown color) and $AgBr_6$ (blue color) and Cs atoms with (violet color).

The electronic band structure and its related parameters are important physical features for describing the optoelectronic properties of materials [27–30] . In fact, a precious knowledge of band features of semiconducting materials permits an accurate information about their synthesis and devices fabrication [31–33]. In the present work, the electronic structure of $Cs_2AgInBr_6$ double perovskite has been computed using the functional hybrid B3LYP approach as mentioned in Section 2. Our findings are displayed in Fig. 2. The picture seems to be similar to those commonly reported for semiconducting materials [34,35]. The main difference lies in the materials fundamental energy gap. Note that Fermi level does not cross the energy bands. This indicates that the material in question is a semiconductor material. A close inspection of Fig. 2 indicates that $Cs_2AgInBr_6$ has a direct ($\Gamma \rightarrow \Gamma$) gap energy since both valence band top and lowest conduction band are located at point in the Brillouin zone. The lowest conduction band is dominated by σ^* antibonding. It is essentially composed of Ag-s states of $AgBr_6$ octahedran and In-s orbitals of the $InBr_6$ octahedran. The valence band maximum is dominated by Ag-d and Br-p orbitals of the $AgBr_6$ octahedran with the small In-d orbitals of the $InBr_6$ octahedran [13]. The direct ($\Gamma \rightarrow \Gamma$) energy gap of $Cs_2AgInBr_6$ recorded by the authors results is 1.427 eV. This value is larger than that of 0.58 eV reported in Refs. [12,13] and obtained by using local density approximation (LDA). As a matter of fact, LDA methods are known to underestimate the band gap values with respect to experiment [36,37].

To assess the stability of this compound, a phonon spectrum calculation has been realized. In fact, in order to understand many aspects in solid materials requires a good knowledge of their lattice-dynamical properties where phonons play an interesting role. For that, the lattice dynamics calculations have been performed and the phonon dispersions curves have been obtained. As a matter of fact, a crystal lattice that has n atoms per unit cell will has 3 n branches, three among them are acoustic and the rest of them are optical. The dynamical stability conditions for a structure tell us that all normal vibration modes must show real and finite frequency. Our results are shown in Fig. 3. From this figure, one can see that the imaginary frequencies (below zero in the ordinate scale of Fig. 3) exist for $Cs_2AgInBr_6$ structure. Hence, the present calculations predict that $Cs_2AgInBr_6$ is unstable dynamically in this structure. Note that the phonon spectrum calculations are extended up to about -175 cm^{-1} showing negative values which indicate that the phonon spectrum is negative in this region.

The theoretical electron effective mass in general turns out to be a tensor. Hence, the electron effective mass is a direction dependent quantity. However, for a very idealized simple case, the electron effective mass becomes a scalar which does not depend on the direction. Hence, we use only one scalar effective mass. In this approach, the electron effective mass of $Cs_2AgInBr_6$ has been used in the electron conduction band minimum from the band curvature. Thus, the electron effective mass of $Cs_2AgInBr_6$ has been computed. Our results gives a value of m_e^*=3.47 m_0 , where m_0 is the electron free-particle mass. In the absence for other theoretical or experimental data for this value to compare with, our result is a prediction.

The partial density of states (PDOS) have been computed so as to investigate the distribution of the electrons on various orbitals. In this context, PDOS has been plotted in Fig. 4 for $Cs_2AgInBr_6$ double perovskite. A close examination of Fig. 4 shows that the first region of PDOS is the most tightly bound energy band. The contribution of the Ag-d and Br-p electrons is predominant in the interval energy from −4 to 0.5 eV, whereas that of the Ag-s and In-p electrons is predominant in the interval energy ranging from 1 to 5 eV. The upper valence bands are formed of the Ag-d and Br-p orbitals antibonding states, whereas conduction bands

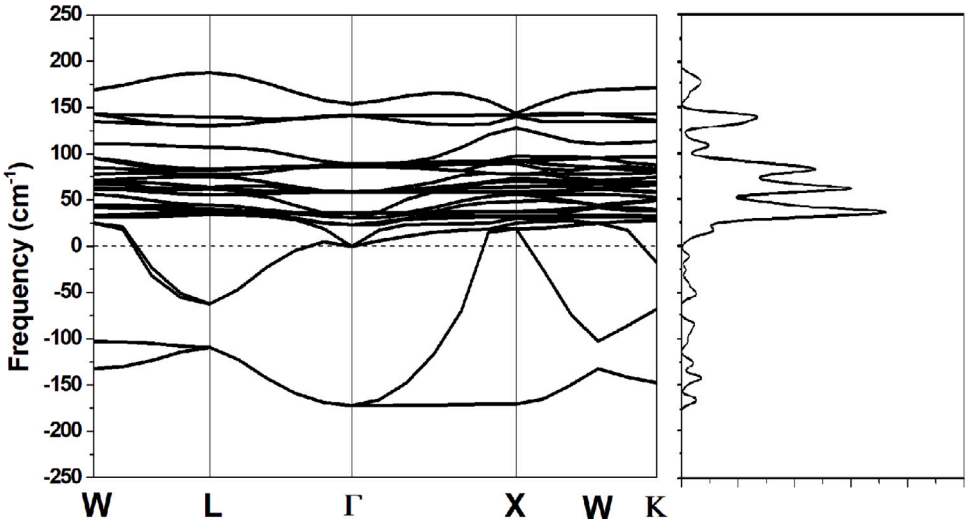

Fig. 3. Phonon spectrum calculation for cubic double perovskite $Cs_2AgInBr_6$. (For interpretation of the references to color in this figure legend, the reader is referred to the web version of this article.)

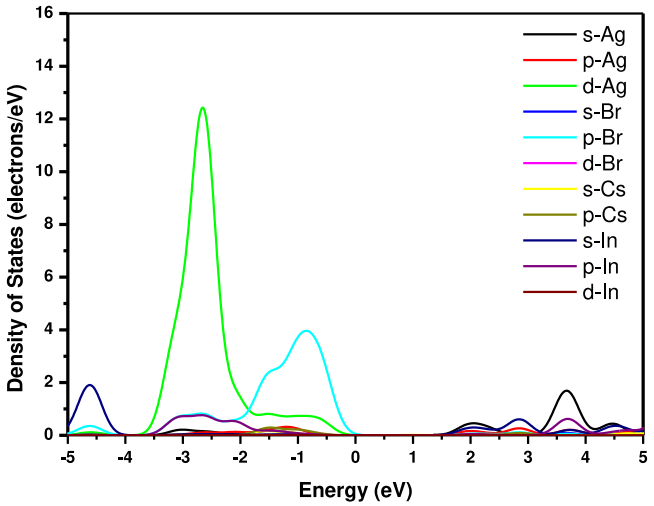

Fig. 4. Partial density of states (PDOS) of cubic double perovskite $Cs_2AgInBr_6$. (For interpretation of the references to color in this figure legend, the reader is referred to the web version of this article.)

are in antibonding manner predominated by the In-s/p orbitals with the Br-p orbital. For energy bands near the Fermi level of the $Cs_2AgInBr_6$ double perovskite material, the contribution of the Ag-d electrons is the predominant. This indicates that the Ag-d electrons have an interesting role for the conductibility in the perovskite under focus.

The optical properties of solid materials are useful features to be used in research and device applications [16,38–43]. The refractive index (n) is an important optical feature which is useful for designing and fabricating devices. It can be regarded as the parameter by which the radiation speed and wavelength are reduced with respect to their vacuum values. In the current work, n is obtained against the photon energy for $Cs_2AgInBr_6$ material. The n(E) spectrum, is illustrated in Fig. 5. At zero photon energy, the static refractive index is recorded as n(0)=2.09. Due to the lack of both theoretical and experimental values regarding n(0) for $Cs_2AgInBr_6$, to the authors knowledge, the present finding is a prediction. We observe that the values of n are large in low photon energy region but decreases in high photon energy region. A presence of peaks that come from the excitonic transitions is noticed. The peaks are more pronounced in low photon energy region than in high photon energy region. The effect of excitonic tends to increase the oscillator strength at M_0 and M_1 points [44,45]. The main peak of n(E) is related essentially to the 2D exciton transitions (E_1).

The optical absorption coefficient $\alpha(\omega)$ is among the important evaluation criteria of semiconductors for their use for photovoltaic devices. This optical parameter characterizes the distance traveled by the incident light inside the material before being absorbed [46]. In the present work $\alpha(\omega)$has been calculated for $Cs_2AgInBr_6$. The authors findings are plotted in Fig. 6. We observe

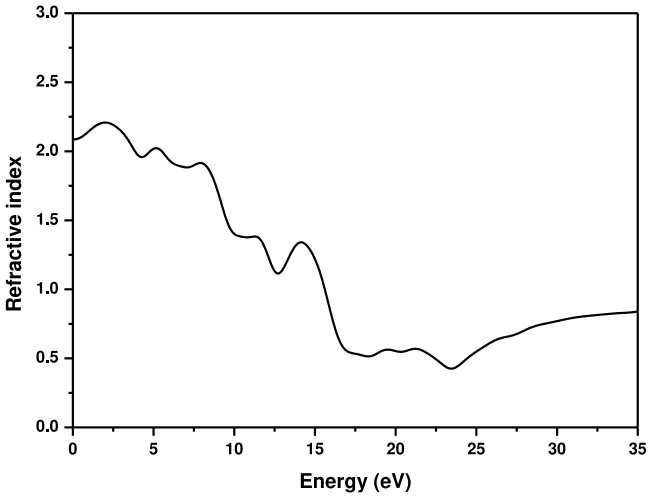

Fig. 5. Refractive index spectrum for cubic double perovskite $Cs_2AgInBr_6$. (For interpretation of the references to color in this figure legend, the reader is referred to the web version of this article.)

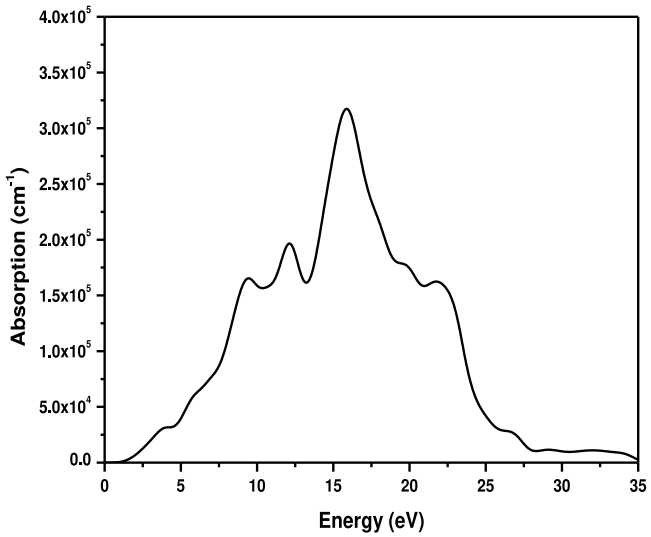

Fig. 6. Absorption coefficient spectrum for cubic double perovskite $Cs_2AgInBr_6$. (For interpretation of the references to color in this figure legend, the reader is referred to the web version of this article.)

that α is practically zero for photon incident energies smaller than the fundamental absorption edge. We see then peaks at the energy threshold, accompanied by a plateau, and afterwards an abrupt decrease of α . The absorption of light seems to be higher in the low photon wavelengths. This is due to the augmentation of the number of electrons that have an energy allowing them to interact with photons. Near threshold, the contribution of the absorption comes from the dominant value bands of the optical transition channels of Ag-d/Br-p orbitals to the In-s/p conduction bands orbitals [14]. The top of $\alpha(\omega)$ for $Cs_2AgInBr_6$ seems to occur at a photon energy of about 17 eV. The perovskite in question presents a band of absorption in the energy interval of about 2.5–35 eV. A high absorption of light in the visible spectrum can be technological applications.

The elastic parameters are interesting physical quantities which are linked to different properties of materials. They describe solid mechanical properties and provide information about their stability [47–50]. For cubic crystals which possess symmetry elements, the number of independent stiffness constants is three which are C_{11}, C_{12} and C_{44}. In the present contribution, C_{11}, C_{12} and C_{44} have been determined for $Cs_2AgInBr_6$ double perovskite material. Our results yield values of C_{11}=35.73, C_{12}=12.08 and C_{44}=10.71 GPa. These values seem to be low which makes strains occur easily in $Cs_2AgInBr_6$. Due to the lack of data in the literature to compare with, to the authors knowledge, our results are only for reference.

Table 1
Power density of each standard spectrum with the proportion of blue light in the 300–475 nm-wavelength region [53].

Solar conditions	Power density (W m^{-2})	Spectral proportion useful for down-shifters (%)
AM0	1366.1	17.3
AM1.5G	1000	14.5
AM1.5D	900	12.5
AM1.5Diff	100	34.7

The mechanical stability of $Cs_2AgInBr_6$ double perovskite at equilibrium are examined via C_{ij}'s based on the criteria of stability described in Refs. [51,52].

$$(C_{11} - C_{12}) > 0 \quad (1)$$

$$C_{11} > 0 \quad (2)$$

$$C_{44} > 0 \quad (3)$$

$$(C_{11} + 2C_{12}) > 0 \quad (4)$$

According to our obtained C_{ij}'s, all the stability criteria are satisfied. However, according to the phonon spectrum calculation, as has been discussed above, the stability is not extended up to about -175 cm^{-1} .

The solar spectrum varies during the day and with location. This makes the down-shifter efficiency dependent on the spectral energy distribution [53]. The efficiency of the down-shifter has been estimated. Under excellent atmospheric conditions, around 13.5% of the incident energy going from a wavelength range from 300 to 475 nm has been evaluated. This proposition is much higher, that is, 22.5% under diffuse atmosphere conditions. This makes the down-shifter much more efficient for the solar cell. The absorption spectroscopy is among the spectroscopic techniques which measure the absorption of radiation as a function of frequency. The energy is observed by the sample, i.e. phonons. The variation of the intensity of the absorption versus frequency is the absorption spectrum. For efficiency meant, the different kinds of reference spectra are: (1) The air mass zero spectrum referred to as AMO. (2) The air mass 1.5 global spectrum referred to as AM1.5G (3) The air mass 1.5 direct spectrum refereed to us AM1.5D (4) The air mass 1.5 diffused spectrum referred to as AM1.5Diff. It is defined as, AM1.5Diff=AM1.5G-AM1.5D (5) The Xenon lamps, which produce a bright white light.

In Table 1, one can show the power density for each standard spectrum with the preparation of blue light in the 300–475 nm-wavelength region. A down-shifter may be taken to be efficient with 34.7% of 'blue light' and inefficient with 12.5% of 'blue-light'.

4. Conclusions

The electronic, optical and elastic properties of cubic halide double perovskite $Cs_2AgInBr_6$ material were investigated. The DFT computations were carried out using ab initio norm-conserving pseudopotential plane-wave method within the GGA-PBE exchange–correlation functional. To improve the accuracy of the fundamental gap, a functional hybrid B3LYP was used. The cubic $Cs_2AgInBr_6$ being studied here showed a direct to band gap with a value of 1.427 eV. The study of optical absorption coefficient indicated that $Cs_2AgInBr_6$ exhibits a large absorption coefficient (>10^4 cm^{-1}) within a wide band of band. The refractive index spectrum was analyzed and discussed, and the static refractive index for the material in question was estimated to be 2.09. Although, the stability of the perovskite under focus was verified via the elastic constants showing that $Cs_2AgInBr_6$ is stable mechanically, the phonon spectrum calculation showed a negative value of about -175 cm^{-1} . The information derived from the present study could be useful for applications of photovoltaic's.

Declaration of competing interest

The authors declare that they have no known competing financial interests or personal relationships that could have appeared to influence the work reported in this paper.

References

[1] A. Kojima, K. Teshima, Y. Shirai, T. Miyasaka, J. Am. Chem. Soc. 131 (2009) 6050.
[2] R.F. Service, Science 344 (2014) 458.
[3] H.J. Snaith, J. Phys. Chem. Lett. 4 (2013) 3623.
[4] N.-G. Park, J. Phys. Chem. Lett. 4 (2013) 2423.
[5] K.T. Butler, J.M. Frost, A. Walsh, Mater. Horiz. 2 (2015) 228, and references therein.
[6] A. Walsh, J. Phys. Chem. C 119 (2015) 5755.
[7] J. Yang, P. Zhang, S.-H. Wei, J. Phys. Chem. Lett. 9 (2018) 31.
[8] R. Fu, Y. Chen, X. Yong, Z. Ma, L. Wang, P. Lv, S. Lu, G. Xiao, B. Zou, Nanoscale 11 (2019) 17004.
[9] G. Garcia-Espejo, D. Rodríguez-Padrón, R. Luque, L. Camacho, G. de Miguel, Nanoscale 11 (2019) 16650.

[10] Z. Zhang, C. Wu, D. Wang, G. Liu, Q. Zhang, W. Luo, X. Qi, X. Guo, Y. Zhang, Y. Lao, B. Qu, L. Xiao, Z. Chen, Org. Electron. 74 (2019) 204.
[11] L. Schade, A.D. Wright, R.D. Johnson, M. Dollmann, B. Wenger, P.K. Nayde, D. Prabhakaran, L.M. Herz, R. Niclolas, H.J. Snaith, P.G. Radaelli, ACS Energy Lett. 4 (2019) 299.
[12] G. Volonakis, A.A. Haghighirad, R.L. Milot, W.H. Sio, M.R. Filip, B. Wenger, M.B. Johnston, L.M. Herz, H.J. Snaith, F. Giustino, J. Phys. Chem. Lett. 8 (2017) 772.
[13] Z. Zhang, J. Su, J. Hou, Z. Lin, Z. Hu, J. Chang, J. Zhang, Y. Hao, J. Phys. Chem. Lett. 10 (2019) 1120.
[14] X.-G. Zhao, D. Yang, Y. Sun, T. Li, L. Zhang, L. Yu, A. Zunger, J. Am. Chem. Soc. 139 (2017) 6718.
[15] Y. Liang, J. Alloys Compd. 862 (2021) 158575.
[16] N. Ravindra, P. Ganapathy, J. Choi, Infrared Phys. Technol. 50 (2007) 21.
[17] S. Adachi, J. Appl. Phys. 61 (1987) 4869, and references therein.
[18] M. Boucenna, N. Bouarissa, Optik 125 (2014) 6611.
[19] S.J. Clark, M.D. Segall, C.J. Pickard, P.J. Hasnip, M.J. Probert, M.I.J. Refson, M.C. Payne, First principles methods using CASTEP, Z. Krist. 220 (2005) 567.
[20] J.P. Perdew, K. Burke, M. Ernzerhof, Phys. Rev. Lett. 77 (1996) 3865.
[21] H.J. Monkhorst, J.D. Pack, Phys. Rev. B 13 (1976) 5188.
[22] V. Milman, M.C. Warren, J. Phys.: Condens. Matter 13 (2001) 241.
[23] A. Reuss, Z. Angew. Math. Mech. 9 (1929) 49.
[24] W. Voigt, Lehrbuch Der Kristallphysik Teubner, Leipzig, 1928.
[25] R. Hill, Proc. Phys. Soc. A 65 (1952) 349.
[26] R. Hill, J. Mech. Phys. Solids 11 (1963) 357.
[27] M.L. Cohen, J.R. Chelikowsky, Electronic Structure and Optical Properties of Semiconductors, Springer-Verlag, Berlin, 1989.
[28] R.M. Martin, Electronic Structure: Basic Theory and Practical Methods, Cambridge University Press, 2004.
[29] N. Bouarissa, J. Phys. Chem. Solids 67 (2006) 1440.
[30] K. Kassali, N. Bouarissa, Microelectron. Eng. 54 (2000) 277.
[31] I. Vurgaftman, J.R. Meyer, L.R. Ram-Mohan, J. Appl. Phys. 89 (2001) 5815, and references therein.
[32] S. Adachi, Properties of Semiconductor Alloys: Group-IV, III-V and II-VI Semiconductors, John Wiley Sons Ltd., Chichester, 2009.
[33] N. Bouarissa, Mater. Sci. Eng. B 86 (2001) 53.
[34] N. Bouarissa, Phys. Lett. A 245 (1998) 285.
[35] N. Bouarissa, Phys. Status Solidi b 231 (2002) 391.
[36] S. Saib, N. Bouarissa, Solid State Electron. 50 (2006) 763.
[37] S. Zerroug, F. Ali Sahraoui, N. Bouarissa, Eur. Phys. J. B 57 (2007) 9.
[38] S. Ozaki, S. Adachi, J. Appl. Phys. 75 (1994) 7470.
[39] K.I. Suzuki, S. Adachi, J. Appl. Phys. 83 (1998) 1018.
[40] F. Mezrag, W. Kara Mohamed, N. Bouarissa, Physica B 405 (2010) 2272.
[41] N. Bouarissa, Mater. Chem. Phys. 72 (2001) 387.
[42] A. Bouarissa, A. Gueddim, N. Bouarissa, S. Djellali, Polym. Bull. 75 (2018) 3023.
[43] S. Saib, N. Bouarissa, P. Rodríguez-Hernández, A. Muñoz, Physica B 403 (2008) 4059.
[44] P.Y. Yu, M. Cardona, Fundamentals of Semiconductors, Physics and Materials Properties, Springer-Verlag, Berlin, 1996.
[45] A. Gueddim, S. Zerroug, N. Bouarissa, J. Lumin. 135 (2013) 243.
[46] A. Khaldi, N. Bouarissa, L. Tabourot, J. Supercond. Nov. Magn. 31 (2018) 1643.
[47] N. Bouarissa, K. Kassali, Phys. Status Solidi B 228 (2001) 663;
N. Bouarissa, N. Kassali, Physica Status Sol. B 231 (2002) 294.
[48] K. Kim, W.R.L. Lambrecht, B. Segall, Phys. Rev. B 53 (1996) 16310.
[49] N. Bouarissa, Mater. Chem. Phys. 100 (2006) 41.
[50] S. Daoud, N. Bioud, N. Bouarissa, Mater. Sci. Semicond. Process. 31 (2015) 124.
[51] Z.-J. Wu, E.-J. Zhao, H.-P. Xiang, X.F. Han, X.-J. Liu, J. Meng, Phys. Rev. B 76 (2007) 054115.
[52] N. Bouarissa, Comput. Condens. Matter 22 (2020) e00435.
[53] Y. Jestin, Compr. Remarkable Energy 1 (2012) 563.

Special issue: ICCESEN-2019

Band Structure and Optical Spectra of Double Perovskite $Cs_2AgBiBr_6$ for Solar Cells Performance

A. Menedjhi[a,b], N. Bouarissa[a,b,*], S. Saib[a,b], M. Boucenna[b] and F. Mezrag[a,b]
[a]Laboratory of Materials Physics and Its Applications, University of M'sila, 28000 M'sila, Algeria
[b] Physics Department, Faculty of Science, University of M'sila, 28000 M'sila, Algeria

The present study reports on the electronic band structure and optical properties of $Cs_2AgBiBr_6$ double-perovskite material using a pseudopotential plane-wave method within the generalized gradient approximation. Our results show that $Cs_2AgBiBr_6$ has a good absorption in the visible spectrum region, nevertheless, it has an indirect band gap of magnitude of 1.32 eV. This limits its application in photovoltaics. An alternative is proposed to overcome this shortcoming.

DOI: 10.12693/APhysPolA.137.486

PACS/topics: optoelectronic properties, double perovskite materials, solar cells

1. Introduction

Perovskite-type materials have attracted much attention in the field of photovoltaic devices. This is due to their important optical and electronic properties [1–9]. As a matter of fact, the power conversion efficiencies of perovskite solar cells were improved by about 20% in ten years, which makes them comparable with polycrystalline silicon solar cells.

Generally, perovskite solar cells with excellent performance are based on lead which is toxic and are instable [10]. This severely limits their applications in photovoltaics. To overcome this shortcoming, a new generation of perovskites materials such as $Cs_2AgBiBr_6$ was proposed [11–14]. These materials are inorganic, stable, and non-toxic. Besides, they are regarded as useful materials for photovoltaic applications since they were reported to be successfully synthesized [15].

The fundamental properties of perovskite solar cell materials, mainly the electronic and optical properties play a crucial role in the design and fabrication of devices based on these materials. For that, the current contribution attempts to investigate the electronic band structure and absorption coefficient of the double perovskites material $Cs_2AgBiBr_6$ using first-principles calculations.

2. Computational method

The computations realized in this paper are based on a pseudopotential plane-wave method using the CASTEP code [16]. The exchange and correlation potential is described using the generalized gradient approximation (GGA) of Perdew et al. (PBE) [17].

*corresponding author; e-mail: n_bouarissa@yahoo.fr

The plane wave cut off energy is taken to be 1400 eV. The Monkhorst and Pack k-point meshes [18] are used so as to perform the Brillouin zone integrations with a $10 \times 10 \times 10$ special k points mesh.

3. Results and discussion

The electronic band structure is an effective means for studying the electronic and optical properties of semiconductors [19–23]. The accurate knowledge of these parameters is an important information for synthesizing and fabricating devices based on these semiconductors [24–27]. In this regard, the electronic band structure of $Cs_2AgBiBr_6$ double perovskite has been computed using the GGA-PBE approach. Our findings are displayed in Fig. 1. The picture appears to be qualitatively similar to those of other semiconducting materials [28, 29]. A close inspection of Fig. 1 shows the absence of intersection points between the Fermi level and energy bands. This indicates that the material of interest is a semiconductor. By observing Fig. 1, one can note that the valence band maximum is located at the high symmetry point L in the Brillouin zone, whereas the conduction band minimum occurs at the Γ point. This suggests that the material in question is an indirect (L-Γ) band gap semiconductor. The computed magnitude of this band gap is found to be 1.32 eV. As a matter of fact, the nature of the band gap of $Cs_2AgBiBr_6$ limits its application in photovoltaics. In this case, we suggest replacing Bi by In in order to change the nature of the band gap. Work is in progress in this respect and will be reported in due course.

The optical properties of semiconductors are important physical parameters that are required to model quantum structures [30, 31]. Before being absorbed, the incident light of a given wavelength penetrates into a material and travels a certain distance. This distance

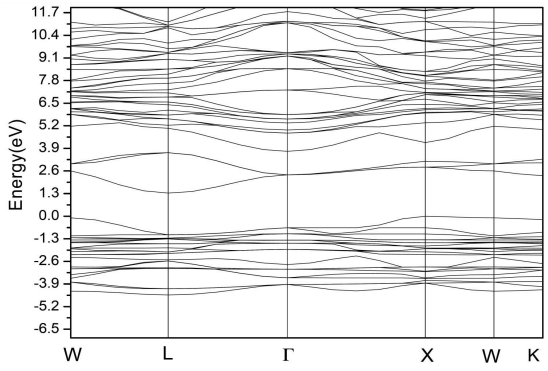

Fig. 1. Electronic band structure for $Cs_2AgBiBr_6$.

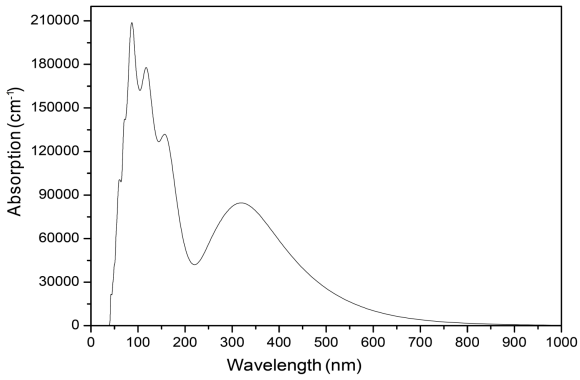

Fig. 2. Optical absorption coefficient spectrum for $Cs_2AgBiBr_6$.

is characterized by a physical parameter termed as the absorption coefficient [32–34]. Figure 2 illustrates the evolution of the absorption coefficient as a function of the photon incident energy. Note that the absorption coefficient is practically null for photon incident energies lower than the fundamental absorption edge and then it increases in magnitude. This is attributed to the increase in the number of electrons which have the energy that permits them to interact with photons. The magnitude of the optical absorption coefficient depends on that of the frequency of the electromagnetic wave. As far as the material of interest is concerned, the latter shows a good absorption of light in the visible spectrum region.

4. Conclusion

The electronic band structure and optical properties of $Cs_2AgBiBr_6$ double perovskite have been investigated using a pseudo-potential plane-wave method within the GGA-PBE approach. The material of interest showed a good absorption in the visible spectrum region. However, its fundamental band gap energy was found to be indirect. This suggests that its application in photovoltaics is limited. We propose to replace Bi by In in order to change the nature of the gap. Work is in progress in this regard.

References

[1] A. Kojima, K. Teshima, Y. Shirai, T. Miyasaka, *J. Am. Chem. Soc.* **131**, 6050 (2009).

[2] R.F. Service, *Science* **344**, 458 (2014).

[3] H.J. Snaith, *J. Phys. Chem. Lett.* **4**, 3623 (2013).

[4] N.-G. Park, *J. Phys. Chem. Lett.* **4**, 2423 (2013).

[5] K.T. Butler, J.M. Frost, A. Walsh, *Mater. Horiz.* **2**, 228 (2015) and references therein.

[6] X. Lu, D. Yang, *Emerg. Mater. Res.* **6**, 234 (2017).

[7] R. Kusum, M. Chhikara, S.P.K. Shishodia, *Emerg. Mater. Res.* **5**, 259 (2017).

[8] N.B. Singh, M. Gilan, D. House, R. Yanamaddi, V. Razdan, B. Arnold, *Emerg. Mater. Res.* **2**, 344 (2013).

[9] H. Sampath, T.I. Jayaraj, R. Oommen, U.R. Parthasarathy, *Emerg. Mater. Res.* **4**, 286 (2015).

[10] A. Walsh, *J. Phys. Chem. C* **119**, 5755 (2015).

[11] Z. Zhang, C. Wu, D. Wang, et al., *Org. Electron.* **74**, 204 (2019).

[12] L. Schade, A.D. Wright, R.D. Johnson, et al., *ACS Energy Lett.* **4**, 299 (2019).

[13] J. Yang, P. Zhang, S.H. Wei, *J. Phys. Chem. Lett.* **9**, 31 (2018).

[14] R. Fu, Y. Chen, X. Yong, Z. Ma, L. Wang, P. Lv, S. Lu, G. Xiao, B. Zou, *Nanoscale* **11**, 17004 (2019).

[15] G. Garcia-Espejo, D. Rodríguez-Padrón, R. Luque, L. Camacho, G. de Miguel, *Nanoscale* **11**, 16650 (2019).

[16] S.J. Clark, M.D. Segall, C.J. Pickard, P.J. Hasnip, M.I.J. Probert, K. Refson, M.C. Payne, *Z. Krist.* **220**, 567 (2005).

[17] J.P. Perdew, K. Burke, M. Ernzerhof, *Phys. Rev. Lett.* **77**, 3865 (1996).

[18] H.J. Monkhorst, J.D. Pack, *Phys. Rev. B* **13**, 5188 (1976).

[19] N. Bouarissa, *Mater. Sci. Eng. B* **86**, 53 (2001).

[20] M.L. Cohen, J.R. Chelikowsky, in: *Electronic Structure and Optical Properties of Semiconductors*, Springer-Verlag, Berlin 1989.

[21] N. Bouarissa, *Phys. Status Solidi B* **231**, 391 (2002).

[22] A. Bechiri, F. Benmakhlouf, N. Bouarissa, *Mater. Chem. Phys.* **77**, 507 (2003).

[23] R.M. Martin, *Electronic Structure: Basic Theory and Practical Methods*, Cambridge Univ. Press, 2004.

[24] N. Bouarissa, *Mater. Chem. Phys.* **73**, 51 (2002).

[25] I. Vurgaftman, J.R. Meyer, L.R. Ram-Mohan, *J. Appl. Phys.* **89**, 5815 (2001).

[26] S. Adachi, *Properties of Semiconductor Alloys: Group-IV, III-V and II-VI Semiconductors*, Wiley, Chichester 2009.

[27] N. Bouarissa, F. Annane, *Mater. Sci. Eng. B* **95**, 100 (2002).

[28] N. Bouarissa, *Phys. Lett. A* **245**, 285 (1998).

[29] L. Hannachi, N. Bouarissa, *Physica B* **404**, 3650 (2009).

[30] F. Mezrag, W. Kara Mohamed, N. Bouarissa, *Phys. B* **405**, 2272 (2010).

[31] S. Saib, N. Bouarissa, P. Rodriguez-Hernández, A. Muñoz, *Physica B* **403**, 4059 (2008).

[32] S. Djaili, A. Gueddim, A. Guibadj, N. Bouarissa, *Optik* **200**, 163421 (2020).

[33] A. Bouarissa, A. Gueddim, N. Bouarissa, S. Djellali, *Polym. Bull.* **75**, 3023 (2018).

[34] A. Khaldi, N. Bouarissa, L. Tabourot, *J. Supercond. Nov. Magn.* **31**, 1643 (2018).